Effector Protein SidM from *Legionella pneumophila* in complex with the Human protein Rab1A

Von der Fakultät für Lebenswissenschaften

der Technischen Universität Carolo-Wilhelmina zu Braunschweig

zur Erlangung des Grades eines

Doktors der Naturwissenschaften

(Dr. rer. nat.)

genehmigte

D i s s e r t a t i o n

von Edukondalu Mullapudi

aus Sindhanur/Indien

1. Referent: Prof. Dr. Michael Steinert
2. Referent: Prof. Dr. Wolf-Dieter Schubert
eingereicht am: 05.08.2014
mündliche Prüfung (Disputation) am: 01.10.2014
Druckjahr 2015

Vorveröffentlichungen der Dissertation

Teilergebnisse aus dieser Arbeit wurden mit Genehmigung der Fakultät für Lebenswissenschaften, vertreten durch den Mentor der Arbeit, in folgenden Beiträgen vorab veröffentlicht:

Tagungsbeiträge:

Mullapudi E., Schubert W.-D.: Structural and functional characterization of the protein SidM of *Legionella pneumophilia* and its complex with human guanosine triphosphatase Rab1A. (Vortrag) Biotechnology Research Open Day, University of the Western Cape, Faculty of Natural Sciences, Cape Town, South Africa (2010) awarded 2nd prize for best PhD oral presentation.

Mullapudi E., Schubert W.-D.: Structural and functional characterization of the protein SidM of *Legionella pneumophilia* and its complex with human guanosine triphosphatase Rab1A. (Vortrag) Biotechnology Research Day, University of the Western Cape, Cape Town, South Africa (2011).

Table of Contents

TABLE OF CONTENTS **2**

ABBREVIATIONS **4**

SUMMARY **6**

1 INTRODUCTION **7**

1.1 LEGIONELLA PNEUMOPHILA 7
1.2 PATHOGENESIS OF *L. PNEUMOPHILA* 8
1.3 SECRETION SYSTEMS OF L. PNEUMOPHILA 9
1.3.0 TYPE IVA SECRETION SYSTEM (T4ASS) 10
1.3.1 TYPE IVB SECRETION SYSTEM (T4BSS) 10
1.4 RAB GTPASES 12
1.4.1 STRUCTURE OF RAB GTPASES 15
1.4.2 RAB ACTIVATION BY GEFS 17
1.5 HIJACKING OF RAB GTPASES BY L. PNEUMOPHILA 18
1.5.1 SIDM/DRRA 18
1.5.2 SIDD, LEPB, AND LIDA 20
1.6 AIM OF THE WORK 20

2 MATERIALS AND METHODS **21**

2.1 STANDARD MATERIALS 21
2.1.1 CHEMICALS, ENZYMES AND KITS 21
2.1.2 MOLECULAR WEIGHT STANDARDS AND KITS 21
2.1.3 CRYSTALLIZATION SCREENS 22
2.1.4 OLIGONUCLEOTIDES 22
2.1.5 PLASMIDS 23
2.1.6 RECOMBINANT PLASMIDS 23
2.1.7 BACTERIAL STRAINS 24
2.1.8 OTHER CHEMICALS 25
2.1.9 ANTIBIOTICS 25
2.2 MEDIA AND BUFFERS 25
2.3 MICROBIOLOGY 27
2.3.1 PREPARATION OF AGAR PLATES 27
2.3.2 LIQUID CULTURE 27
2.3.3 PREPARATION OF GLYCEROL STOCKS 27
2.4 MOLECULAR BIOLOGY 28
2.4.1 TRANSFORMATION OF COMPETENT BACTERIA 28
2.4.2 EXTRACTION OF PLASMID DNA 28
2.4.3 AGAROSE GEL ELECTROPHORESIS 29
2.4.4 SITE-DIRECTED MUTAGENESIS 29
2.4.5 RESTRICTION FREE CLONING 30
2.4.6 CO-EXPRESSION 30
2.5 PROTEIN PRODUCTION AND PURIFICATION 30
2.5.1 EXPRESSION TEST 30
2.5.2 RECOMBINANT PROTEIN PRODUCTION 31
2.5.3 PURIFICATION OF RAB1A AND SIDM$_{317-545}$ 32
2.6 PROTEIN ANALYTICAL METHODS 33
2.6.1 CONCENTRATION OF PROTEINS 33
2.6.2 SDS-POLYACRYLAMIDE GEL ELECTROPHORESIS (SDS-PAGE) 34
2.6.3 SURFACE PLASMON RESONANCE (SPR) SPECTROSCOPY 34
2.6.4 ISOTHERMAL TITRATION CALORIMETRY (ITC) 34

2.7 Crystallization 35
2.8 X-ray Data Collection 36
2.9 Data Processing and Structure Solution 36

3 RESULTS 37
3.1 Human Rab1A, a small GTPase 37
3.1.1 Production and purification of recombinant Rab1A 37
3.1.2 C-terminal deletions of Rab1A 38
3.1.3 Production and purification of stable $Rab1A_{1-175}$ 40
3.2 Type IVB effector protein SidM of *Legionella pneumophila* 41
3.2.1 Production and Purification of $SidM_{317-545}$ 41
3.2.3 Crystallization of $SidM_{317-545}$ 43
3.3 Complex formation of $SidM_{317-545}$ /$Rab1A_{1-175}$ 44
3.3.1 Purification and analysis of $SidM_{317-545}$ /$Rab1A_{1-175}$ complex 44
3.3.2 Stability of $SidM_{317-545}$ /$Rab1A_{1-175}$ complex 46
3.3.3 Co-expression of $SidM_{317-545}$ and $Rab1A_{1-175}$ 47
3.4 Surface Mutagenesis of Rab1A 48
3.4.1 $Rab1A^{K55S-K58S}$ and $Rab1A^{E168A-K170S-K171A-R172S}$ variants 48
3.5 Structure of $SidM_{317-545}$ /$Rab1A_{1-175}$ complex 49
3.5.1 Crystallization of $SidM_{317-545}$ /$Rab1A_{1-175}$ 49
3.5.2 Data collection and processing 50
3.5.3 Structure of $Rab1A_{1-175}$ 51
3.5.3 Structure of $SidM_{317-545}$ 53
3.5.4 The $SidM_{317-545}$ /$Rab1A_{1-175}$ Complex 54
3.5.5 Interface of the $SidM_{317-545}$ /$Rab1A_{1-175}$ Complex 55
3.5.6 Switch I of $Rab1A_{1-175}$ contacts α2, α5, α6 and L_F of $SidM_{317-545}$ 56
3.5.7 Switch II contacts of $Rab1A_{1-175}$ with $SidM_{317-545}$ 57
3.5.8 P-Loop and other contacts of $Rab1A_{1-175}$ with $SidM_{317-545}$ 58
3.6 Isothermal Titration Calorimetry (ITC) Measurements 59
3.6.1 State A- Rab1A: GDP/$SidM_{317-545}$ 60
3.6.2 State B: EDTA treatment of Rab1A/$SidM_{317-545}$ 60
3.6.3 Effect of $Rab1A^{K55A-K58S}$ variant on binding affinity with SidM 61
3.6.4 Effect of Rab1 variants E35A, Y37A and I41A on binding to SidM 62

4 DISCUSSION 66
4.1 SidM Manipulates Rab1A Function for Legionella pneumophila Survival 66
4.2 SidM Induces Structural Changes on Rab1A 66
4.2.1 Structural mechanism of nucleotide exchange by SidM 67
4.3 SidM affinity for nucleotide-free Rab1A is higher than for Rab1A:GDP 69
4.4 Role of Switch I in SidM binding 70
4.4 Comparison of SidM/Rab1A with other GEF/Rab Complexes 70
5 Conclusions and Outlook 72

6 REFERENCES 74

ACKNOWLEDGEMENTS 80

CURRICULUM VITAE 82

Abbreviations

aa	Amino acid
Å	Ångström
AMP	Adenosine mono phosphate
AP	Alkaline phosphatise
APS	Ammonium persulphate
Bis-Tris	Bis(2-hydroxyethyl)amino-tris(hydroxymethyl)methan
CDP	Cytosine diphosphate
CV	Column volume
kDa	Kilo Dalton
E. coli	*Escherichia coli*
DMSO	Dimethyl sulfoxide
DOT	Defect in orgnalle trafficking
EDTA	Ethylenediaminetetraacetic acid
ER	Endopalsmic reticulum
GAP	GTPase activating protein
GDP	Guanosine di phosphate
GTP	Guanosine tri phosphate
GEF	Gaunosine nucleotide exchange factor
GDI	Guanosine nucleotide dissociation Inhibitor
GDF	GDI displacement factor
GGTase	Geranylgeranyltransferase
LCV	Legionella containing vacuole
ICM	Intracellular multiplication
ITC	Isothermal titration calorimetry
IEC	Ion exchange chromatography
IMAC	Immobilized metal ion affinity chromatography
IPTG	Isopropyl-β-D-thiolgalactoside
KPi	KH_2PO_4/K_2HPO_4
MWCO	Molecular weight cut off

Mg^{2+}	Magnesium ions
Ni-NTA	Nickel-nitrilotriacetic acid-agarose
NMR	Nuclear magnetic resonance
OD_{600}	Optical density at 600 nm
PAGE	Polyacrylamid gel electrophoresis
PCR	Polymerase chain reaction
PDB	Protein data bank
Pi	Inorganic phosphate
PI(4)P	Phosphatidylinositol 4-phosphatase
Rab	Ras-related proteins in brain
REP	Rab escort protein
SDS	Sodium dodecyl sulphate
SEC	Size exclusion chromatography
SNARE protein receptor	Soluble N-ethylmaleimide-sensitive factor attachement
SPR	Surface plasma resonance
TAE	Tris-acetate-EDTA
TBS	Tris buffered saline
TCA	Trichloroacetic acid
TEMED	N, N, N', N' – Tetramethylendiamin
Tris	Tris (hydroxymethyl) aminomethane
T4ASS	Type 4 A secretion system
T4BSS	Type 4 B secretion system
UTI	Urinary tract infection
WHO	World Health Organization
wt	Wild type

Amino acids are abbreviated using 1 or 3 letter code.

Latinisms are written in italic.

Summary

Rab1 is a small GTPase that regulates intracellular trafficking between the endocytoplasmic reticulum (ER) and the Golgi complex. In common with other GTPases, cytosolic Rab1 is normally kept in a GDP-bound, inactive state by a dedicated GDP-dissociation inhibitor (GDI). To activate Rab1, a GDI-displacement factor (GDF) is required to remove the GDI before a GTP exchange factor (GEF) can induce the release of GDP to allow for subsequent uptake of GTP and activation of Rab1. SidM is a type IV secretion system effector protein from *Legionella pneumophila* that has both GEF and GDF activity for Rab1GTPase. SidM recruits Rab1 to the *Legionella*-containing vacuole (LCV) as part of generating a specialized vacuole that resembles the host's rough endoplasmic reticulum. Within this vacuole *L. pneumophila* creates a replication niche allowing it to evade destruction by lysosomal fusion. To understand the SidM/Rab1 complex at the atomic level, the central domain of $SidM_{317-545}$ and $Rab1A_{1-175}$ were each purified and co-crystallized. Complex formation of SidM/Rab1 was analysed by size exclusion chromatography and isothermal calorimetry. The structure of the SidM/Rab1A complex was determined by X-ray crystallography revealing that the GEF domain of SidM is structurally distinct from known eukaryotic GEFs. The structure of the complex further revealed that SidM induces several conformational changes in Rab1A to facilitate GDP release. ITC experiments show that SidM has a higher affinity for unbound Rab1A compared to GDP-bound Rab1.

1 Introduction

Infectious diseases pose a significant threat to the global population. Recent reports from World Health Organization (WHO) have shown that infectious diseases account for more than 17 million deaths every year, the majority of which are due to bacterial infections (Millar et al., 2007). Bacterial infections result in acute to chronic illnesses especially in elderly people, children and immunocompromised patients. Common bacterial infections include pneumonia, diarrhea, urinary tract infections, ear and skin infections. Despite the availability of broad range of antibiotics, new bacterial strains are emerged that develop resistant to antibiotics. According to the latest reports from WHO, antibiotic resistant bacterial infections annually result in ~ 25 thousand deaths in the European Union alone (Reports from European Center For Disease Prevention And Control (ECDC, 2012). The associated medical costs and lost productivity are estimated to be around € 1.5 billion per year (Reports from European Center For Disease Prevention And Control (ECDC, 2012).
Pathogenic bacteria have developed numerous strategies to escape the host immune system and survive inside host cells. Understanding the molecular mechanisms involving host-pathogen interactions is essential for the development of novel antimicrobial drugs and vaccines. In recent years, structural biology has become a powerful tool in the field of modern drug discovery. Use of structural biology methods such as X-ray crystallography and NMR will allow us to solve the three dimensional structures of biological proteins. This information can be used to design the therapeutic agents against the target proteins involved in the infectious diseases.

1.1 *Legionella pneumophila*

The genus *Legionella* is a Gram negative, aerobic, rod shaped motile bacterium that belong to the family of Legionellaceae (Edelstein 2007). To date more than 50 species of *Legionella* have been identified. Among them, *Legionella pneumophila* is a pathogenic bacterium that is universally found in freshwater environments such as ponds, lakes and also in association with amoeba and man-made aquatic environments like swimming pools, air-conditioning systems, cooling towers, water tanks, refrigerators, showers, respiratory devices etc.

In humans, *L. pneumophila* causes two forms of infections: Legionnaires' disease and Pontiac fever. Legionnaires' disease is a severe form of a pneumonia characterized by high fever, body pains, headache, nausea, shortness of breath and respiratory disorders that leads to chronic lung disease and can cause death in 5 to 30 % of the infected individuals (Edelstein 2007); (Tronel and Hartemann 2009; Cunha and Syed 2010) Legionnaires' disease was named after a massive outbreak of pneumonia affecting veterans at the American Legion convention in Philadelphia in 1976. Legionnaires' disease most commonly occurs in individuals suffering from chronic lung diseases, diabetes, AIDS/HIV, smokers, alcoholics and other immunocomprimised individuals. The second manifestation of the disease, Pontiac fever, is a mild sickness. The symptoms include fever, dry cough, chillness, muscle pains, and headaches but no pneumonia (Pancer and Stypulkowska-Misiurewicz 2003).

1.2 Pathogenesis of *L. pneumophila*

L. pneumophila is transmitted to humans through the inhalation of contaminated aerosols into the lungs. *L. pneumophila* has the ability to cause disease because it survives inside the host cells by escaping the bacteriocidal activities of the alveolar macrophages (Horwitz and Silverstein 1980) and resembles its lifecycle in amoebae. After uptake into macrophages, *L. pneumophila* resides inside the phagosome and survives inside the host cell by inhibiting the phagosome-lysosome fusion and the early endocytic pathway (Horwitz 1983). *L. pneumophila* utilizes a specialized system to manipulate the functions of host effector proteins like Rab1 and Arf1 involved in vesicle trafficking and thereby recruiting the vesicles derived from endoplasmic reticulum (ER) and ribosomes to the Legionella containing vacuole (LCV). Legionella makes use of the existing host machinery to form a specialized vacuole resembling the host rough endoplasmic reticulum (ER) studded with ribosomes (Derre and Isberg 2004). In the rough ER like vacuole, *L. pneumophila* replicates and eventually disrupts the vacuole membrane and lyses the host cell, which releases the bacterium into the extracellular environment for infecting neighbouring cells (Fig 1).

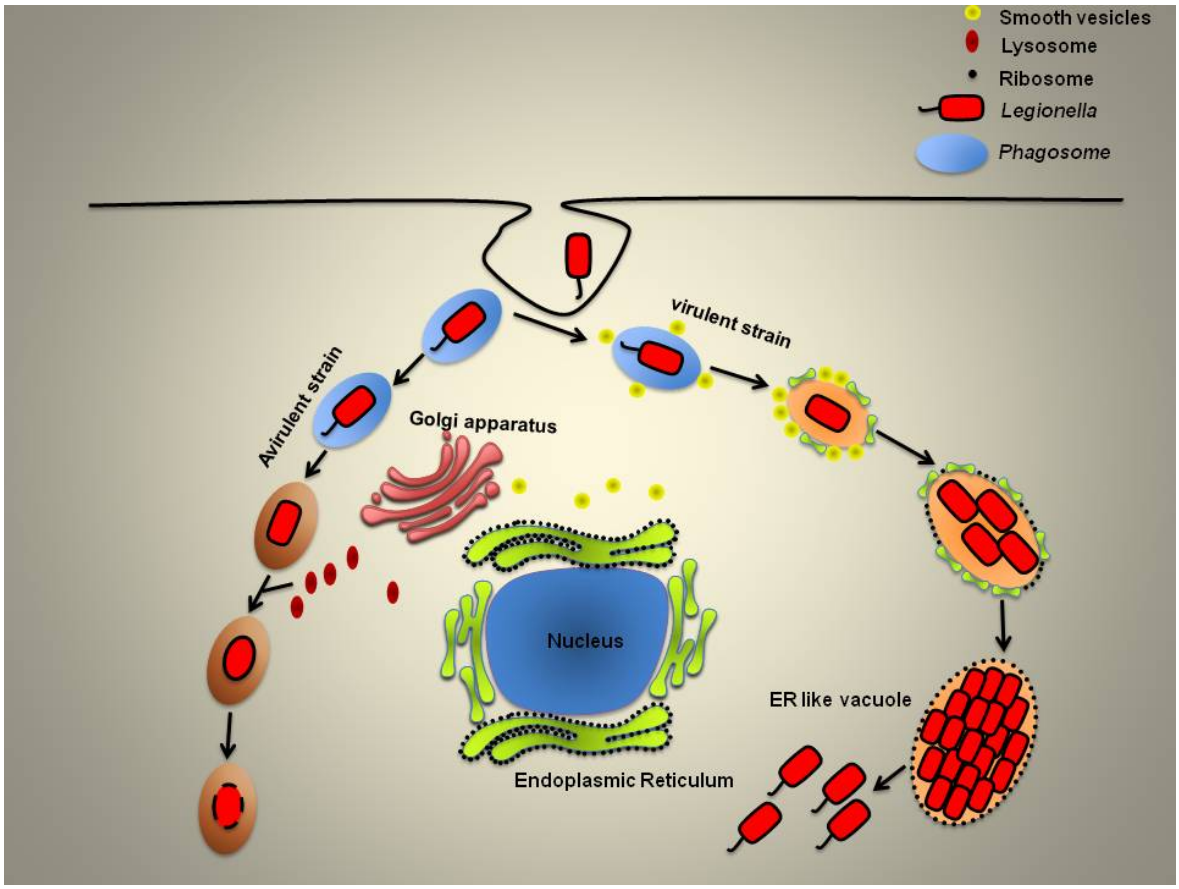

Figure 1: Life cycle of *L. pneumophila* after entry into a host cell. A bacterium of *L. pneumophila* is engulfed by macrophages by phagocytosis and resides in a phagsosme. Endoplasmic reticulum derived vesicles are recruited to fuse with the phagosome to form ER-like vacuoles studded with ribosomes, where *L. pneumophila* establishes replication niche and subsequently lyses the host cell. Avirulent strains of *L. pneumophila* (or other bacteria) fail to recruit ER-derived vesicles and enter the endocytic pathway, killing bacteria by phagosome-lysosome fusion. (adopted from Jiannin and Feng, 2011)

1.3 Secretion Systems of L. pneumophila

The interaction of a pathogen with its host is critical for its infection process. For this purpose, bacteria utilize specialized secretion systems to deliver virulence proteins into the cytosol of the host cells. In Gram-negative bacteria such as *L. pneumophila*, effector proteins need to cross the inner and the outer bacterial membrane, and the host plasma membrane to reach their destined location. This is accomplished by secretion machineries exist in the Gram-negative bacteria. *L. pneumophila* contains four secretion systems namely, type I Lss, type II pilD-dependent Lsp, type IVA Lvh, type IVB Icm/Dot and type V secretion system respectively (Gerlach and Hensel 2007). Among these, a type IV

secretion system is important for the virulence of *L. pneumophila*. Type IV secretion system are subdivided into type IVA and type IVB.

1.3.0 Type IVA Secretion System (T4ASS)

The T4ASS, resembles the *Agrobacterium tumefaciens* T-DNA transfer system or Vir system and is named as *Legionella vir* homologues (Lvh) system. Based on experimental evidences it was shown that *L. pneumophila* encodes 11 *lvh* genes (*lvhB2, B3, B4, B5, B6, B8, B9, B10, B11, D4),* and these are shown to be important in the virulence of *L. pneumophila* (Segal, Russo et al. 1999; Samrakandi, Ridenour et al. 2002).

1.3.1 Type IVB Secretion System (T4BSS)

The current work is mainly focused on effector proteins of T4BSS of *L. pneumophila*. Ralph Isberg and colleagues have identified approximately 20 *L. pneumophila* genes essential for intracellular replication and infection (Berger and Isberg 1994; Brand, Sadosky et al. 1994; Vogel, Andrews et al. 1998). Later these genes were collectively named *dot* (defect in organelle trafficking) or *icm* (intracellular multiplication). The *dot/icm* genes encode a T4BSS also known as Dot/Icm system, closely related to the Inc bacterial conjugative DNA-transfer systems (Segal and Shuman 1997; Vogel, Andrews et al. 1998). Several effector proteins of *L. pneumophila* are translocated into the cytosol of host cells using the Dot/Icm secretion system or T4BSS (Nagai, Kagan et al. 2002; Hubber and Roy 2010).

The Dot/Icm system is composed of mainly two subcomplex units, the outer membrane core transport complex and the coupling protein complex. The outer membrane core transport complex is composed of DotC, DotD, DotF, DotG and DotH proteins in which the inner membrane proteins DotF (interacts with secreted substrates) and DotG (homology to the VirB10 protein of the *A.tumefaciens*) form a complex and the C-terminal domain of DotG interacts with the outer membrane complex DotC, DotD and DotH. DotC and DotD are the outer membrane lipoproteins that recruit DotH an intrinsic periplasmic protein to the outer membrane, thereby forming a DotC-DotD-DotH-DotF-DotG outer membrane core transport complex [Fig 2 (Vincent, Friedman et al. 2006)]. However, more

detailed study is needed to get a better understanding of the T4BSS or Icm/Dot secretion system of *L. pneumophila*.

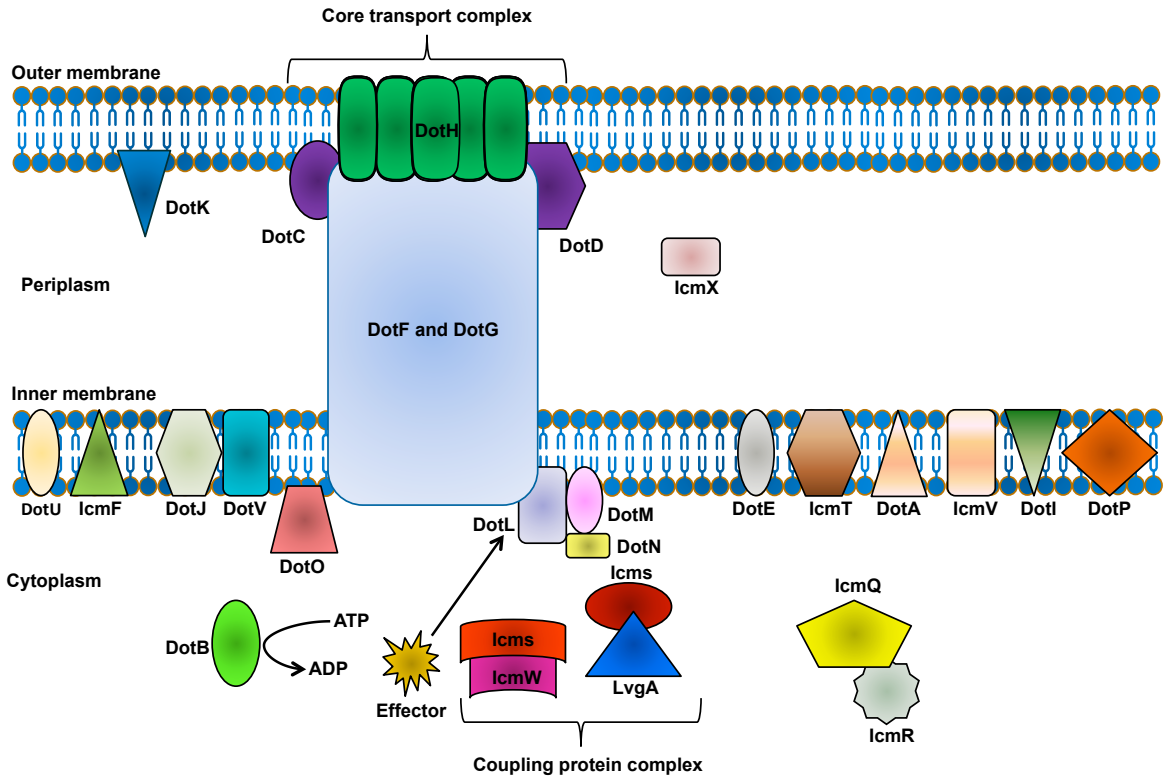

Figure 2: Components of type IVB secretion system (T4BSS) of *L. pneumophila*. The core transport complex that links the inner and outer membranes is composed of DotC, DotD, DotF, DotG and DotH [(Dot-Defect in organelle trafficking). The inner membrane proteins DotF and DotG interact and form a subcomplex with the outer membrane lipoproteins DotC, DotD and DotH. The coupling protein complex is composed of DotL (recruits IcmSW substrates to the transport complex), DotM, DotN, IcmS and IcmW [adapted from (van Schaik, Chen et al. 2013)].

To date biochemical, genetic and bioinformatics analyses have identified ~250 Dot/Icm substrate proteins (Nagai, Kagan et al. 2002; Conover, Derre et al. 2003; Luo and Isberg 2004; Campodonico, Chesnel et al. 2005; de Felipe, Pampou et al. 2005; Ninio, Zuckman-Cholon et al. 2005; Shohdy, Efe et al. 2005; Laguna, Creasey et al. 2006; Machner and Isberg 2006; Murata, Delprato et al. 2006; VanRheenen, Luo et al. 2006; Zusman, Aloni et al. 2007; Altman and Segal 2008; Kubori, Hyakutake et al. 2008; Zhu, Hu et al. 2010). The biochemical function of some substrates was identified while others remain to be studied. Some have C-terminal translocation signals for the substrate identification (Details are given in section 1.5).

1.4 Rab GTPases

Eukaryotic cells consist of several distinct intracellular compartments, which require well defined regulation of transport of vesicles to their designated location (Jordens, Marsman et al. 2005). The process of membrane trafficking occurs in a series of steps, where the donor membranes protrude to form vesicles. Rab GTPases deliver these vesicles to the acceptor membranes via microtubules or actins by recruiting motor adaptor proteins. In the next step, vesicles fuse to their target membrane with the help of rod-shaped tethering factors and SNAREs (Soluble N-ethylmaleimide-sensitive factor attachment protein receptor) by a process called as tethering (Stenmark 2009). Cell biology studies on membrane trafficking have shown that Rab (Ras-related proteins in brain) GTPases are involved in regulating the membrane trafficking events by binding to the diverse group of effector proteins, motor proteins and tethering complexes (Segev 2001; de Renzis, Sonnichsen et al. 2002; Hammer and Wu 2002; Novick, Medkova et al. 2006; Cai, Reinisch et al. 2007).

Rab proteins belong to the Ras super family of small GTPases (Wennerberg, Rossman et al. 2005). To date more than 60 Rab genes have been identified in the human genome (Pereira-Leal and Seabra 2000; Bock, Matern et al. 2001; Pereira-Leal, Hume et al. 2001). Rab proteins are located on the endoplasmic reticulum, Golgi apparatus, endosomes, lysosomes, nucleus, plasma membrane and mitochondria (Schwartz, Cao et al. 2007). Rab GTPases are involved in membrane trafficking, signalling events, regulation of cell proliferation and differentiation (Bucci and Chiariello 2006; Schwartz, Cao et al. 2007).

Rab GTPases operate in two conformations, one is guanosinediphosphate (GDP)-bound ‘inactive’ state and the other one is gunaosine triphosphate (GTP)-bound ‘active state’ (Stenmark, Valencia et al. 1994; Zerial and McBride 2001). Rabs do not exhibit high nucleotide exchange and hydrolysis activities, so the exchange of GDP to GTP or vice versa is accomplished by specialized proteins called guanine nucleotide exchange factors (GEFs) and GTPase-activating proteins (GAPs). In the cytosol, GDP Rab is solubilized by being in complex with guanine nucleotide dissociation inhibitor (GDI). For the membrane insertion of C-terminus of Rab, GDI need to be displaced from Rab:GDP and this is accomplished by GDI displacement factor (GDF) (Pfeffer and Aivazian 2004). Once

Rab:GDP is targeted to the membrane by GDF, GEF activates Rab by catalyzing the exchange of GDP for GTP. The GTP-bound active Rab interact with their downstream effector proteins to regulate several cellular functions such as membrane trafficking, signalling events, regulation of cell proliferation and differentiation. Eventually, the GTP-bound 'active' Rab is converted back to the GDP-bound 'inactive' by the GAP, which

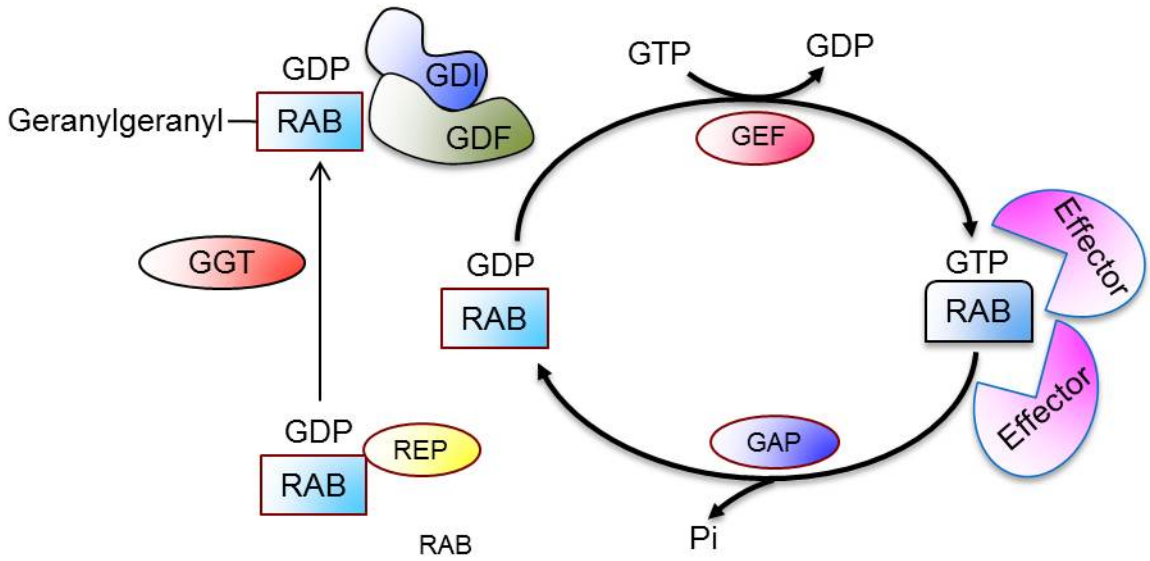

Figure 3: Rab GTPase Cycle. Rab GTPases operate between GDP and GTP-bound forms. Exchange of GDP for GTP is catalyzed by the GDP/GTP exchange factor (GEF). The GTP-bound 'active' form interacts with its effector proteins and is converted back to the GDP-bound 'inactive' form by the GTPase activating protein (GAP), which promotes hydrolysis of GTP and releases an inorganic phosphate (Pi). Rab escort protein (REP) presents the newly synthesized GDP-bound Rab to a prenylating enzyme Rab geranylgeranyltransferase (RabGGTase), which geranylgeranylates one or two carboxy-terminal Cys residues of the Rab. The geranylgernaylated, GDP-bound Rab is further recognized by Rab GDP dissociation inhibitor (GDI). The GDI displacement factor (GDF), releases GDI from the Rab-GDI complex and recruits GDP-bound Rab to the target membrane [adapted from (Stenmark and Olkkonen 2001).

effector proteins to regulate several cellular functions such as membrane trafficking, signalling events, regulation of cell proliferation and differentiation. Eventually, the GTP-bound 'active' Rab is converted back to the GDP-bound 'inactive' by the GAP, which facilitates the hydrolysis of GTP by releasing inorganic phosphate (Pi). The Rab GTPase cycle is circumvented by the extraction of Rab:GDP from the target membrane to the cytoplasm by GDI [(Fig 3) (Somsel Rodman and Wandinger-Ness 2000; Esters, Alexandrov et al. 2001; Gurkan, Lapp et al. 2005)].

Rab GTPases are targeted to specific membranes by a post-translational modification known as prenylation, where 20-carbon geranylgeranyl group is attached to one or two carboxy-terminal Cys residues of the Rab (Andres, Seabra et al. 1993). The prenylation of Rab GTPases is carried out by two conserved paralogs, Rab escort protein (REP) and Rab-GDI (Alory and Balch 2001; Pereira-Leal, Hume et al. 2001). REP is responsible for presenting the newly synthesized Rab proteins to the prenylating enzyme Rab geranylgeranyltransferase (RabGGTase) for geranyl-geranylation process and then delivers Rab proteins to target membranes. Rab GDI is important for Rab recycling by extracting inactive Rab proteins from membranes after GTP hydrolysis. The GDF, releases GDI from the Rab-GDI complex and recruits GDP-bound Rab to the target membrane (Ullrich, Stenmark et al. 1993; Sivars, Aivazian et al. 2003). REP binds either prenylated or unprenylated GDP bound Rab proteins with high affinity, whereas GDI binds prenylated Rab with higher affinity than to unprenylated Rab proteins (Plutner, Cox et al. 1991; Wu, Tan et al. 2007).

1.4.1 Structure of Rab GTPases

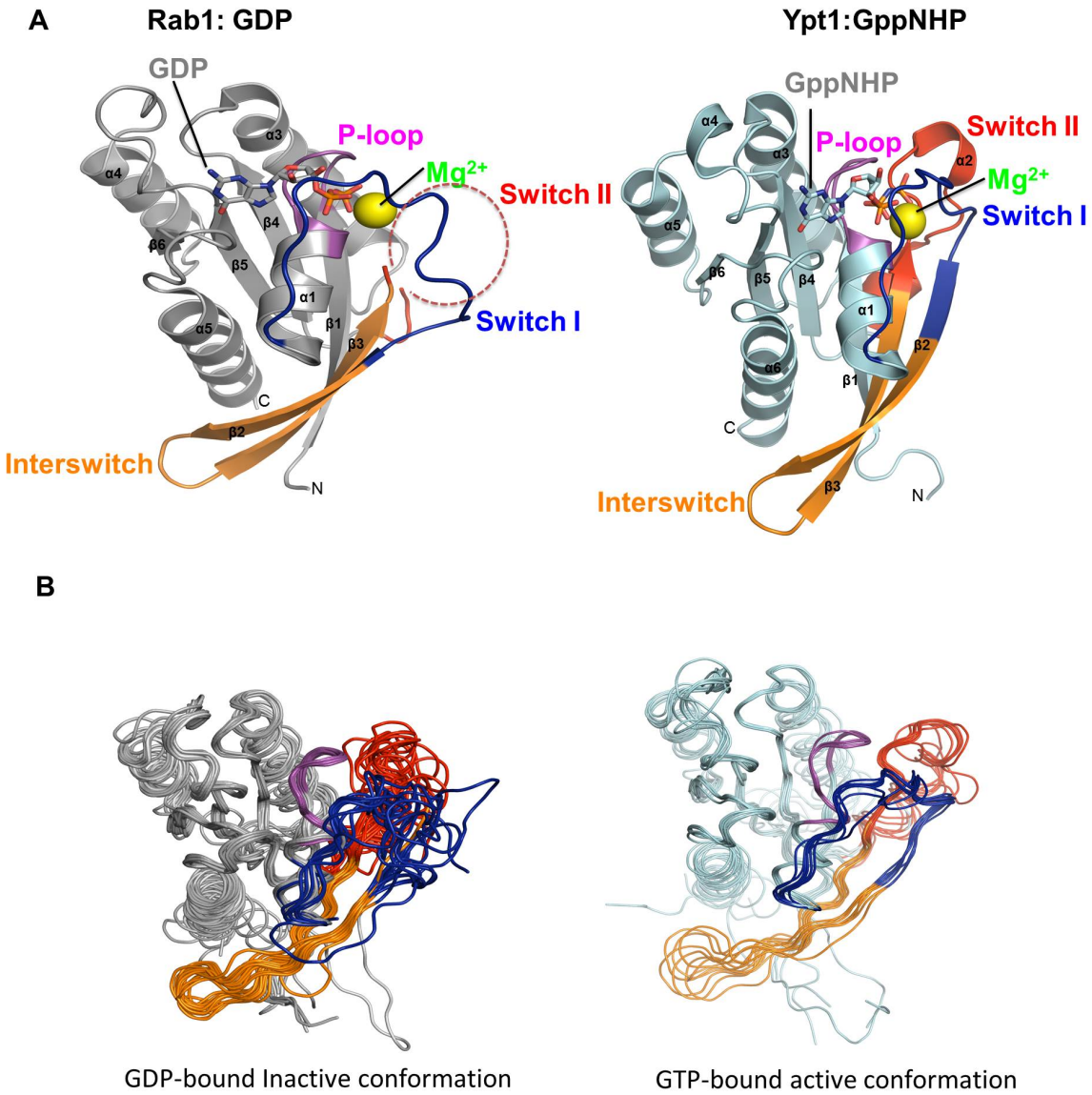

Figure 4: Crystal structures of Rab GTPases in GDP-bound, inactive and GTP-bound active conformation. (A) Structure of Rab1A bound to GDP and Mg^{2+} showing switch II in disordered conformation (Left). Structure of Ypt1:Guanosine 5′-[β, γ-imido] triphosphate (GppNHP: non- hydrolyzable analogue of GTP) showing switch II adopted ordered confirmation (Right). **(B)** Several Rab GTPase structures in active and inactive bound conformations are aligned showing structural differences (Left: GDP bound inactive conformations, Right: GTP bound active conformations). Structural elements; P-loop coloured in magenta, switch I in blue, switch II in red and interswitch regions in orange, GDP and Mg^{2+} are shown in stick and sphere representation (Details of the above structures are given in Table 1).

Table 1: Structures of Rab GTPases represented in Figure 4 are summarized below

Protein	Ligand	PDB ID
Rab/GDP (Fig 5)		
Rab1A	GDP	2FOL
Rab2A	GDP	1Z0A
Rab3B	GDP	3DZ8
Rab3D	GDP	2GF9
Rab4B	GDP	2O52
Rab5B	GDP	2HEI
Rab5C	GDP	1ZOD
Rab6A (Q72L)	GDP	4DKX
Rab7	GDP	1VG1
Rab12	GDP	2IL1
Rab14	GDP	1ZOF
Rab21	GDP	1ZOI
Rab23	GDP	1Z22
Rab25	GDP	2OIL
Rab43	GDP	2HUP
Rab/GTP /GppNHP (Fig 5)		
Ypt1	GppNHP	1YZN
Rab3A	GppNHP	3RAB
Rab4A	GppNHP	2BME
Rab6A	GTP	2GIL
Rab6	GppNHP	1YZQ
Rab7	GppNHP	1VG8
Rab28	GppNHP	3E5H
Ypt7	GppNHP	1KY2
Ypt51	GppNHP	1EKO

Rab/GDI/REP(Fig 6)		
Rab7/REP1	GDP	1VGO
REP1/RabGGTase		1LTX
Ypt1/GDI	GDP	1UKV

Rab proteins exhibit common structural features of Ras-related GTPases, comprising of a six-stranded-β sheet, with five parallel strands and one antiparallel strand, enclosed by five α- helices (Vetter and Wittinghofer 2001). Crystallographic analysis of various Rabs in the GDP- and GTP-bound states shows that the protein adopts two different conformations and these conformational changes are confined to two regions namely switch I and switch II (Fig 4 A&B). Magnesium ions (Mg^{2+}) are important for the high affinity binding of nucleotide to the Rab GTPases. Guanine nucleotides interact with residues from five G-motifs that are highly conserved in all GTPases. The G1 motif also commonly known as P-loop (phosphate binding loop) consists of consensus sequence GxxxxGKS/T that binds to phosphate and Ser/Thr is coordinated by the Mg^{2+}. The G2 motif in the switch I region has threonine residue that interacts with γ-phosphate and the Mg^{2+} ion. The G3 motif in the switch II region has a conserved DxxGQ sequence where the aspartate establishes water mediated ionic interaction with Mg^{2+}, the glycine interacts with the γ-phosphate and the glutamine acts as a catalytic residue for the GTP hydrolysis. The residues in the G4 and G5 motifs interact with the guanine base and also distinguish from other nucleotides (Khosravi-Far, Lutz et al. 1991; Vetter and Wittinghofer 2001).

Several crystal structures are available for RabGTPases in the GDP bound inactive state and GTP bound active state (Table 1). In the GDP bound inactive state, the switch regions are largely disordered or adopts ordered conformations based on the crystal packing, where in the GTP-bound active state, the switch regions adopts ordered conformation [(Eathiraj, Pan et al. 2005) (Fig 4B)].

1.4.2 Rab activation by GEFs

As explained in the previous section, activation of Rab GTPases is regulated by the switch between GDP bound inactive state and GTP bound active state. Rab GTPases form multiple contacts with guanosine nucleotides involving G motifs and Mg^{2+}. The affinity of GDP to Rab family is high and hence the release of GDP from Rab GTPases occurs at a

very slow rate by itself and this process is accelerated by GEF. GEFs establish competition with nucleotides for binding to GTPases. To date only few Rab GEFs have been identified because of their diversity in the sequence, structure, size and complexity (Lee, Mishra et al. 2009). Structures of five Rab-GEFs in complex with their specific Rab GTPases have been determined. They are MSS4-Rab8, Sec2p-Sec4p, Rabex-5-Rab21, TRAPP1-Ypt1p and DENN1B-S-Rab35. These structures will be explained in detail in the discussion chapter. Briefly, based on the available structural information about GEF-GTPase complex, it was explained that GEFs induces structural changes on Rab GTPases, especially on the nucleotide binding sites of switch I and switch II regions. These structural rearrangements lead to the wide opening of the nucleotide binding pocket and release of Mg^{2+}. This results in reducing the binding affinity between nucleotide and Rab GTPases.

1.5 Hijacking of Rab GTPases by L. pneumophila

L. pneumophila able to survive inside the host cell by modulating several functions of host proteins by delivering large set of effector proteins in to the host cytosol via T4BSS also known as Dot/Icm. Some of the Dot/Icm effector proteins namely SidM/DrrA, SidD and LepB mimic the function of host GEF, GAP and GDF proteins that are involved in the activation and inactivation of Rab1 GTPase.

1.5.1 SidM/DrrA

Figure 5: Domain organization of SidM/DrrA. N-terminus harbouring AMPlyation domain, central part with GEF domain and C-terminal P4M domain

SidM, a Dot/Icm effector protein of *L. pneumophila* recruits Rab1 onto the LCV. Rab1 is a small GTPase involved in the regulation of vesicle trafficking between ER and Golgi complex. SidM also named as DrrA contains 647 amino acid residues comprises of three domains: a C-terminal novel phosphatidylinositol 4-phosphatase (PI(4)P)-binding domain,

a central domain exhibiting GEF and GDF activity for Rab1 and an N-terminal domain displaying adenylyl transferase (AMPylation) activity (Fig 5). Inside the host cell, SidM is anchored to the LCV by the action of PI4P domain that binds with high affinity to PI4P located on the vacuolar membrane (Brombacher, Urwyler et al. 2009; Schoebel, Blankenfeldt et al. 2010; Zhu, Hu et al. 2010). The central GEF/GDF domain of SidM enables the recruitment of Rab1 to the LCV by detaching GDI from Rab:GDP:GDI complex and activates Rab by catalyzing the GDP/GTP exchange (Machner and Isberg 2006; Murata, Delprato et al. 2006; Ingmundson, Delprato et al. 2007). The N-terminal domain with adenylation activity catalyses transfer of adenosine mono phosphate (AMP) to a conserved Tyr 77 in the switch II region of Rab1:GTP. This modification inhibits the hydrolysis of GTP to GDP, maintaining Rab1 in the active form (Muller, Peters et al. 2010). By the action of SidM, Rab1 efficiently remodulates the LCV into an ER- like derived vesicle, where *L. pneumophila* replicates and escapes the lysosomal fusion. This is how the multi functional SidM/DrrA is important for the pathogenicity of *L. pneumophila*.

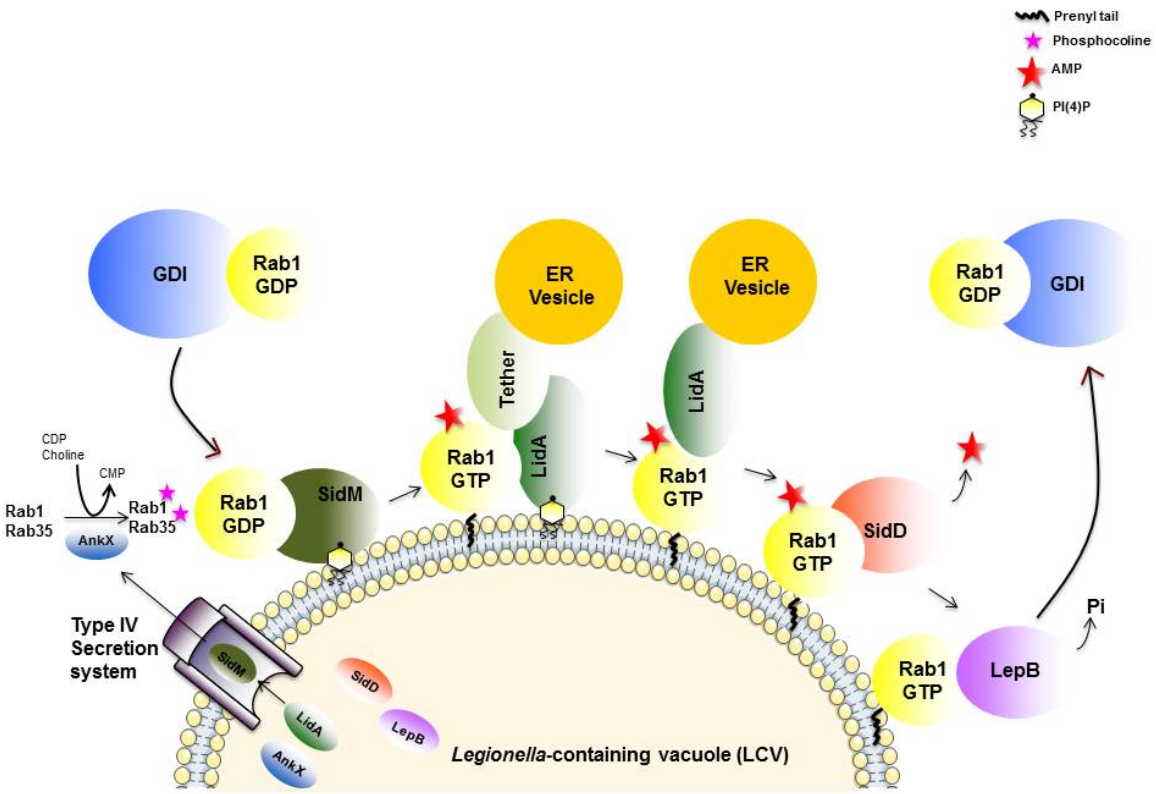

Figure 6: Regulation of Rab1 activity cycle by Dot/Icm effector proteins of *L. pneumophila* on the LCV. *L. pneumophila* secretes effector proteins into the host cytosol via T4BSS or Dot/Icm. SidM is anchored to the LCV by PI(4)P binding to recruit GDP-bound Rab1 to the LCV by detaching it from the Rab1-GDI complex and later activates Rab1 by catalyzing the exchange of GDP for GTP. SidM then

AMPylates (adding AMP) GTP-bound Rab1 at Tyr 77 to retain Rab1 in its active form, which is not accessible to GAPs. SidD deAMPylates (remove AMP) Rab1, which makes it accessible for inactivation by LepB mediated GTP hydrolysis. Finally, inactive GDP-bound Rab is accessible for GDI to remove it from the LCV membrane [Adopted from (Neunuebel and Machner 2012)] .

1.5.2 SidD, LepB, and LidA

SidD is another Dot/Icm effector protein consisting of 507 amino acids, deAMPylates Rab1 by harbouring protein phosphatase-like catalytic domain (Neunuebel, Chen et al. 2011; Tan and Luo 2011). SidD makes Rab1 accessible for inactivation by LepB. LepB also a T4B effector protein exhibits GAP activity and inactivates Rab1 by promoting hydrolysis of GTP to GDP and removes Rab1 from the LCV (Ingmundson, Delprato et al. 2007). The inactive GDP-bound Rab1 is extracted from the membrane by the action of GDI. LidA, the other T4B effector protein binds to various Rabs regardless with the bound nucleotide form, but shows higher affinity towards Rab1-GTP (Conover, Derre et al. 2003; Machner and Isberg 2006). LidA is also thought to involve in assisting SidM for the recruitment of Rab1 onto the LCV and in maintaining bacterial cell integrity (Machner and Isberg 2006; De Buck, Anne et al. 2007). The mechanism of its function is not clearly known.

The combined action of SidM/DrrA catalysed nucleotide exchange and AMPylation, SidD catalyzed deAMPylation and LepB-catalysed GTP hydrolysis of Rab1A explains the unique mechanism of *L. pneumophila* in regulating the Rab1 cycle (Fig 6).

1.6 Aim of the work

The T4B or Icm/Dot effector protein SidM of *L. pneumophila* is shown to have GEF and GDF activity towards Rab1 GTPase. One aim of this work is to produce and purify $SidM_{317-545}$ and Rab1a to analyse the stable complex formation of two proteins by size exclusion chromatography (SEC) and Isothermal titration calorimetry (ITC). The second aim is to solve the crystal structure of $SidM_{317-545}$ and $SidM_{317-545}$/Rab1a complex by X-ray crystallography to elucidate the mode of interaction between two proteins.

2 Materials and Methods

2.1 Standard Materials

If not mentioned otherwise, all chemicals and reagents used were purchased from Qiagen, Sigma Aldrich, Fluka, Invitrogen, GE Healthcare, Millipore, Hampton Research, Roche, Merck, Stratagene, Pall and Inqaba Biotech.

2.1.1 Chemicals, Enzymes and Kits

Table 1: Enzymes

Enzyme	Source
Benzonase	Structural Biology Group, HZI
DNaseI	Roche
PreScission Protease	Structural Biology Group, HZI
TEV protease	Structural Biology Group, HZI
Pfu DNA polymerase	Invitrogen
DpnI	Fermentas
T4 DNA Ligase	New England Biolabs
Hen egg-white lysozyme (HEWL)	Fluka
Restriction endonucleases: BamHI, EcoRI, NcoI, NdeI and XhoI	New England Biolabs

2.1.2 Molecular Weight Standards and Kits

Table 2: Molecular weight standards

Name	Type	Usage	Company
Smart Ladder	DNA	Agarose gel electrophoresis	Fermentas
Prestained protein Marker	Protein	SDS-PAGE	Fermentas
Unstained protein Marker	Protein	SDS-PAGE	Fermentas

Table 3: Kits

Kits	Source
QIAprep Spin Miniprep Kit	Qiagen
QIAquick PCR Purification Kit	Qiagen
QuickChange Site-Directed Mutagenesis Kit	Stratagene

2.1.3 Crystallization Screens

The following commercial screens were used to screen for initial crystallization conditions.

Table 4: Crystallization screens

Crystallization kits	Source
The $AmSO_4$ Suite The Compas Suite The Cryo Suite The Classic I–II Suite The Classic Lite Suite The JCSG+ Suite The JCSG I-IV Suite The PACT Suite The PEGs Suite The pH Suite The Pro-complex Suite The MPD Suite	Qiagen
Pre-crystallization Test Additive Screen Detergent Screen Grid Screen Ammonium Sulfate	Hampton Research Corp.

2.1.4 Oligonucleotides

Primers used for site-directed mutagenesis and PCR reactions were purchased from MWG and Inqaba Biotech (desalted and HPLC-purified).

Table 5: Oligonucleotides for PCR and site-directed mutagenesis. Point mutations are highlighted bold and underlined.

Primer	Length (bp)	Sequence
Rab1A C178S C179S	47	5' CAAGCAGTCAGGTGGAGGT**TCCTCC**CATCATCATCATCATCATTAAC 3'
Rab1A 5aaΔ	42	5' TTAAAATTCAGAGCACTGGTGGAGGTTCCTCCCATCATCATC 3'
Rab1A 10aaΔ	41	5' TGCTGAGAAGTCCAATGTTGGTGGAGGTTCCTCCCATCATC 3'
Rab1A 15aaΔ	35	5' AGCAACAGCTGGTGGTGCTGGTGGAGGTTCCTCCC 3'
Rab1A 18aaΔ	35	5' TCCCCGGAGCAACAGCTGGTGGAGGTTCCTCCCATC 3'
Rab1A 20aaΔ	38	5' AATGGGTCCCGGAGCAGGTGGAGGTTCCTCCCATCATC 3'
Rab1A 23aaΔ	42	5' CTGAGATTAAAAAGCGAATGGGTGGTGGAGGTTCCTCCCATC 3'
Rab1A His Stop	35	5' GATTAAAAAGCGAATGCCGTGAGGTTCCTCCC 3'
Rab1AK56AK58S	49	5' GAGTTAGACGGG**GC**AACAATCA**GT**CTTCAAATATGGGACACAGCAGGCC 3'
Rab1AK128S K129S	49	5' GGAACAAATGTGATCTGACCACA**GC**GA**GC**GTAGTAGACTACACAACAGC 3'

Rab1A E168A K170S K171A R172S	53	5' CATGACGATGGCAGCTG**C**GATTA**GTGC**G**A**G**A**ATGGGTGGTGGAGGTTCCTCCC 3'
Rab1A D16A	28	5' TTACTTCTGATTGGC**GCA**TCAGGGGTTG 3'
Rab1A E35A	33	5' GCAGATGATACATATACA**GCA**AGCTACATCAGC 3'
Rab1A Y37A	31	5' CATATACAGAAAGC**GCC**ATCAGCACAATTGG 3'
Rab1A I41A	30	5' GCTAACATCAGCACA**GCA**GGTGTGGATTTC 3'
Rab1A W62A	29	5' GCTTCAAATA**GCC**GACACAGCAGGCCAGG 3'
Rab1A R69A	30	5' GCAGGCCAGGAA**GCA**TTTCGAACAATCACC 3'
pETM30-SidM FW	46	5'CGTTTGGTGGTGGCGACCATCCTCTGGAAGTTCTGTTCCAGGGGCC 3'
pETM30-SidMRV	52	5' CTCAGTGGTGGTGGTGGTGGTGTTATTTTATCTTAATGGTTTGTCTTTCTTG 3'
SidM E337A E340A K343S K344A	53	5' CGTGTCACAAGGATTG**C**AAATCTGG**C**AAATGCCA**GCGC**GTTGTGGGACAACGC 3'
SidM (K454A K457S K459A)	54	5' GCGAGCAACCCCTGATCCAGATTTT**GC**GGTTGGGA**GC**TCT**GC**AATTTTAGTAGG 3'

2.1.5 Plasmids

Table 6: Plasmids

Plasmid	Size (Kb)	Selection	Tag	Position	Cleavage site	Source
pGEX-6P-1	4.9	Amp^R	GST	N-terminal	PreScission Protease	GE Healthcare
pETM-30	6.3	Kan^R	GST His_6	N-terminal C-terminal	TEV Protease	EMBL, Protein Expression Facility
pET-21	5.4	Amp^R	His_6	C-terminal		Novagen

2.1.6 Recombinant Plasmids

Recombinant plasmids used in this work are summarized in Table 7

Table 7: Recombinant plasmids

Plasmid	Features	Source
pGEX-6P-1_*sidM*317-545	684 bp *BamH*I/*Hind*III fragment of *sidM* (317-545) in pGEX-6P-1	MP Machner, NICHD, USA
pGEX-6P-1_*rab1A*1-210	630 bp *BamH*I/*Hind*III fragment of *rab1A* (1-210) in pGEX-6P-1	MP Machner, NICHD, USA
pGEX-6P-1_*rab1A*1-200	Site-directed mutagenesis of pGEX-6P-1_*rab1A*1-210	this work

pGEX-6P-1_*rab1A*1-195	Site-directed mutagenesis of pGEX-6P-1_*rab1A*1-210	this work
pGEX-6P-1_*rab1A*1-190	Site-directed mutagenesis of pGEX-6P-1_*rab1A*1-210	this work
pGEX-6P-1_*rab1A*1-187	Site-directed mutagenesis of pGEX-6P-1_*rab1A*1-210	this work
pGEX-6P-1_*rab1A*1-175	Site-directed mutagenesis of pGEX-6P-1_*rab1A*1-210	this work
pGEX-6P-1_*rab1A*K55A/K58S	Site-directed mutagenesis of pGEX-6P-1_*rab1A*1-210	this work
pGEX-6P-1_*rab1A*K168A/K172S	Site-directed mutagenesis of pGEX-6P-1_*rab1A*1-210	this work
pGEX-6P-1_*rab1A*D16A	Site-directed mutagenesis of pGEX-6P-1_*rab1A*1-175	this work
pGEX-6P-1_*rab1A*E35A	Site-directed mutagenesis of pGEX-6P-1_*rab1A*1-175	this work

2.1.7 Bacterial Strains

The following bacterial strains were used

Table 8: Bacterial strains

***E.coli* strains**	**Antibiotic Resistance**	**Source**
Rosetta 2 (DE3)	Chloramphenicol	Novagen
Top 10		Invitrogen
XL1 Blue super competent cells	Ampicillin	Stratagene
BL21	Ampicillin	Stratagene
BL21 (DE3) codon plus	Chloramphenicol	Stratagene

2.1.8 Other Chemicals

Table 9: Other chemicals

Chemical	Source
Complete-Protease Inhibitor Cocktail Tablets	Roche
Complete-EDTA free Protease Inhibitor Cocktail Tablets	Roche
Bug Buster Protein Extraction Reagent	Novagen

2.1.9 Antibiotics

Table 10: Stock solutions of antibiotics

Antibiotic	Final concentration
Ampicillin	100 µg/mL in H_2O
Chloramphenicol	34 µg/mL in ethanol
Kanamycin	30 µg/mL in H_2O

2.2 Media and Buffers

Media and buffers used in this study are summarized in **Table 11** and **Table 12**. All media were sterilized by autoclaving while heat-sensitive components were sterile filtered (0.2 µM filters). Antibiotics were added after media had been allowed to cool to below 50 °C.

Table 11: Media

Culture Media	Ingredients	Final concentration
Luria Bertani Medium (LB)	Bactotryptone	10 g/L
	Yeast extract	5 g/L
	NaCl	10 g/L
SOB-Medium	Bactotryptone	20 g/L
	Yeast extract	5 g/L
	NaCl	10 mM
	KCl	2.5 mM

SOC-Medium	Tryptone	20 g/L
	Yeast extract	5 g/L
	NaCl	10 mM
	KCl	2.5 mM
	MgCl2	10 mM
	Glucose	20 mM

Table 12: Solutions and buffers

Buffers/Solutions	**Composition**
Lysis buffer	1 x PBS (Phosphate Buffered Saline) pH 7.0, 2.5 mM $MgCl_2$, Complete EDTA-free Protease Inhibitor Cocktail Tablet, 5 mM β-mercaptoethanol and DNaseI (10 µg/mL)
PreScission protease cleavage buffer	10 mM Tris/HCl pH 7.0, 150 mM NaCl, 5 mM β-mercaptoethanol
Ni-NTA binding buffer	1 x PBS pH 7.0, 10 mM imidazole, 5 mM β-mercaptoethanol,
Ni-NTA elution buffer	1x PBS pH 7.0, 250 mM imidazole, 5 mM β-mercaptoethanol
TEV cleavage buffer	50 mM Tris/HCl pH 7.5, 150 mM NaCl, 20 mM EDTA, 5 mM β-mercaptoethanol
Anion exchange buffer A1 (Rab1A)	20 mM Tris/HCl pH 7.0, 10 mM NaCl, 5 mM β-mercaptoethanol
Anion exchange buffer B1 (Rab1A)	Buffer A1 (Rab1A) + 1 M NaCl
Cation exchange buffer A1 (SidM)	20 mM Tris/HCl pH 8.0, 10 mM NaCl, 5 mM β-mercaptoethanol
Cation exchange buffer B1(SidM)	Buffer A1 (SidM) + 1M NaCl
Anion exchange buffer A2 (Rab1A/SidM)	20 mM Tris/HCl pH 7.0, 10 mM NaCl, 5 mM β-mercaptoethanol
Anion exchange buffer B2 (Rab1A/SidM)	Buffer A1 (Rab1A/SidM) + 1M NaCl
Gel filtration buffer (Rab1A/SidM)	50 mM Tris/HCl pH 7.5, 150 mM NaCl, 5 mM β-mercaptoethanol
ITC buffer	50 mM HEPES pH 8.0, 50 mM NaCl
TAE buffer	40 mM Tris/HCl pH 7.5, 20 mM sodium acetate, 1 mM EDTA. Adjust pH to 8.2 with acetic acid
10 x DNA loading buffer	70 % (w/v) sucrose, 0.25 % (w/v) bromphenol blue, 0.1 M EDTA
SDS-PAGE lower buffer (4 x)	1.5 M Tris/HCl pH 8.8
SDS-PAGE upper buffer (4 x)	0.5 M Tris/HCl pH 6.8, 0.4 % (w/v) SDS
SDS-PAGE running buffer	25 mM Tris/HCl, 192 mM glycine, 0.1 % (w/v) SDS
SDS-PAGE sample buffer (8 x)	16 mL 10 % SDS, 4 mL glycerol, 2.2 mL Tris/HCl, pH 6.8, 800 µL β-mercaptoethanol,

	1 spatula tip bromophenol blue
SDS-PAGE separating gel (15 %)	15 mL acrylamide/bisacrylamide 30 % (w/v)/ 0.8 % (w/v), 7.6 mL 1.5 M Tris/HCl, pH 6.8, 300 µL 10 % (w/v) SDS, 10 mL ddH_2O, 40 µL TEMED, 100 µL 25 % (w/v) APS
SDS-PAGE stacking gel (5 %)	1.5 mL acrylamide/bisacrylamide 30 % (w/v)/0.8 % (w/v), 2.5 mL 0.5 M Tris/HCl, pH 6.8, 5.9 mL ddH_2O, 15 µL TEMED, 25 µL 25 % (w/v) APS
SDS-PAGE Staining solution	0.25 % (w/v) Coomassie Brilliant Blue R-250, 30 % (v/v) ethanol, 10 % (v/v) acetic acid
SDS-PAGE destaining solution	40 % (v/v) ethanol, 10 % (v/v) acetic acid

2.3 Microbiology

2.3.1 Preparation of Agar Plates

Agar plates were used to culture bacteria on solid medium. Agar plates were prepared following standard procedure: 15 g agar was added to 1 L LB-medium. The solution was sterilized by autoclaving and allowed to cool to ~55 °C. Required antibiotics were added and 25 mL of agar was poured into each Petri dish). Bacteria were plated on LB agar plates with respective antibiotics on a sterile clean bench with sterile beads or spreading inoculation loops.

2.3.2 Liquid culture

Bacteria were grown in liquid medium using Erlenmeyer flasks for proper aeration and agitation. The flasks containing inoculated liquid medium with appropriate antibiotics were incubated at 37 °C with a rotation speed of 160-180 rpm overnight. Liquid bacterial cultures were made for precultures, protein production, preparation of DNA and glycerol stocks.

2.3.3 Preparation of Glycerol Stocks

Glycerol stocks were prepared for long-term storage of the bacterial cells containing plasmid of interest. 5 mL LB-medium was inoculated with bacteria harboring a plasmid of

interest. Appropriate antibiotics were added and incubated overnight at 37 °C and a rotation speed of 160-180 rpm. 900µL of this culture was mixed with 100 µL of sterile 80 % glycerol (cryoprotectant) in a 1 mL cryo-vial and then stored at -80 °C.

2.4 Molecular Biology

2.4.1 Transformation of Competent Bacteria

Competent bacterial cells were transformed with plasmid DNA for plasmid amplification and recombinant gene expression. Positive clones were selected by plating the transformation mixture on LB agar plates containing antibiotics corresponding to plasmid resistance genes.

Heat shock transformation

Plasmid DNA (1-2 µL) obtained from ligation reactions was added to 50 µL of competent cells that were thawed on ice. The cells were incubated on ice for 30 minutes and treated with heat shock for 45 s at 42 °C, followed by fast cooling on ice for 2 min. 800 µL of SOC or LB medium were added to the cells and shaken at 37 °C for 1 h on a thermo-mixer. The transformation mixture was plated on LB agar plates containing appropriate antibiotics and incubated at 37 °C overnight.

Electroporation

Plasmid DNA (1-2 µL) was transferred in to a pre-cooled electroporation cuvette, followed by the addition of 50 µL competent cells (thawed on ice). The cuvette was dried and an electric pulse of 2.5 kV, 200 Ω and 125 µF was applied to the cells using Gene Pulser electroporation equipment (Bio-Rad). 800 µL of SOC or LB-medium was added immediately to the cells and incubated at 37 °C for 1h on a thermo-mixer. The transformation mixture was plated on LB agar plates using appropriate antibiotics.

2.4.2 Extraction of Plasmid DNA

Freshly transformed *E. coli* XL1 blue cells were transferred to 5 mL of LB medium with appropriate antibiotics and allowed to grow at 37 °C in a shaking incubator overnight. Plasmid DNA was isolated using QIAGEN mini prep kit. Purification of the plasmid DNA was performed according to the manufacturer's instructions. The yield of DNA was measured by detecting the absorption at 260 nm (A_{260}) using a Nanodrop ND-1000 spectrophotometer (peqLab, Erlangen, Germany)

2.4.3 Agarose gel electrophoresis

Agarose gel electrophoresis is a common method for analyzing DNA samples. In this method, DNA migrates through the agarose matrix when an electric current is applied. Phosphate groups on the DNA impart a negative charge to the molecule and migrate towards a positively charged pole. 1 % agarose gel was prepared by dissolving 0.5 g of agarose in 50 mL of TAE buffer, brought to boil in a microwave for 1min. The agarose solution was allowed to cool down to ~60 °C and SYBR Green was added to visualize the DNA samples. DNA samples were mixed with 10 % loading buffer (10 x) and loaded into the sample wells. Gels were run at 5 V/cm for 60 min and later visualized under a UV illuminator.

2.4.4 Site-directed mutagenesis

Site-directed mutagenesis is a technique to replace, delete or insert a number of nucleotides into a target DNA by PCR using appropriately designed primers. Mutagenesis reactions were performed using the Quick Change Kit (QIAGEN). The reaction products were treated with DpnI restriction enzyme for 1 h at 37 °C to digest the methylated template DNA. The DpnI digested products were transformed into XL1 blue competent cells. The transformation mixture was plated on LB agar plates with appropriate antibiotics. Positive clones were analyzed by DNA sequencing. Given below are the parameters for PCR

Table 13: Reaction mixture

Reaction components	Volume (µL)	Concentration
10x PFU Ultra II buffer	10.0	1 x
Template DNA	1.0	50 ng
Mutagenesis forward primer	1.25	10 pmol/µL
Mutagenesis reverse primer	1.25	10 pmol/µL
dNTP'smix	1.0	10 µM
Pfu Ultra HS II DNA-polymerase (Stratagene)	1.0	1 U
Total volume	50.00	

Table 14: Mutagenesis reaction programme

Step1	Initial denaturation	95 °C	1 min
Step2	Denaturation	95 °C	50 s
Step3	Annealing	55°C	50 s
Step4	Elongation	68 °C	7 min

Step5	Final elongation	68 °C	9 min
Repeat steps 2-4 18 times			

2.4.5 Restriction free cloning

Restriction free (RF) cloning is a simple method compared to conventional cloning whereby a gene of interest can be inserted at any desired location into a vector, independent of restriction sites, ligation or any modifications in both vector and gene. In this work, the gene *sidM* was cloned into pETM-30 vector using this method. A set of primers 50 bases in length were designed harboring complementary sequences to both *sidM* and to the vector. The forward primer had an overlap of 24 bases with the vector sequence complementary to the 5'-end of the target site of insertion, followed by a start codon and 20-25 bases of the 5'-end of *sidM*. The reverse primer of 24 bases was complementary to the 3' end of the vector at the target site of insertion (Fusinita et al., 2006). The reaction mixture containing the template, primers, dNTP's, polymerase and buffer was amplified by PCR and the resultant products were analyzed by agarose gel electrophoresis. The double-stranded, blunt-ended PCR product was used as a set of primers for a second PCR to insert the amplified gene into the desired vector. The final product was digested with DpnI for 1 h at 37 °C and transformed into XL1 blue cells. Positive clones were analyzed by DNA sequencing.

2.4.6 Co-expression

The vectors pGEX-6P-1_Rab1A$_{1-210}$ and pETM30_SidM$_{317-545}$ were co-transformed into *E. coli* BL21-CodonPlus cells (Stratagene) for co-expression of the two respective genes. The transformation mixture was plated on LB-agar plates containing ampicillin, kanamycin and chloramophenicol. Positive clones were confirmed by protein expression test.

2.5 Protein Production and Purification

2.5.1 Expression Test

To optimize the expression of a target recombinant gene (Table 8), various parameters such as temperature, isopropyl-β-D-1-thiogalacto pyranoside (IPTG) concentration and induction time were tested. The recombinant plasmids harboring a gene of interest (Table 8) were transformed into *E. coli* BL21 and/or Rosetta 2 expression cells. In each case, a single colony was picked from the LB agar plate and transferred to 5 mL of LB-medium

with appropriate antibiotics and grown overnight at 37 °C in a shaking incubator. The overnight pre-culture cells were transferred into 50 mL of LB-medium with appropriate antibiotics and incubated at 37 °C, 180 rpm until cell density reached an OD_{600} value of 0.5-0.8. Expression of the target genes was induced with 0.1 mM IPTG. Samples were taken before induction and every 2 h after induction i.e. at 2, 4, 6 h and overnight. Samples were then centrifuged for 1 min at 13000 rpm. The bacterial pellet containing total cell extract was resuspended in 100 µL Bug-Buster reagent and incubated at room temperature for 20 min, followed by centrifugation for 20 min at 13000 rpm. The supernatant containing all soluble proteins was collected for the analysis of the target recombinant protein production. The pellet was resuspended in an equal volume of 8 M urea. Samples of the soluble and insoluble fractions were analyzed by SDS-PAGE.

2.5.2 Recombinant Protein Production

In this work pGEX-6P-1_$SidM_{317-545}$, pGEX-6P-1_$Rab1A_{1-210}$ and pGEX-6P-1_Rab1A plasmid constructs were expressed in *E. coli*. BL21, BL21-CodonPlus and Rosetta 2. Cells harboring the respective recombinant plasmids were thawed from glycerol stocks and grown in 50 mL LB-medium containing appropriate antibiotics at 37 °C and 180 rpm overnight. The resulting 0.1 OD_{600} pre-culture was transferred to 2 L of LB-medium with appropriate antibiotics. The cells were permitted to grow at 37 °C and 180 rpm until they reached an OD_{600} of 0.5-0.8. The expression of the gene of interest was induced by 0.1 mM IPTG and the cultures were incubated at 18, 25, 37 °C, 180 rpm respectively. After overnight incubation, cells were harvested by centrifugation: 15 min, 4 °C, 6000 rpm. The supernatant was discarded and the cell pellet resuspended in 15 mL lysis buffer per 1 L culture at 4 °C. The cell suspension was passed through a homogenizer (Constant systems 20 kPa, 4 °C, 2-3 runs for efficient cell lysis. After cell lysis DNase I was added to degrade DNA and reduce sample viscosity. The lysate was centrifuged for 1 h at 4 °C and 16000 rpm to separate the soluble protein fraction from cell debris and inclusion bodies. Soluble and insoluble fraction samples were collected to analyze the target protein production by SDS-PAGE.

2.5.3 Purification of Rab1A and $SidM_{317-545}$

Affinity chromatography

Affinity chromatography is based on the principle of strong and specific binding of affinity tag fused to the N- or C-terminus of the target protein to an immobilized matrix. In this work, the central domain of $SidM_{317-545}$ was produced as a fusion protein with an N-terminal glutathione S-transferase (GST) tag whereas $Rab1A_{1-210}$ and variants were produced with an N-terminal GST and a C-terminal His_6-tag.

Glutathione/Glutathione-S-Transferase Affinity Chromatography

This method is based on the high affinity of GST for its substrate glutathione. GST is used as an affinity tag fused to a target protein. In this work, both SidM and Rab1A were purified by producing N-terminal GST fusion proteins. After cell lysis, the soluble fraction was added to the PBS pre-equilibrated glutathione sepharose (GS) beads and incubated at 4 °C for 1 h with agitation to allow the target protein to bind. The flow through was collected to check for possible unbound fusion protein. Loaded GS beads were washed 4 times (50 mL) with PBS buffer to remove unbound and non-specifically bound proteins and further washed 3 times (30 mL) with PreScission Protease Cleavage Buffer. The GST-SidM and -Rab1A fusion proteins were proteolytically cleaved by adding PreScission protease and incubating the GS at 4 °C overnight. SidM and Rab1A proteins were eluted from the GS beads using 60 mL PreScission Protease Cleavage Buffer.

Ni-NTA affinity chromatography

Ni-NTA agarose beads are used for the purification of recombinant proteins with so-called His_6-tags. Histidine residues of the His_6-tag bind to the immobilized nickel ions with high specificity and affinity. In this study, $Rab1A_{1-210}$ and variants thereof were produced as fusion proteins bearing a C-terminal His_6-tag. Elution fractions of Rab1A from glutathione affinity chromatography purification were pooled and coupled to the pre-equilibrated (PBS buffer) Ni-NTA agarose beads at 4 °C for 1 h. The flow-through was collected to check for the presence of unbound fusion protein followed by extensive washing of beads with PBS. The beads harboring the His_6-tagged target protein were further washed with10 column volumes (CV) wash buffer containing 10 mM imidazole (Table 12) to remove impurities. The pure His_6-tag protein was eluted with 5 CV of elution buffer containing 250 mM imidazole. The efficiency of protein fusion binding, yield of fusion protein and purity were analyzed by SDS PAGE.

Ion exchange chromatography

Ion exchange chromatography separates protein samples based on their electrostatic properties. In cation exchange chromatography, positively charged protein molecules bind to a negatively charged resin and *vice versa* in anion ion exchange chromatography. Before applying the sample, the column was washed with buffer containing a high NaCl concentration to displace all other charged species. Washing with a low ionic strength buffer then removes all unbound Na^+ and Cl^- ions. After binding and washing, the bound proteins were eluted using a linear NaCl gradient. The binding of the protein to the resin depends on the pH of the solvent.

In this work, $Rab1A_{1-210}$ and $Rab1A_{1-210}/SidM_{317-545}$ complex were purified by anion exchange chromatography (MonoQ HR 10/100 GL, GE Healthcare) and $SidM_{317-545}$ by cation exchange chromatography (MonoS HR 10/100GL, GE Healthcare). The peak fractions were collected and analyzed on the SDS-PAGE for the target protein.

Size exclusion chromatography

Size exclusion chromatography (SEC) is also referred to as gel permeation chromatography or gel filtration. It separates proteins based on their molecular size (hydrodynamic volume). Proteins larger than the pores size of the resin material unable to enter the porous particles will pass through the space in between the beads and will elute first. Smaller molecules will be retained in the porous particles and elute at slower rate. In this work, affinity purified $Rab1A_{1-210}$ and $SidM_{317-545}$ were mixed and subjected to SEC. The peak fractions were collected and analyzed on the SDS-PAGE to analyze the formation of $Rab1A_{1-210}$ /$SidM_{317-545}$ complex. All the SEC experiments were conducted on ÄKTA purifiers with HiLoad Superdex 75 and 200 10/30, 16/60 and 26/60 columns.

2.6 Protein Analytical Methods

2.6.1 Concentration of Proteins

Protein samples were concentrated for SEC, Isothermal Titration Calorimetry (ITC) and crystallization experiments by ultracentrifugation using Vivaspin 2, 6 and 20 concentrators with desired molecular weight cut-offs. The molecular weight cut-off of the concentrators was selected at least 10 kDa smaller than the protein. The concentration of purified proteins were measured by measuring the absorption at 280 nm (A_{280}) using a Nanodrop ND-1000 spectrophotometer (peqLab, Erlangen, Germany)

2.6.2 SDS-Polyacrylamide Gel Electrophoresis (SDS-PAGE)

Protein samples were analyzed by sodium dodecyl sulfate (SDS) polyacrylamide gel electrophoresis (PAGE). This technique separates proteins based on their molecular weight. SDS is a strong anionic detergent that binds non-covalently to proteins disrupting their native structure. SDS treated proteins are negatively charged and migrates towards a positively charged anode in an electric field. Protein samples were mixed with 8x sample buffer (10 µL protein +2 µL sample buffer). Samples were heated at 95 °C for 5 min to denature the protein. The protein samples were loaded onto the gel and run at constant 40 mA for 30-35 min. The gel was stained for 15-20 min in a Coomassie Brilliant Blue R-250 solution and excess stain was removed by destaining solution.

2.6.3 Surface Plasmon Resonance (SPR) Spectroscopy

Surface Plasmon Resonance (SPR) is a biosensing technique to measure biomolecular interactions in a label free environment. One of the interactants (ligand) is immobilized onto the metal film (Gold layer), whereas the second (analyte) is passed over the surface in a continuous flowing aqueous solution. Plane polarized light is reflected off the opposite side of the metal film. At a certain angle the light excites the electrons in the gold layer generating a surface plasmon and resulting in a loss of reflection. Binding of analyte to the immobilized ligand increases the refractive index and hence the angle at which absorption of energy occurs. This change in angle is relayed in response units (RUs) and is directly proportional to the amount of analyte bound to the ligand. In this work, binding studies between Rab1A (ligand) and SidM (analyte) were carried out using a Biacore X instrument. Different dilutions of $Rab1A_{1-210}$ were passed over the surface of a Ni-NTA sensor chip (20 µL/min flow rate, 25 °C) to immobilize the ligand via its C-terminal His_6-tag until sufficient ligand had bound (corresponding to 200? RU). Thereafter, 1-5 µM solutions of $SidM_{317-545}$ were passed over the immobilized $Rab1A_{1-210}$ to allow for binding analysis.

2.6.4 Isothermal Titration Calorimetry (ITC)

Isothermal Titration Calorimetry (ITC) was also employed to analyze the binding affinity between $Rab1A_{1-210}$ and $SidM_{317-545}$. In this work, ITC experiments were performed using an ITC200 Titration Calorimetry System (Microcal, GE Health care). Prior to the

experiment, both protein samples were subjected to buffer exchange (50 mM HEPES pH8.0, 50 mM NaCl) using SEC and concentrated by ultracentrifugation using Vivaspin-concentrators. All buffers and protein samples were filtered and degassed to avoid air bubbles during the experiment. Cells and the syringe of the ITC200 were extensively washed with buffer (50 mM HEPES pH 8.0, 50 mM NaCl). 40 µL of the $Rab1A_{1-210}$ solution (1000 µM) was filled into the syringe and titrated against 300 µL of the $SidM_{317-545}$ solution (100 µM) present in the sample cell. All titrations were performed at 25 °C, 500 rpm (syringe rotation). 2 µL were injected per cycle with a total of 18 cycles and 4 s duration between injections. Data were analyzed by Microcal Origin7 software. The peaks obtained after each injection were integrated to calculate the amount of heat absorbed or evolved upon complex formation. The binding affinity constant 'K', the stoichiometry 'n' and the binding enthalpy 'ΔH' were derived by curve fitting using the single set of independent sites model.

2.7 Crystallization

As part of this project both $SidM_{317-545}$ alone and the complex between $SidM_{317-545}$ and $Rab1A_{1-175}$ were crystallized. Methods used were sitting-drop and hanging drop vapor diffusion. Preliminary crystallization trials were carried out using a range of commercial screens (Hampton Research and QIAGEN) in Low Profile Greiner 96 well plates by sitting drop vapor diffusion setup. The reservoir consisted of 80 µL of the screening solution. Crystallization drops were prepared by mixing 200 nL of protein and 200 nL of reservoir solution by Mosquito robot (TTP Labtech Ltd). The crystallization plates were sealed with crystal clear tape and stored at 4 °C, 10 °C and/or 16 °C.

Once suitable starting conditions had been identified, protein crystals were optimized in 24-well plate formats by hanging drop experiments. The reservoir was filled with 500-1000 µL of reservoir solution and the crystallization drops prepared by mixing 1-2 µL of protein solution with 1-2 µL of reservoir solution. The crystallization drop was pipetted onto a siliconised cover slip and inverted over the reservoir with drop facing downwards. Silicone grease was applied to the raised rim of the reservoir to seal each experiment. Parameters that were optimized to improve crystal quality include the protein concentration, precipitant and salt concentrations, the pH of the buffer produce well diffracting crystals.

2.8 X-ray Data Collection

Protein crystals were individually harvested from their mother liquor using a nylon loop, transferred to a suitable cryoprotectant derived from the mother liquor and flash cooled in liquid nitrogen. X-ray diffraction data were collected on a home source comprising a rotating copper anode generator and using a Saturn 944HG charged coupled device (CCD) detector (Rigaku) as well as at the beam line Proxima1-Soleil.

2.9 Data Processing and Structure Solution

X-ray diffraction data of $SidM_{317-545}$ crystals were processed with XDS and scaled with XSCALE (Kabsch 1993), those for $Rab1A_{1-175}/SidM_{317-545}$ complex HKL-Suite 3000 (Otwinowski and Minor 1997). Further processing of data was carried out using the CCP4 Suite (Collaborative Computational Project 4, 1994). Intensities were converted to structure factor amplitudes using TRUNCATE from CCP4 package. The structure of the $Rab1A_{1-175}/SidM_{317-545}$ complex was solved by molecular replacement using the structure of the complex $DrrA_{340-533}/Rab1b_{3-174}$ as a search model in Phaser (Storoni, McCoy et al. 2004). The model from Phaser was refined using restrained refinement in REFMAC5 (Murshudov, Vagin et al. 1997). The model was adjusted manually using COOT (Emsley and Cowtan 2004). The final structure was validated using Molprobity. Protein figures were prepared using PYMOL (http://pymol.sourceforge.net/).

3 Results

In this study, full-length and six C-terminally truncated variants of human Rab1A GTPase as well as the central domain of SidM (residues 317-545), a type IVB effector protein from *Legionella pneumophila*, were studied. The genes of interest were cloned into the expression vector pGEX-6P1 and proteins were produced in *E. coli* and purified by affinity, ion exchange and size exclusion chromatography. The crystal structure of $Rab1A_{1-175}/SidM_{317-545}$ complex was solved by X-ray crystallography and refined to 2.05 Å resolution.

3.1 Human Rab1A, a small GTpase

cDNA for Human Rab1A was provided by Dr. Matthias P. Machner (National Institute of Child Health and Human Development [NICHD], Washington DC, USA. This was transferred to the expression vector pGEX-6P1 (GE Healthcare) coding for an N-terminal GST tag by Ms. Christin Holland (HZI, Braunschweig, Germany) for expression in *E. coli*. As part of this thesis, a C-terminal His_6-tag was added to Rab1A by site-directed mutagenesis (section 2.4.4) to allow purification of C-terminally intact protein by Ni-NTA affinity chromatography.

3.1.1 Production and purification of recombinant Rab1A

For simplicity, the GST and His_6-tagged full-length Rab1A will hereafter be referred to as Rab1A. Rab1A was produced in Rosetta 2 *E. coli* cells overnight at 20 °C following induction with 0.1 mM IPTG. Cells were pelleted, lysed by homogenizer and centrifuged to separate soluble and insoluble fractions. The soluble fraction was applied to glutathione agarose resin and unbound proteins were removed by washing the resin with PBS buffer. The GST fusion tag was cleaved off by adding PreScission protease at 4 °C and incubating overnight. The GST free Rab1A was eluted using PreScission protease cleavage buffer, while GST remained on the column. The yield and purity of the protein were qualitatively analyzed by SDS-PAGE (Fig 3.1). After GST affinity purification, Rab1A was observed to degrade rapidly. This was visualized by SDS-PAGE (Fig 3.1), where Rab1A runs at 23 kDa and degraded product is around 20 kDa. Degradation of Rab1A was assumed to be caused by secreted bacterial host proteases. Prior to purification “Complete” protease inhibitor cocktail tablets, EDTA-free (Roche) were added to all the buffers to avoid degradation. This, however, did not improve the stability of Rab1A.

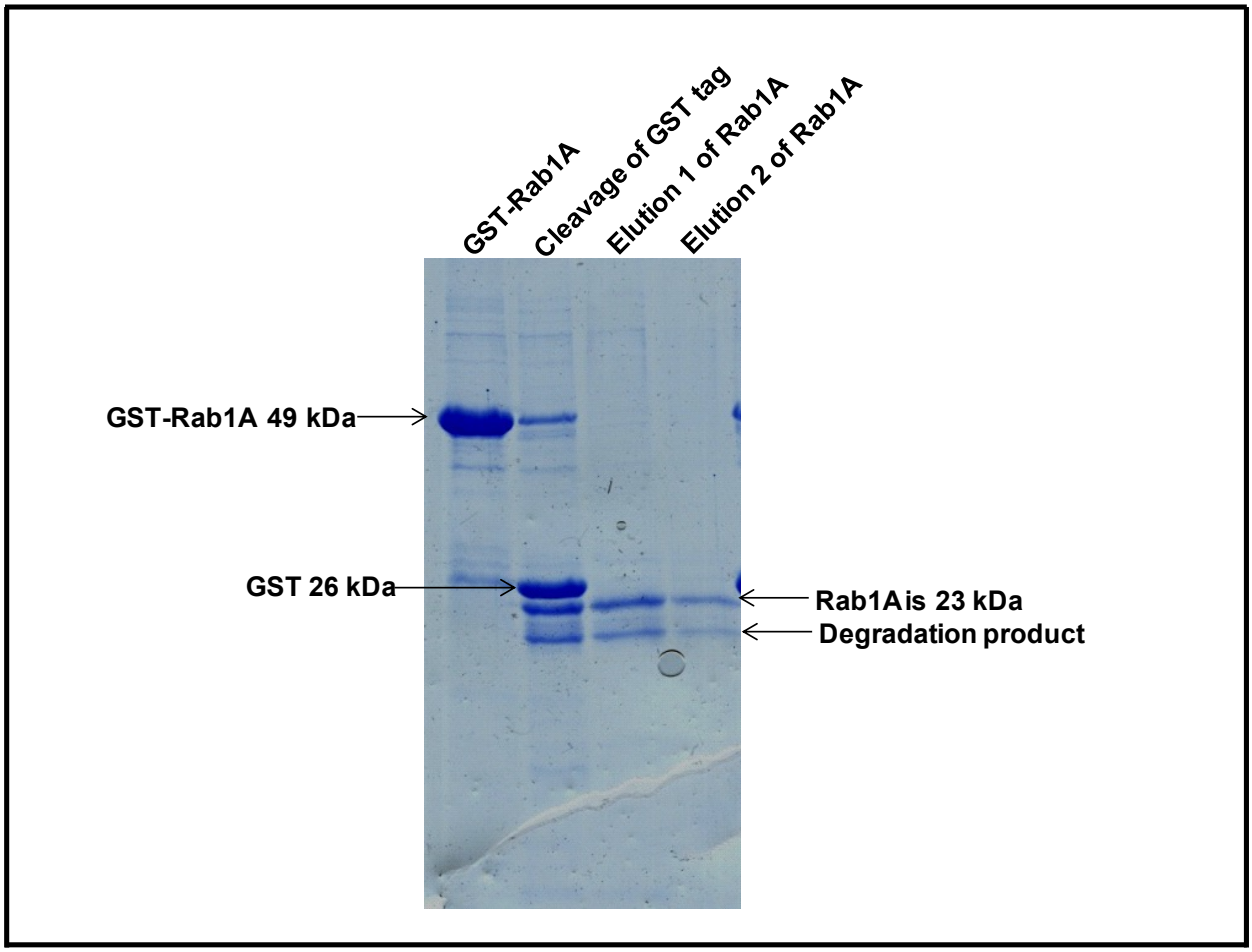

Figure 3.1: Purification of Rab1A by Glutathione affinity chromatography. Coomassie stained SDS-PAGE analysis of GST-Rab1A purification. Lanes from left to right, 1-GST fusion Rab1A, 2-Overnight proteolytic cleavage of GST fusion Rab1Awith PreScission protease, 3 and 4- Elution fractions of Rab1A (Upper band), degradation product of Rab1A (Lower band)

3.1.2 C-terminal deletions of Rab1A

To stabilize Rab1A, 5, 15, 18, 23 and 35 amino acid residues were C-terminally deleted by site-directed mutagenesis using primers designed to retain the His_6-tag - except in the case of $Rab1A_{1-175}$ (Fig 3.2). The resulting Rab1A variants were all produced and purified as for full-length Rab1A. Variants $Rab1A_{1-205,}$ $Rab1A_{1-195}$ and $Rab1A_{1-187}$ similarly prone to degradation as the full-length protein (Fig 3.3).

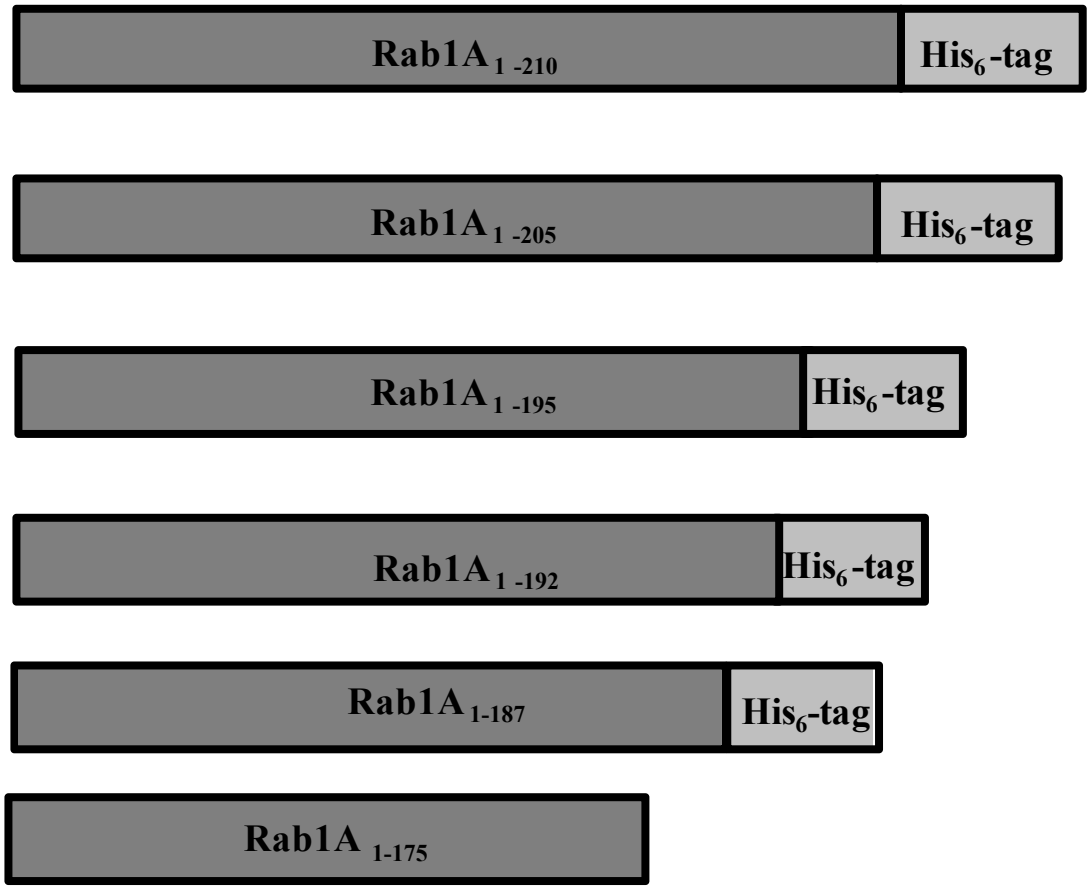

Figure 3.2: C-terminal deletions of Rab1A. Rab1A was C-terminally truncated by site-directed mutagenesis. The C-terminal His_6-tag was retained for all variants except $Rab1A_{1-175}$.

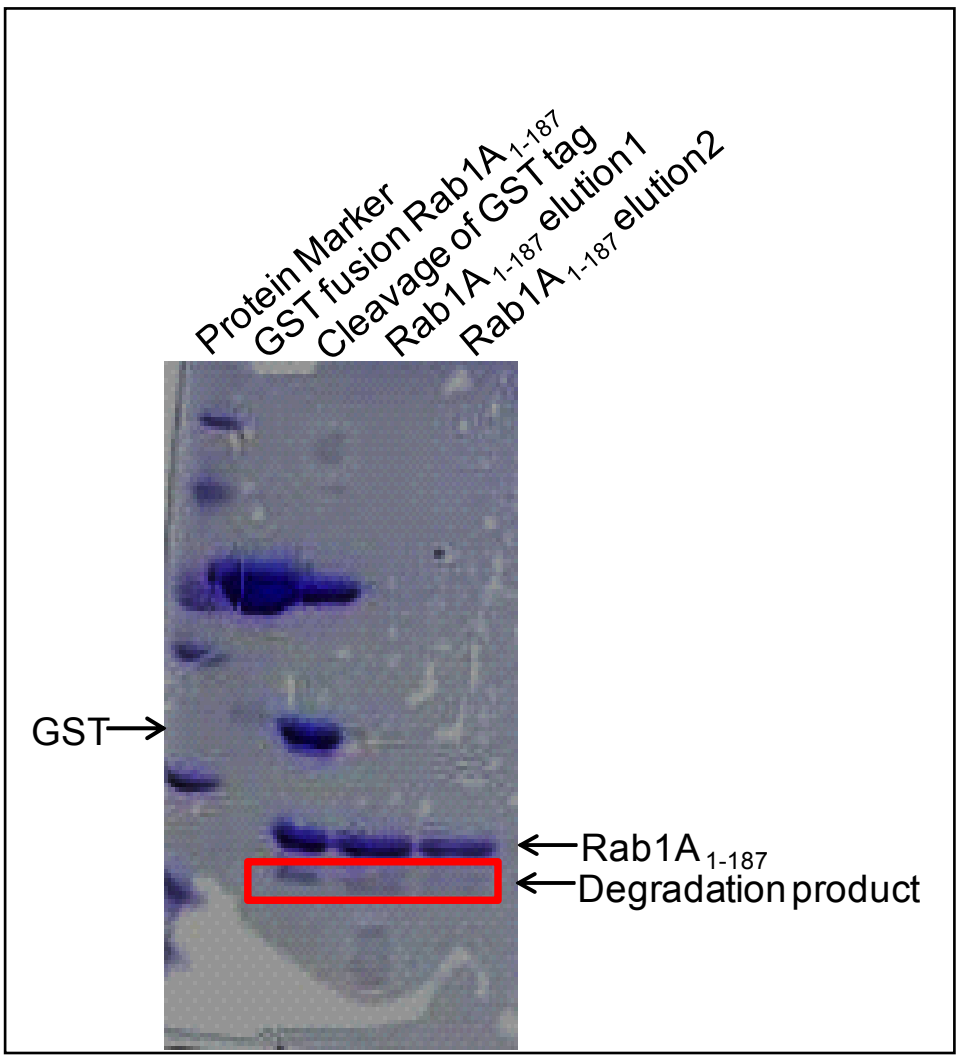

Figure 3.3: Coomassie stained SDS gel showing the instability of Rab1A$_{1-187}$ variant. Lanes from left to right, 1. Protein Marker, 2. GST Rab1A$_{1-187}$ fusion protein, 3. Overnight cleavage of GST fusion Rab1A$_{1-187}$ with PreScission protease, 4. and 5. Elution fractions of Rab1A$_{1-187}$. Degradation of variant Rab1A$_{1-187}$ is indicated by a red rectangular box.

3.1.3 Production and purification of stable Rab1A$_{1-175}$

As outlined above, a range of C-terminal deletions of Rab1A still resulted in unstable protein. Hence, Rab1A was further C-terminally deleted by adding a stop codon prior to residue 35 by site-directed mutagenesis losing the His$_6$-tag in the process. Purification of Rab1A$_{1-175}$ was as described for full-length Rab1A. Rab1A$_{1-175}$ did not show any signs of degradation after GST affinity purification (Fig 3.4A). Rab1A$_{1-175}$ eluted as a single peak during size exclusion chromatography (SEC) using a Superdex 75 16/60 SEC column with an elution volume of 77 mL (Fig 3.4B). Relative to standards the elution volume of Rab1A$_{1-175}$ corresponds to a molecular weight of 20 kDa confirming Rab1A to be monomeric.

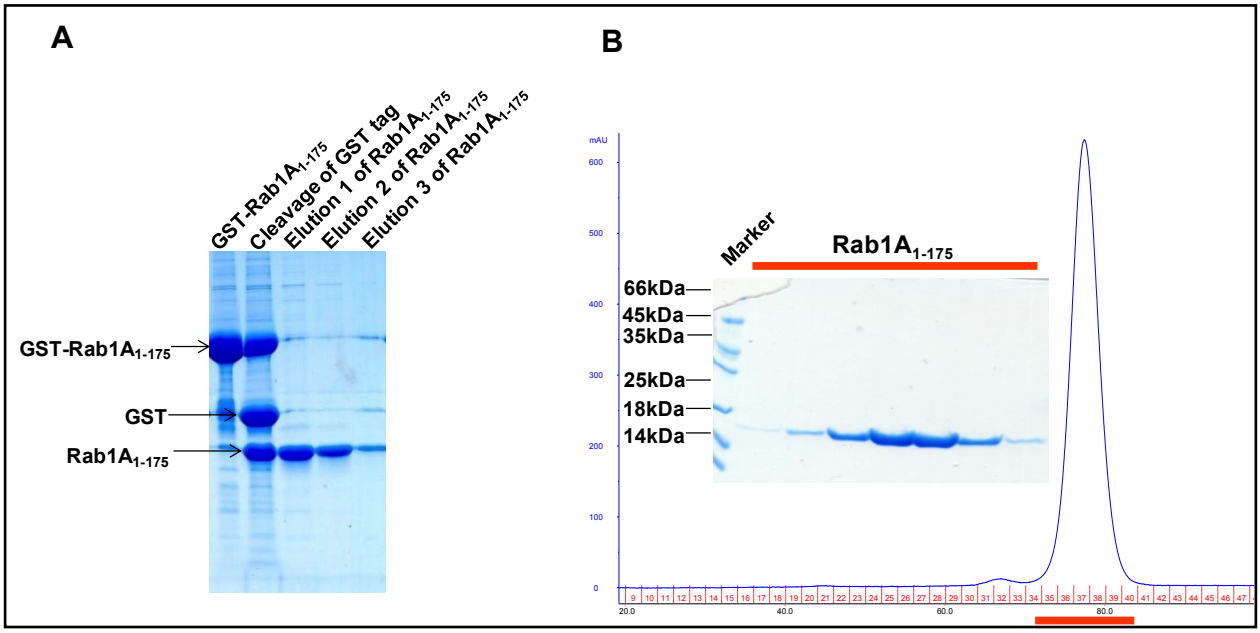

Figure 3.4 Purification profile of Rab1A$_{1-175}$ (A) Coomassie stained SDS-PAGE analysis of glutathione affinity purified Rab1A$_{1-175}$. Lanes from left to right, 1. GST-Rab1A$_{1-175}$ fusion protein; 2. Overnight proteolytic cleavage of the fusion protein with PreScision protease; 3, 4. and 5. In consecutive elution fractions Rab1A$_{1-175}$ appears as a single band. (B) SEC elution profile and corresponding SDS gel of Rab1A$_{1-175}$. Fractions highlighted by red bar on the SDS gel show pure and stable Rab1A$_{1-175}$.

3.2 Type IVB effector protein SidM of *Legionella pneumophila*

3.2.1 Production and Purification of SidM$_{317-545}$

To analyze the interaction of human Rab1A with SidM from *L. pneumophila*, the central domain corresponding to residues 317-545 of SidM was cloned into vector pGEX-6P1. A GST-SidM$_{317-545}$ fusion protein was hence produced in BL21 *E. coli* cells overnight at 37 ºC induced with 0.1 mM IPTG. Cells were harvested, lysed by homogenizer and centrifuged to separate soluble and insoluble fractions. The soluble fraction was applied to glutathione agarose resin, unbound proteins washed off and GST-fusion protein cleaved on column with PreScission protease overnight at 4 ºC. SDS-PAGE analysis of SidM$_{317-545}$ indicated a stable, undegraded protein (Fig 3.5). SidM$_{317-545}$ was further purified by size exclusion chromatography on a Superdex 75 16/60 column. See Figure 6 for the elution profile and SDS-PAGE analysis. The first two peaks, marked by red and green bars, contain SidM$_{317-545}$ co-eluting with impurities while the third peak (blue bar) contains pure SidM$_{317-545}$ with an elution volume of 72 mL. Compared to protein standards this volume indicates molecular weight of 27 kDa for SidM$_{317-545}$, which matches its size on SDS-PAGE gel (Fig 3.6). SidM$_{317-545}$ was concentrated by ultrafiltration to 13 mg/mL for crystallization trials.

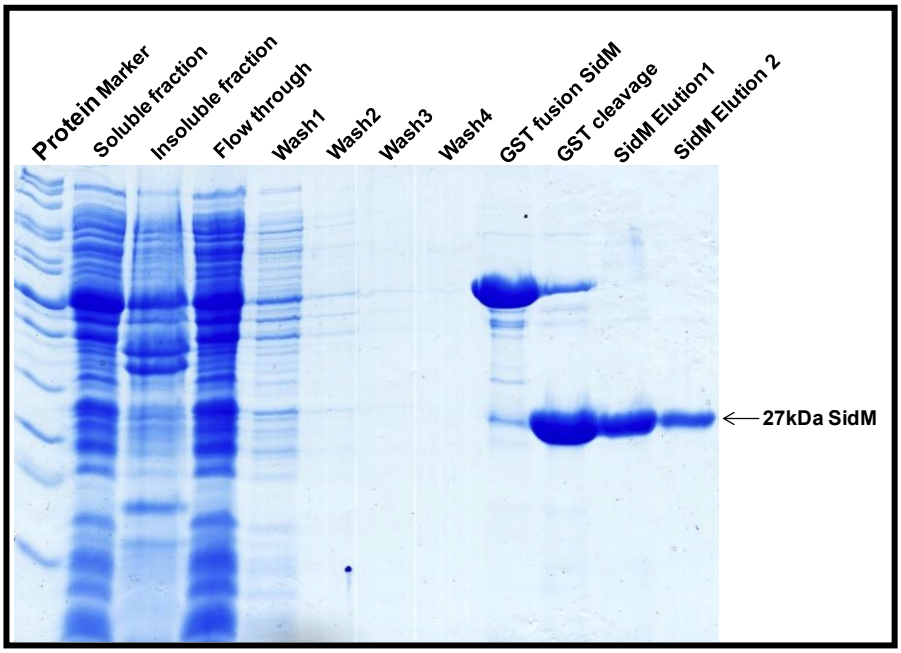

Figure 3.5: Production and purification of SidM$_{317-545.}$ Coomassie stained SDS-PAGE profile of affinity purification of GST-SidM$_{317-545}$ affinity purification. Lanes from left to right, 1. Protein Marker, 2. Soluble fraction, 3. Insoluble fraction, 4. Flow through, 5 to 8 elution of unspecifically bound proteins with 1xPBS, 9. GST fusion SidM, 10. Cleavage of GST–fusion protein with PreScission protease, 11 and 12. Elution of SidM

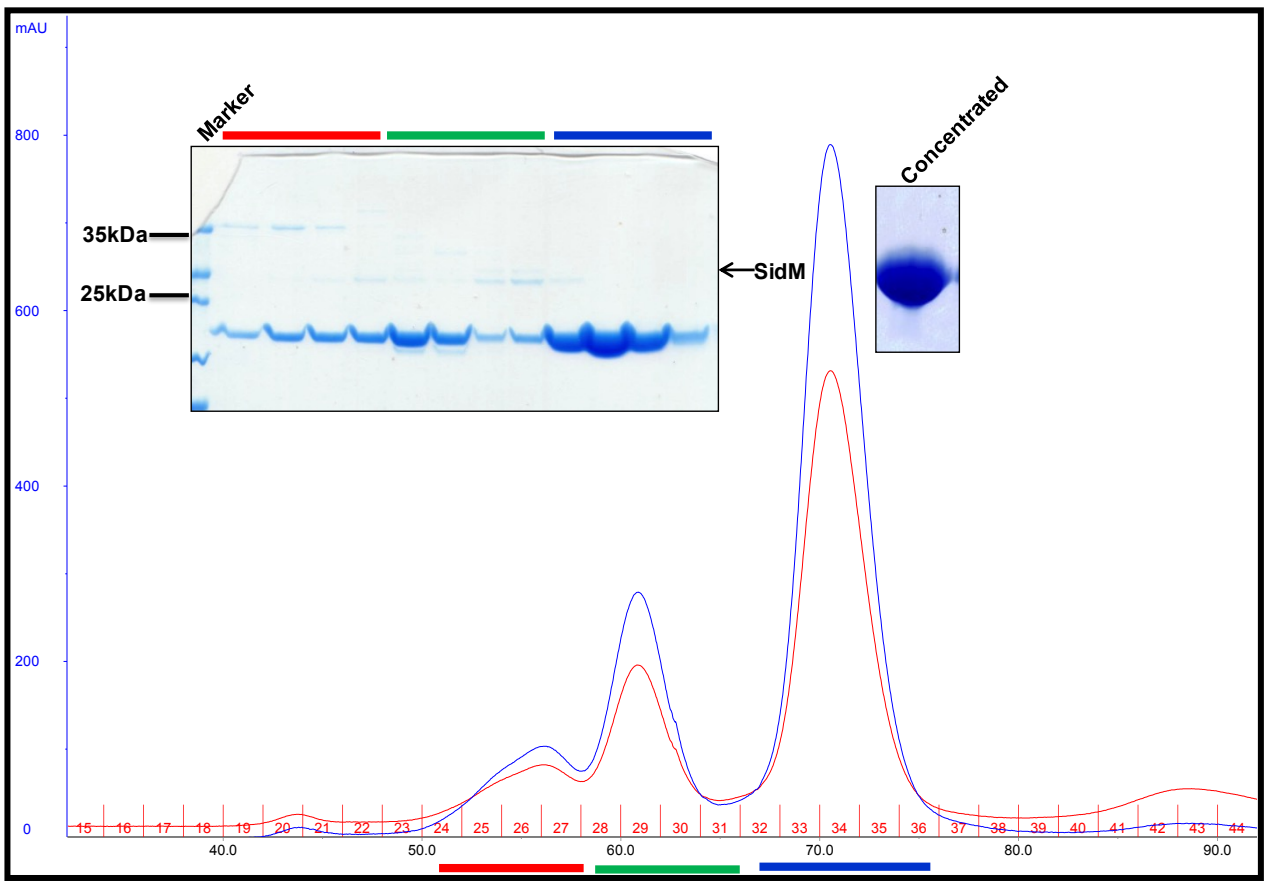

Figure 3.6: Size exclusion chromatography of SidM$_{317-545.}$ Coomassie stained SDS-PAGE gel and chromatogram of

size exclusion chromatography of $SidM_{317-545}$ using a Superdex 75 16/60 column. Peaks one and two, marked by red and green bars contain $SidM_{317-545}$ with other impurities whereas peak 3 indicated by blue bar (elution volume of 72 mL) contains pure $SidM_{317-545}$. Fractions containing pure $SidM_{317-545}$ were pooled and concentrated by Vivaspin. The corresponding SDS-PAGE gel is featured as the right-hand insert.

3.2.3 Crystallization of $SidM_{317-545}$

After final purification of $SidM_{317-545}$ by SEC, the protein was concentrated by ultrafiltration to 15 mg/mL for crystallization. Initial screening for crystallization lead conditions was performed in 96 well plate by sitting drop vapor diffusion. Around a thousand crystallization conditions were screened at both 10 and 16 °C and various protein concentrations. $SidM_{317-545}$ crystals were observed in a condition containing 0.1 M phosphate citrate buffer pH 4.25, 5 % PEG 3000, 12 % 1, 2-propanediol and 10 % glycerol at 16 °C (Fig 3.7A). However, the resultant crystals were in clusters unsuited for single-crystal diffraction experiments. These initial crystals were used to prepare crystallization seeds in crystal optimization trials. Conditions were optimized by varying pH, PEG and protein concentrations, finally yielding individual large crystals (Fig 3.7B). These crystals diffracted X-rays to ~ 3 Å at the Soleil synchrotron (Fig 3.8) and also on an in-house rotating anode generator (Rigaku MicroMax 007 HF) equipped with a CCD detector (Rigaku Saturn944HG). The diffraction data was processed using MOSFLM (Leslie and Powell 2007). Closer inspection of the diffraction pattern indicated $SidM_{317-545}$ crystals to have a modulated structure, meaning the fundamental unit cell can be obtained using strong reflections only. Indexing of these reflections results in a primitive triclinic basis cell with a = 60 Å, b = 151 Å, c = 153 Å, α = 98 °, β = 101 ° and γ = 101 °. These parameters can be transformed to a body centered orthorhombic lattice with unit cell dimensions a = 60 Å, b = 191 Å, c = 229 Å when incorporating the weaker diffraction spots along C-axis. These satellite reflections are represented by incommensurate vector q (personal communication: Dr. Toine Schreurs, BIJVOET Centre for Biomolecular Research, Utrecht University, Utrecht, The Netherlands). Processing of diffraction data with this larger unit cell resulted in a completeness of 30 %, insufficient for structural analysis. Optimization experiments with detergent and additive screens failed to solve the incommensurate crystal problem.

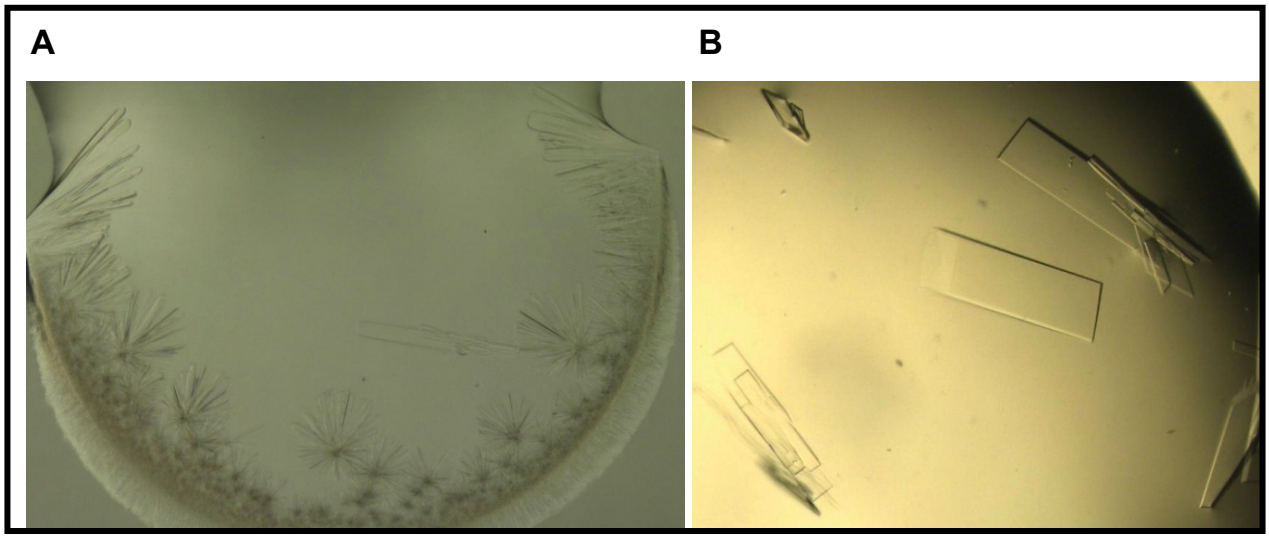

Figure 3.7: Crystallization of SidM$_{317-545}$: A) An initial sitting drop vapor diffusion screen yielded small clustered crystals. B) Micro-seeding using initial crystals as seeds by hanging drop method resulted in plate-like large crystals that diffracted to 3.0 Aº.]

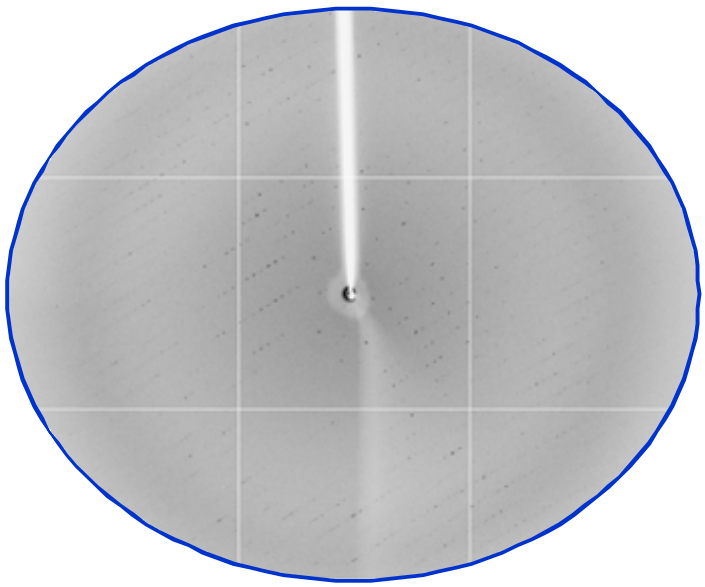

Figure 3.8: A diffraction image of SidM$_{317-545}$ crystal. The blue circle indicates the resolution limit of 3.0 Å

3.3 Complex formation of SidM$_{317-545}$/Rab1A$_{1-175}$

3.3.1 Purification and analysis of SidM$_{317-545}$/Rab1A$_{1-175}$ complex

SidM of *L. pneumophila* was previously shown to interact with the human, small GTPase Rab1A (Machner *et al*, 2007). Structural information for Rab1A was available while the structure of SidM

was unknown. To understand the structural details of the SidM interaction with Rab1A, the central domain of SidM (residues 317-545) was complexed with Rab1A (Fig 3.9). SidM and Rab1A were purified separately by glutathione agarose affinity chromatography (See chapter 2.3.3). Fractions of both proteins eluted following cleavage from GST were analyzed by SDS-PAGE (Fig 3.9A). $SidM_{317-545}$ and $Rab1A_{1-175}$ were mixed and incubated at 4 °C to allow complex formation. The resulting $Rab1A_{1-175}/SidM_{317-545}$ complex was purified by Size Exclusion Chromatography to remove impurities and uncomplexed proteins, and also to establish whether dissociation of the complex occurs. Fig 3.9B combines the chromatogram and SDS-PAGE. As expected, the complex eluted first (highlighted by a red bar, ~47 kDa) followed by excess $SidM_{317-545}$ (magenta bar). Clearly $Rab1A_{1-175}$ and $SidM_{317-545}$ form a tight, 1:1 complex (Fig 3.9B)

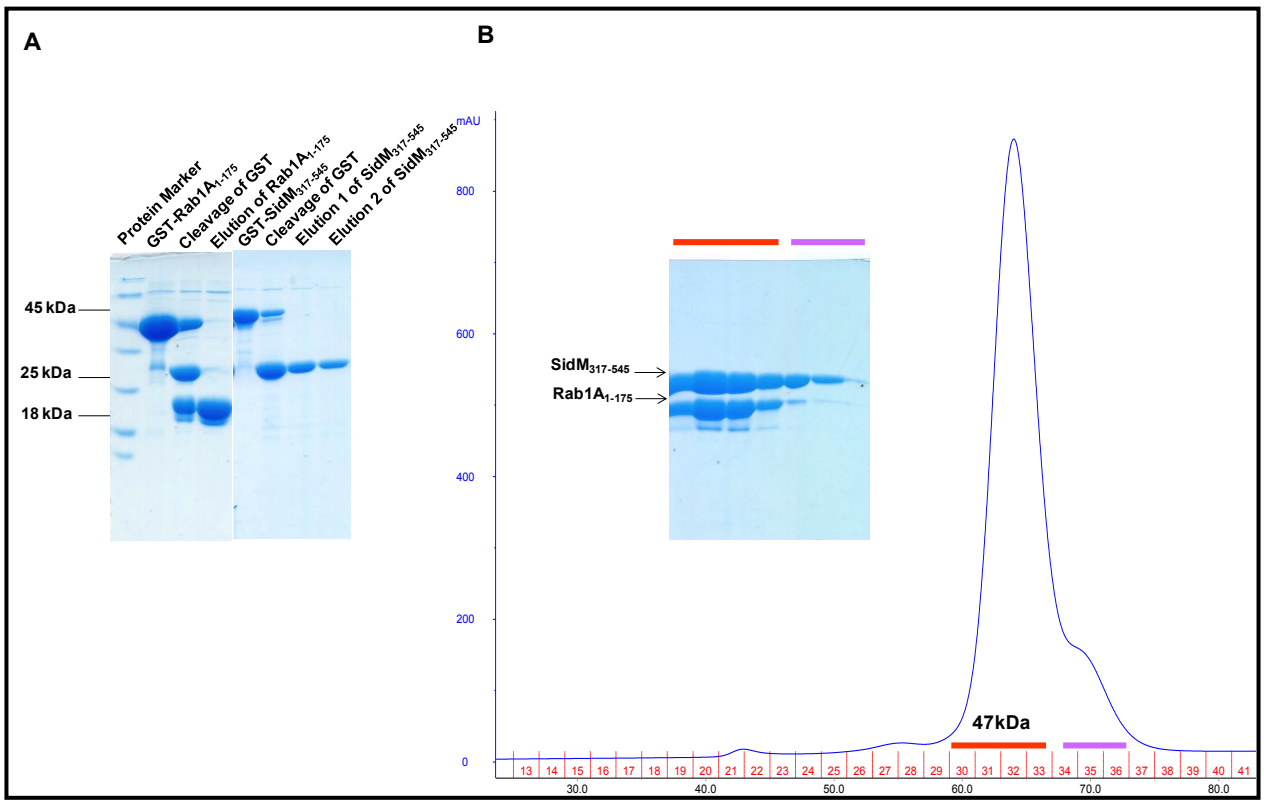

Figure 3.9: Purification profile of SidM/Rab1A complex

(A) Glutathione affinity purification of SidM and Rab1A. Elution fraction of SidM and Rab1A were analyzed by SDS-APGE. (B) Size exclusion chromatography of SidM/Rab1A complex. Coomassie stained SDS-PAGE gel and chromatogram showing the formation of complex, fractions highlighted in red bar indicates SidM/Rab1a complex eluted with an elution volume of 64 mL corresponds to 47 kDa and fractions highlighted in magenta bar indicates excess SidM

3.3.2 Stability of $SidM_{317-545}$ /$Rab1A_{1-175}$ complex

The $SidM_{317-545}$/$Rab1A_{1-175}$ complex was further purified by anion exchange chromatography (AEC). In addition this method would further establish the tightness of the complex. The pH was chosen to allow excess $SidM_{317-545}$ to elute in the flow through rather than binding to the column while the complex did bind and was thereafter eluted using a linear NaCl gradient. The AEC chromatogram (Fig 3.10) reveals a single elution peak, which SDS PAGE analysis confirmed to correspond to homogenous $Rab1A_{1-175}$/$SidM_{317-545}$ complex. Thereafter the $Rab1A_{1-175}$/$SidM_{317-545}$ complex was further purified by SEC to remove excess NaCl prior to crystallization.

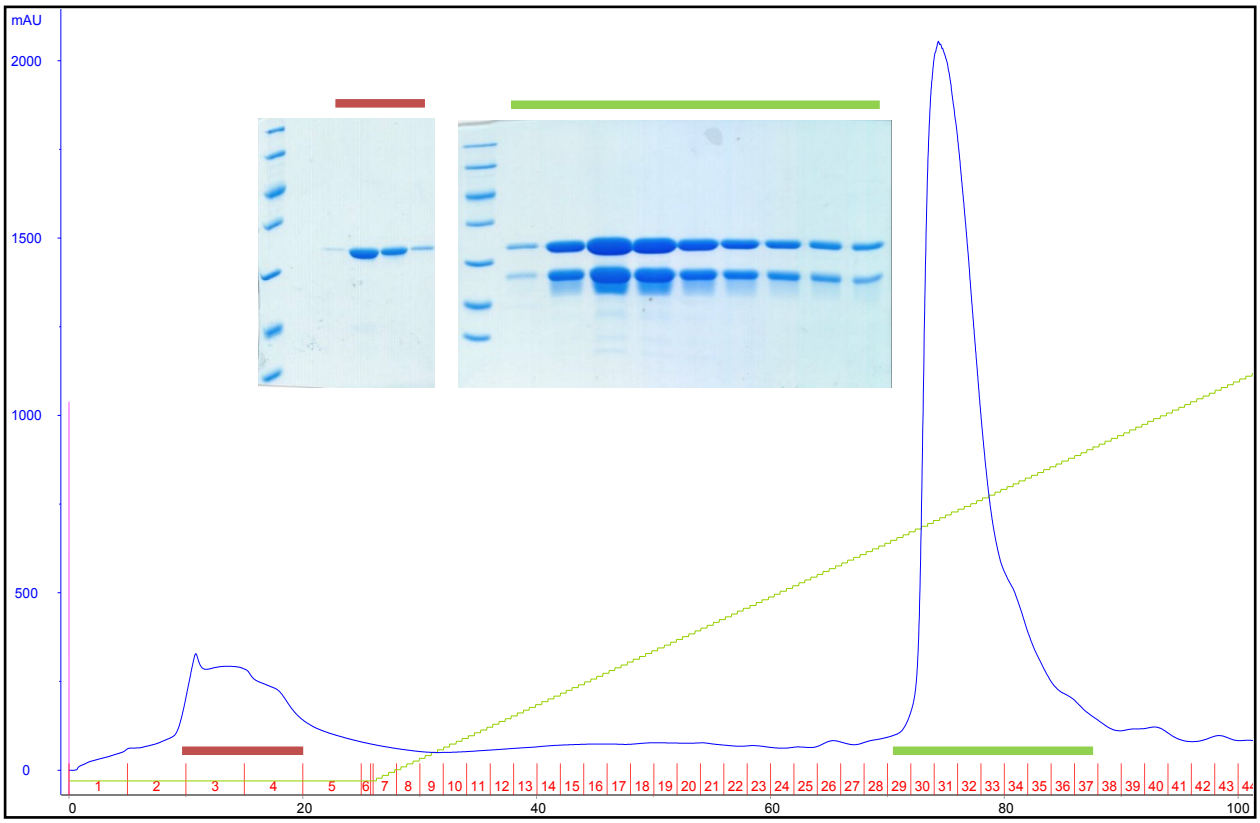

Figure 3.10: Anion exchange chromatography of $SidM_{317-545}$ /$Rab1A_{1-175}$complex

Separation of excess $SidM_{317-545}$ from$SidM_{317-545}$ /$Rab1A_{1-175}$ complex. $SidM_{317-545}$ /$Rab1A_{1-175}$ complex was applied to the anion exchanger and eluted by salt gradient from 0 to 100mM NaCl. Unbound $SidM_{317-545}$ came out in the flow through indicated by red bar and elution fractions of $SidM_{317-545}$ /$Rab1A_{1-175}$ complex were indicated by green bar.

3.3.3 Co-expression of SidM$_{317-545}$ and Rab1A$_{1-175}$

To speed up purification of SidM$_{317-545}$/Rab1A$_{1-175}$ the two proteins were co-expressed in *E. coli* BL21 and Rosetta 2 to allow stable complex formation *in situ*. For this, the gene encoding SidM$_{317-545}$ was cloned into the vector pETM-30 by a restriction free cloning (see section 2.4.5 for details on the method). For Rab1A$_{1-175}$ production the existing pGEX-6P1 (Fig 3.11A & B). As the vector pETM-30 carries kanamycin and pGEX-6P1 ampicillin antibiotic resistance genes, retention of both plasmids can be enforced by adding both antibiotics. Co-expressed SidM$_{317-545}$/Rab1A$_{1-175}$ complex was purified by GST affinity chromatography followed by SEC. Production of soluble SidM$_{317-545}$ and Rab1A$_{1-175}$ was analyzed on SDS-PAGE (Fig 12A). SidM$_{317-545}$ and Rab1A$_{1-175}$ co-eluted from the glutathione agarose column. SidM$_{317-545}$ was, however, markedly more strongly produced than Rab1A$_{1-175}$ (Fig 3.12A). Fractions containing the complex were pooled and further purified by SEC.

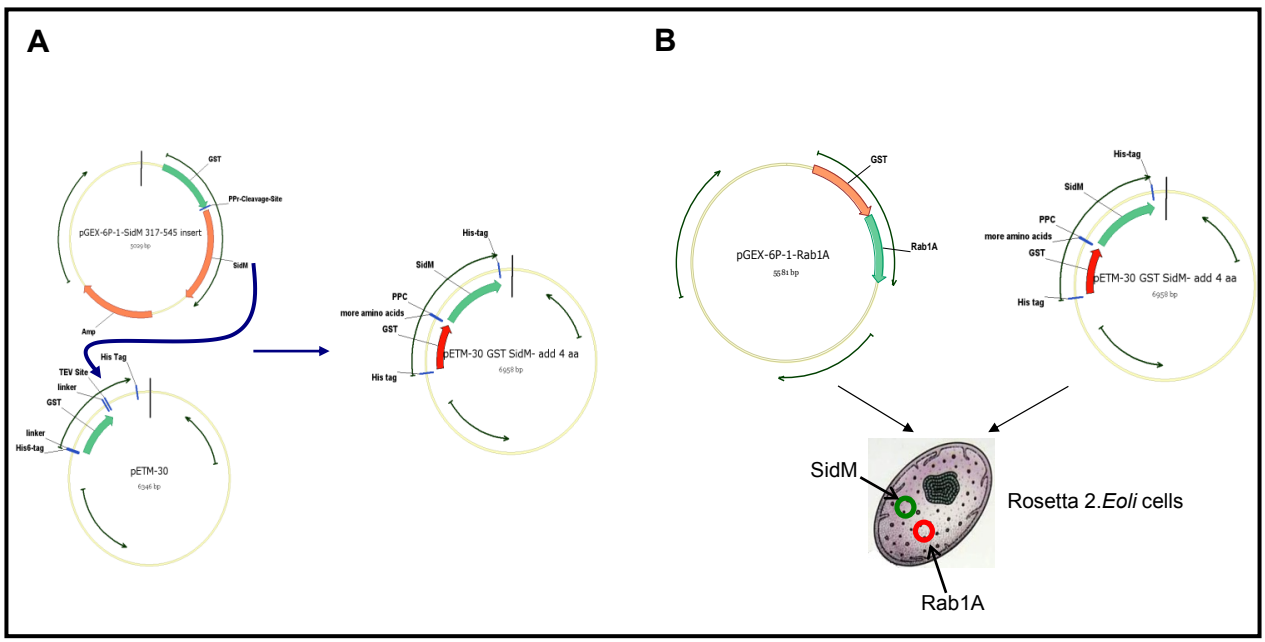

Figure 3.11: Co-expression of SidM$_{317-545}$ and Rab1A$_{1-175}$. (A) Re-cloning of *sidM* in to pETM-30 vector. (B) Co-expression of pGEX-6P1Rab1A$_{1-175}$ and pETM-30 SidM$_{317-545}$ into Rosetta 2.*E. coli* cells

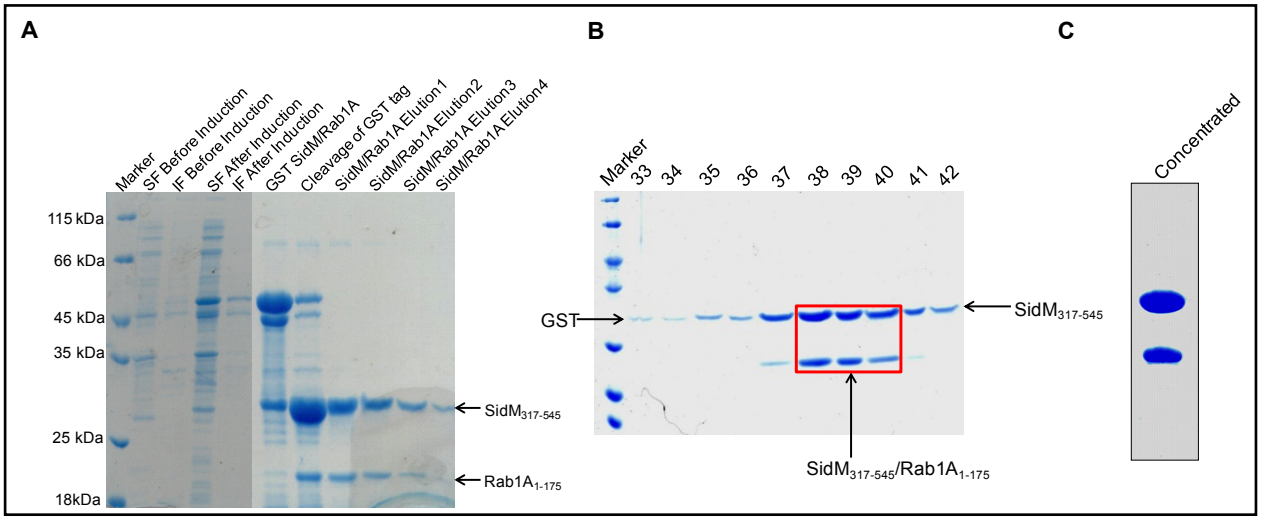

Figure 3.12: Co-expression and purification profile of $SidM_{317-545}/Rab1A_{1-175}$

(A) Coomassie stained SDS-PAGE showing glutathione agarose affinity purification profile of $SidM_{317-545}$ /$Rab1A_{1-175}$, where Rab1A is co-eluted with SidM. **(B)** Coomassie stained SDS-PAGE of SEC of $SidM_{317-545}$ /$Rab1A_{1-175}$. Fractions highlighted by the red rectangle contain $SidM_{317-545}$ /$Rab1A_{1-175}$ (C) SDS-PAGE showing concentrated $SidM_{317-545}$ /$Rab1A_{1-175}$ after SEC.

3.4 Surface Mutagenesis of Rab1A

3.4.1 $Rab1A^{K55S-K58S}$ and $Rab1A^{E168A-K170S-K171A-R172S}$ variants

Following numerous failed attempts to crystallize the $SidM_{317-545}/Rab1A_{1-175}$ complex, the method of entropy reduction was used on Rab1A to increase the likelihood of crystallization. Long, flexible surface residues such as lysine and arginine were replaced by short, less flexible alanines and serines. Two variants of Rab1A were constructed by site-directed mutagenesis: the double variant K55A-K58S and the quadruple variant E168A-K170S-K171A-R172S. Production and purification of the variants were carried out as for full length Rab1A. However, neither of these variants resulted in crystals. Coincidentally though SEC (Fig 3.13) and ITC experiments (Fig 3.24) demonstrated the variant $Rab1A^{K55A-K58S}$ to be strongly impaired for $SidM_{317-545}$ binding compared to wild type Rab1A.

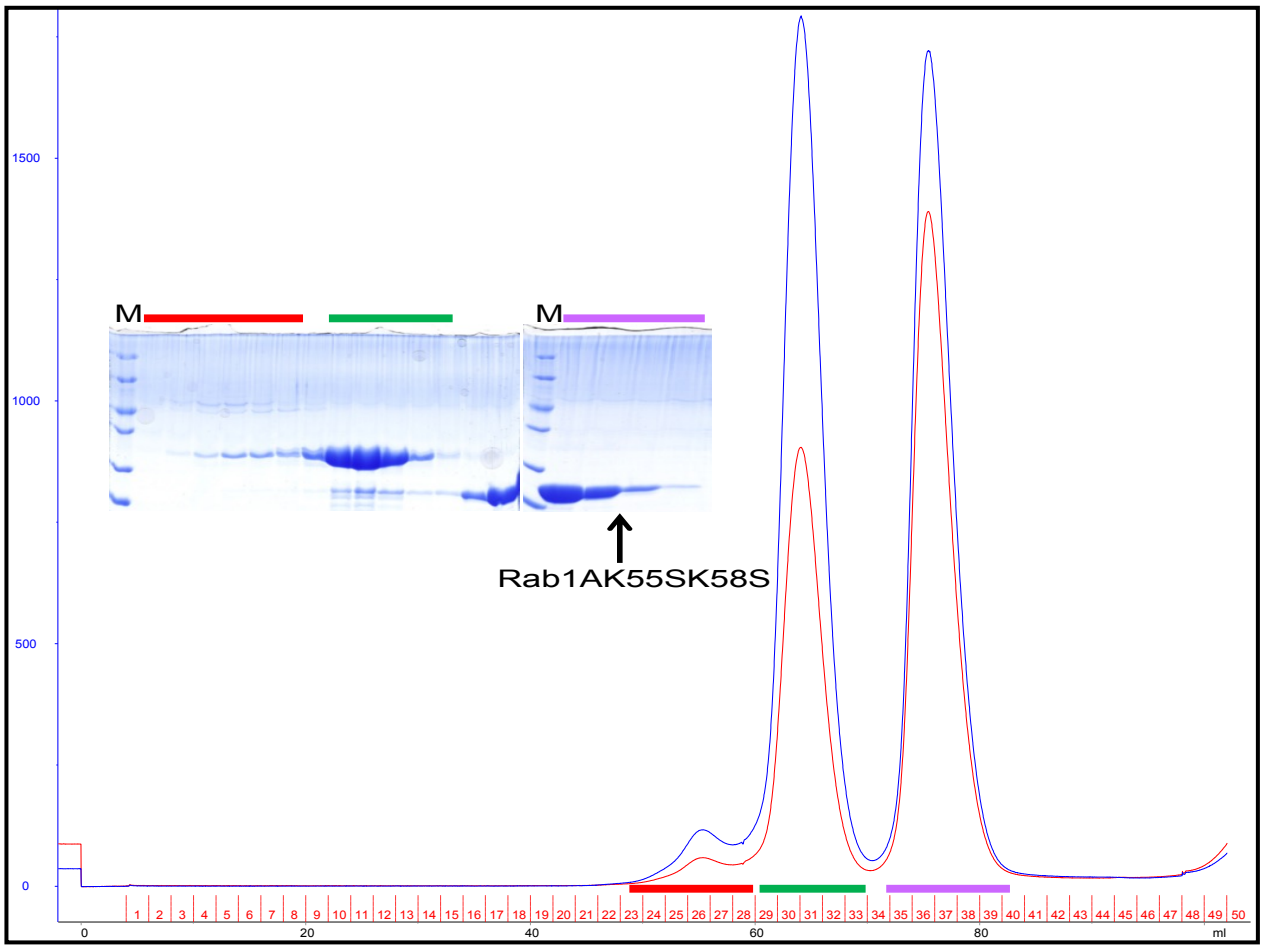

Figure 3.13: SEC purification profile of Rab1A$^{K55A-K58S}$/SidM$_{317-545}$. Rab1A$^{K55A-K58S}$ and SidM$_{317-545}$ are largely separated during SEC purification. Fractions of the first SEC peak highlighted by the red bar contain SidM$_{317-545}$ together with larger impurities. The green bar marks SidM$_{317-545}$ with a small amount of retained Rab1A$^{K55A-K58S}$. The pink bar highlights fractions of the third peak essentially containing unbound Rab1A$^{K55A-K58S}$.

3.5 Structure of SidM$_{317-545}$ /Rab1A$_{1-175}$ complex

3.5.1 Crystallization of SidM$_{317-545}$ /Rab1A$_{1-175}$

As part of this thesis, six truncation variants of human Rab1Awere generated. Each was screened over a wide variety of conditions to generate crystals in complex with SidM$_{317-545}$ with the aim of solving the crystal structure of the complex. All truncation mutants tightly bind SidM$_{317-545}$. However only the complex consisting of SidM$_{317-545}$ and Rab1A$_{1-175}$ and where both genes were co-expressed in *E. coli* was successfully crystallized. The SidM$_{317-545}$ /Rab1A$_{1-175}$ complex was concentrated to 15 mg/mL and crystallization lead conditions were screened for using commercial

screens by sitting drop vapor diffusion experiments in 96 well plates. Crystals of $SidM_{317-545}$ /$Rab1A_{1-175}$ complex were finally observed to grow in wells containing 27.5 % PEG 400 and 0.1 M sodium citrate pH 5.3 at 10 °C (Fig 3.14A). These clustered crystals were optimized by varying the pH and precipitant concentrations in a 26 (6x4) well hanging drop vapor diffusion crystallization plate. Optimization finally resulted in large single crystals in 35 % PEG 400 and 0.1 M sodium citrate pH 5.5 (Fig 3.14B). As the reservoir solution already had the properties of a cryo-protectant, crystals were directly harvested from the drops, cryo-cooled and subjected to X-ray analysis.

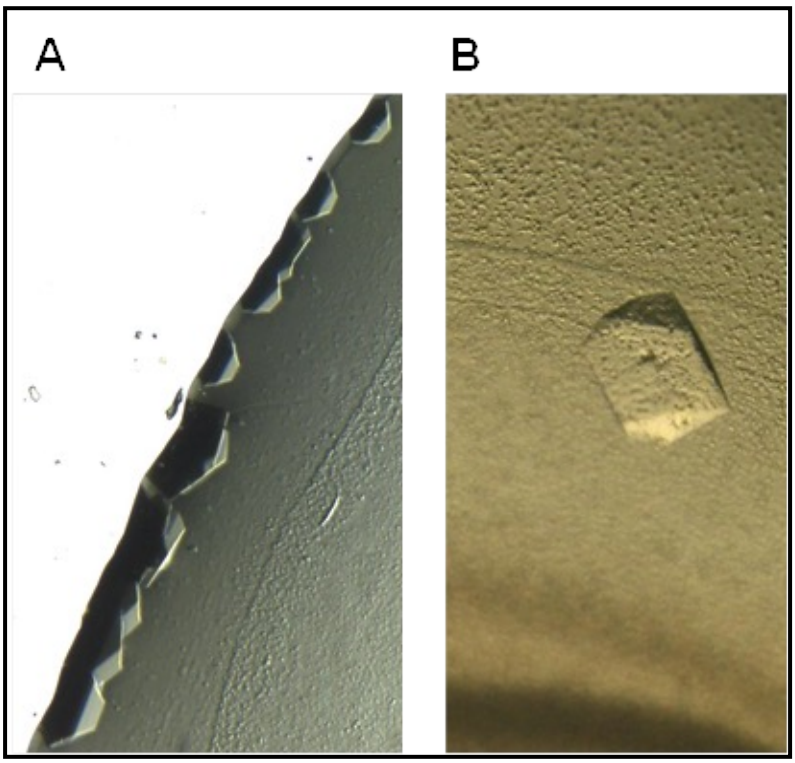

Figure 3.14: Crystals of the $SidM_{317-545}$ /$Rab1A_{1-175}$ Complex

(A) Initial, slightly intergrown crystals of $SidM_{317-545}$/$Rab1A_{1-175}$. **(B)** Optimized $SidM_{317-545}$/$Rab1A_{1-175}$ crystals grown in a hanging drop experiment yielded a single crystal of sufficient size for X-ray diffraction experiments.

3.5.2 Data collection and processing

X-ray diffraction data for $SidM_{317-545}$ /$Rab1A_{1-175}$crystals were collected in-house on a rotating anode generator (Rigaku MicroMax-007HF) and CCD detector (Rigaku Saturn944HG). The diffraction data were indexed, integrated and scaled using the software package HKL3000 (Otwinowski and Minor 1997). The crystals diffracted X-rays to 2.05 Å resolution and crystals were found to belong to the trigonal space group R3 with unit cell dimensions a=b=105.0 Å and

c=118.6 Å α = β = 90° and γ = 120°.Matthews's coefficient analysis (Matthews 1968) suggested a packing parameter V_M = 2.68 $Å^3$/Da corresponding to a solvent content of 54%. This in turn implieda crystal packing with of oneSidM/Rab1A dimer per asymmetric unit.

Structure factors were phased by molecular replacement usingthe programme PHASER (Storoni, McCoy et al. 2004) and the complex of $DrrA_{340-533}$/$Rab1b_{3-174}$ as a search model. The single solution from PHASER was refined by restrained refinement protocol in REFMAC5 (Murshudov, Vagin et al. 1997) alternated cyclically with manual adjustment of the model addition of water moleculesin COOT (Emsley and Cowtan 2004). This procedure gradually improved the model resulting in a final model with R and R_{free} values of 16.0 and 19.0 % respectively.

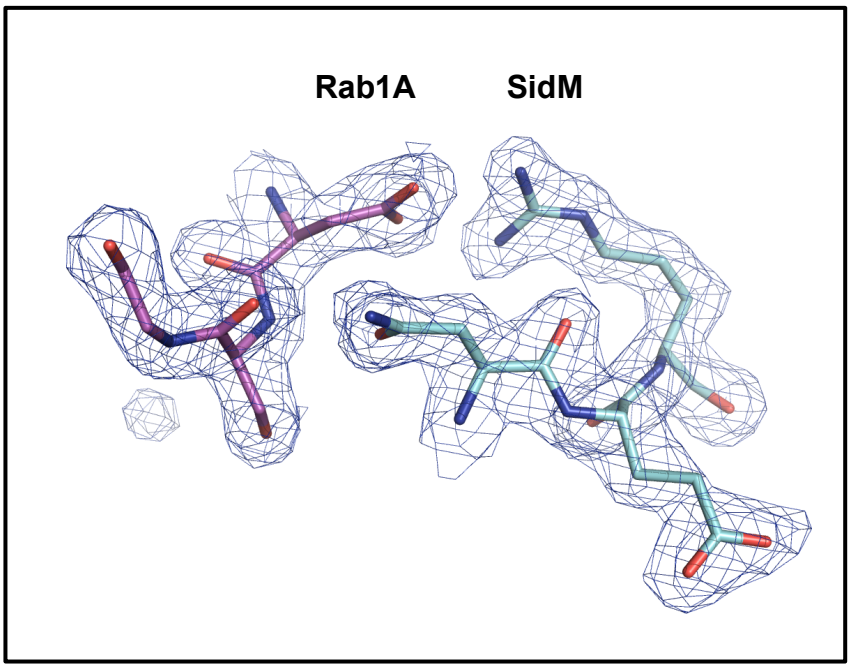

Figure 3.15: Electron density map of the $SidM_{317-545}$/$Rab1A_{1-175}$ Complex after final refinement of the structure. The P-loop of Rab1A is depicted in magenta, SidM in cyan.

3.5.3 Structure of $Rab1A_{1-175}$

Structurally Rab1A shares structural features with other small GTPases (See chapter 4.2) such as the Switch I and Switch II motifs as well as the P-loop. $Rab1A_{1-175}$ displays mixed α-helical and β-sheet structure: a central 6-stranded β-sheet comprised of five parallel ($β1_R$, $β3_R$, $β4_R$, $β5_R$ and $β6_R$ – where the subscript R stands for Rab1A) and one anti-parallel β-strand ($β2_R$) is surrounded by 6 α-helices ($α1_R$ to $α6_R$). The ten connecting loops L1 to L10 are correspondingly denoted $β1_R$-$α1_R$, $α1_R$-$α2_R$, $α2_R$-$β2_R$, etc. Five N-terminal residues of $Rab1A_{1-175}$ are remnants of the PreScision protease cleavage site. Part of the loop between $β6_R$ and $α6_R$ is disordered (Figure 3.16). Structural

elements contributing to switch I (blue in Figure 3.16) include L2, $\alpha2_R$ and L3 (residues 34 to 45). Switch II (red in Figure 3.16) is comprised of L5, $\alpha3_R$ and L6 (residues 63 to 80) .The P-loop (magenta in Figure 3.16) is located in L1 spanning residues 16 and 17.

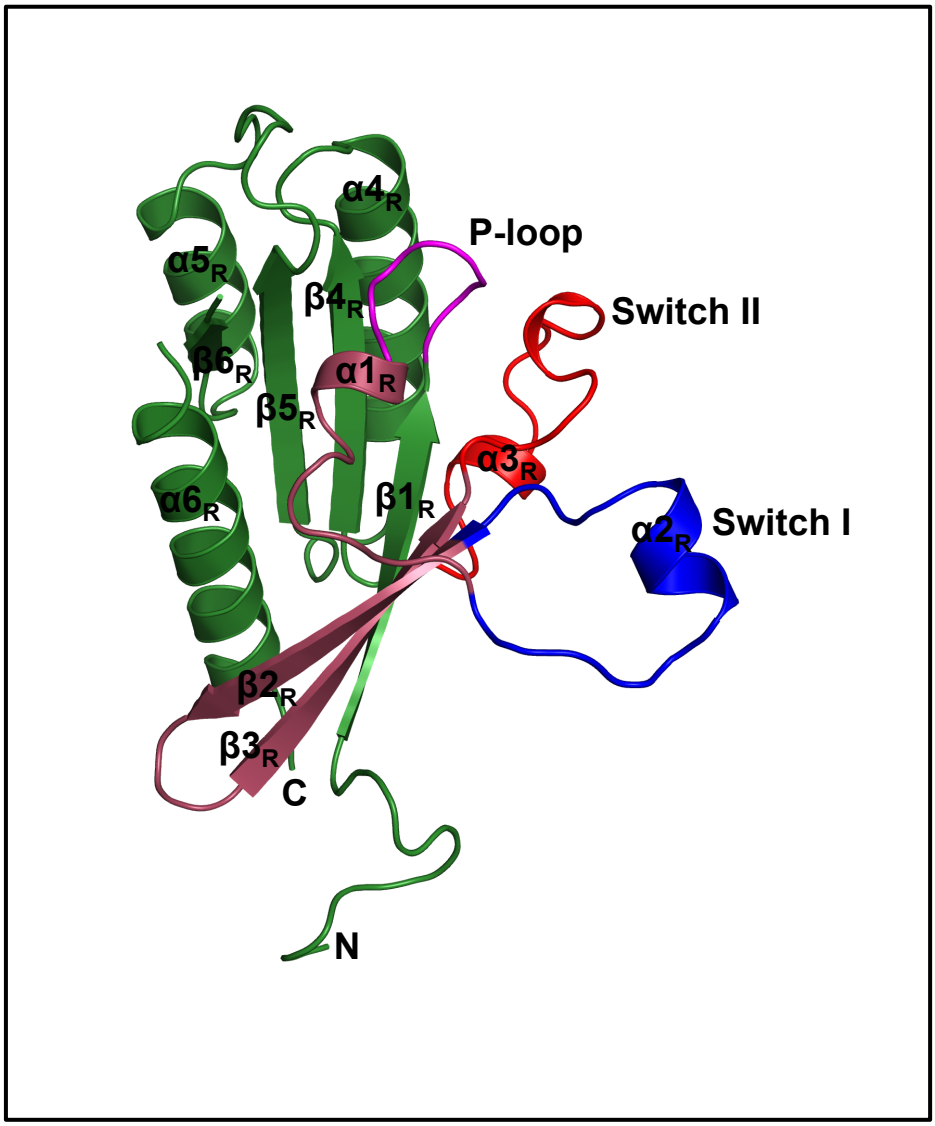

Figure 3.16: Structure of $Rab1A_{1-175}$

Rab1 is shown in green, Switch I domain is represented in blue, Switch II in red, P-loop in magenta and inter switch regions in salmon.

In the crystal structure of the $SidM_{317-545}$ /$Rab1A_{1-175}$ complex, $Rab1A_{1-175}$ displays mixed α-helical and β-sheet structure: a central 6-stranded β-sheet comprised of five parallel ($\beta1_R$, $\beta3_R$, $\beta4_R$, $\beta5_R$ and $\beta6_R$ – where the subscript R stands for Rab1A) and one anti-parallel β-strand ($\beta2_R$) is surrounded by 6 α-helices ($\alpha1_R$ to $\alpha6_R$). The ten connecting loops L1 to L10 are correspondingly

denoted $\beta1_R$-$\alpha1_R$, $\alpha1_R$-$\alpha2_R$, $\alpha2_R$-$\beta2_R$, etc. Five N-terminal residues of $Rab1A_{1-175}$ are remnants of the PreScision protease cleavage site. Part of the loop between $\beta6_R$ and $\alpha6_R$ is disordered (Fig 3. 16A&B). Structurally Rab1A shares structural features with other small GTPases (See section 4.2) such as the Switch I and Switch II motifs as well as the P-loop. Structural elements contributing to switch I include L2, $\alpha2_R$ and L3 residues 34 to 45. Switch II is comprised of L5, $\alpha3_R$ and L6 residues 63 to 80.The P-loop is located in L1 spanning residues 16 and 17.

3.5.3 Structure of $SidM_{317-545}$

$SidM_{317-545}$ has a unique structural fold and is a purely α-helical structure comprising eight α-helices (denoted $\alpha1_S$ to$\alpha8_S$, where "subscript S" indicates the component SidM). The α-helices are connected by seven loops denoted L_A to L_G corresponding to $\alpha1_S$-$\alpha2_S$, $\alpha2_S$-$\alpha3_S$, $\alpha3_S$-$\alpha4_S$ etc. $SidM_{317-545}$ forms a two-layered structure, in which two parallel α-helices $\alpha4_S$ and $\alpha5_S$ constitute the upper layer. This layer coincidentally is the primary contact surface for Rab1A. The lower layer is formed by the roughly parallel α-helices $\alpha1_S$, $\alpha2_S$, $\alpha6_S$ and $\alpha7_S$. The two α-helical layers are oriented at an angle of 90 ° to each other. The other two small helices $\alpha3_S$ and $\alpha8_S$ are located at the end of $\alpha4_S$ and $\alpha5_S$ respectively (Figure 3.17).

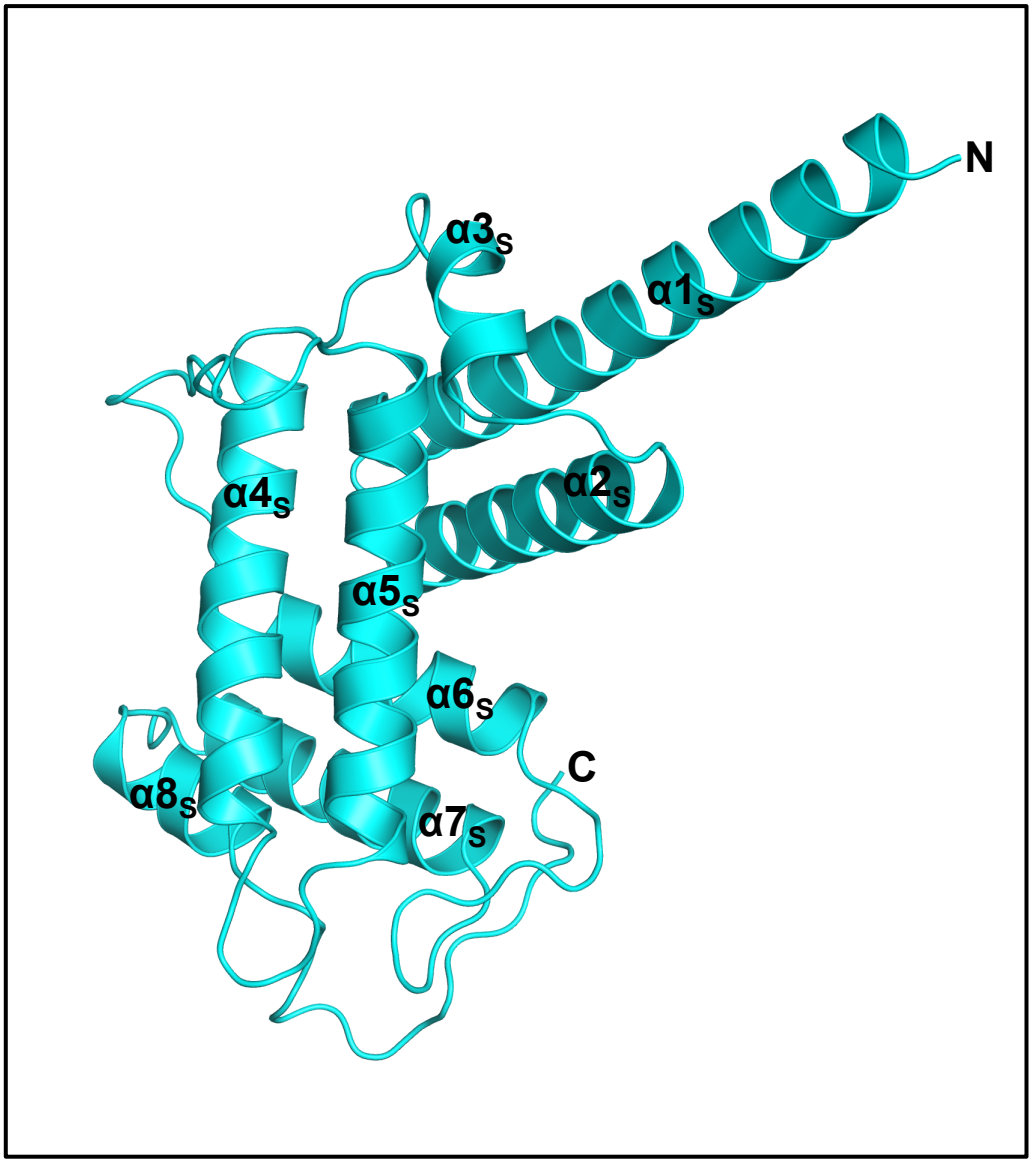

Figure 3.17: Structure of SidM$_{317-545}$ rendered in cyan, helices indicated by numbers

3.5.4 The SidM$_{317-545}$ /Rab1A$_{1-175}$ Complex

SidM and Rab1A form a stoichiometric complex in which SidM binds predominantly to the Switch I, Switch II and P-loop regions of Rab1A (Figure 3.18). SidM binding induces conformational changes on Rab1A structure, where Switch I is displaced away from the nucleotide binding site and Switch II adopts ordered conformation (Detail explanation in section 4.2).

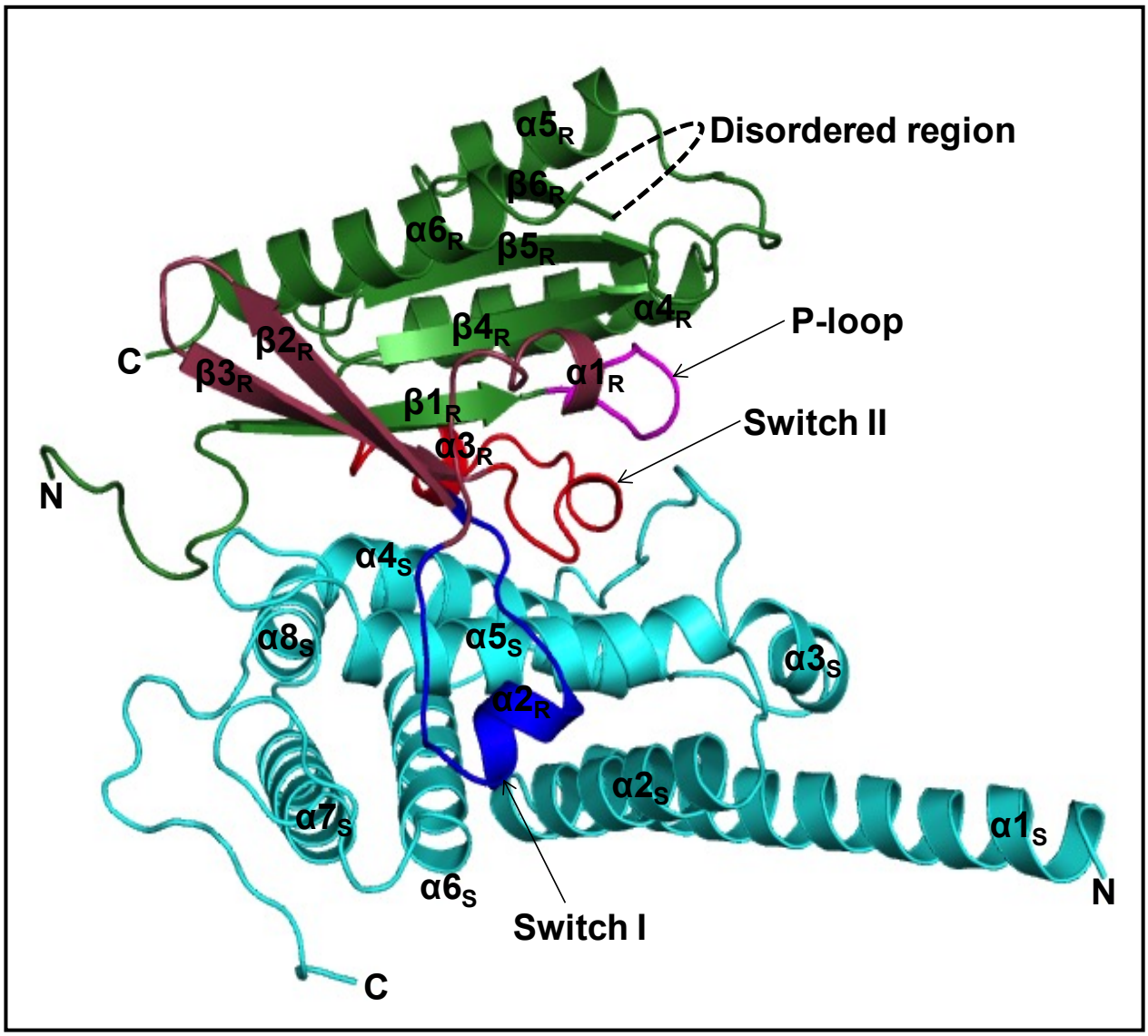

Figure 3.18: The Crystal Structure of the SidM$_{317-545}$/Rab1A$_{1-175}$ Complex. Cartoon representation of the SidM$_{317-545}$/Rab1A$_{1-175}$ complex. SidM$_{317-545}$ interacts with the Switch I, Switch II and P-loop of Rab1A$_{1-175}$. Rab1A$_{1-175}$ is represented in green, with Switch I in blue, Switch II in red, the P-loop in magenta and SidM$_{317-545}$ in cyan. The black dashed line in the Rab1$_{1-175}$ structure indicates the disordered loop.

3.5.5 Interface of the SidM$_{317-545}$/Rab1A$_{1-175}$ Complex

In the crystal structure of the complex, the interactions between the SidM$_{317-545}$ and Rab1A$_{1-175}$ bury surface accessible area of 1816Å as calculated by the PISA server (Krissinel and Henrick, 2007). Structural elements involved in complex formation are the N-terminal loop, $\beta1_R$, $\beta2_R$, Switch I, Switch II and P-loop of Rab1A$_{1-175}$ and the $\alpha2_S$, $\alpha4_S$, $\alpha5_S$, $\alpha6_S$ and $\alpha8_S$ helices and the loops L_D, L_E, L_F of SidM$_{317-545}$ (Figure 3.19).

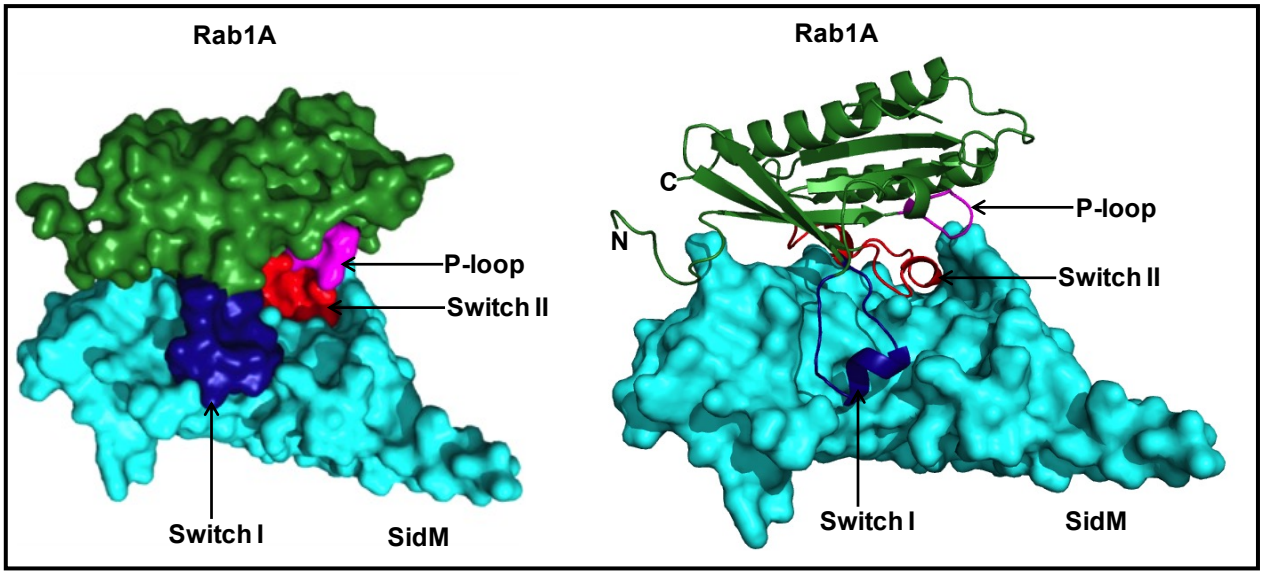

Figure 3.19: Surface representation of the SidM$_{317-545}$ /Rab1A$_{1-175}$ Complex. (A) Rab1A and SidM are shown in surface representation. Switch I of Rab1A is shown in blue, Switch II in red, P-loop in magenta and other regions in green and SidM in cyan (B) The Rab1A interacting region of SidM is shown in surface representation and Rab1A is in cartoon presentation

Based on the contact regions of Rab1A$_{1-175}$, the interactions of the complex can be divided in to four sections

3.5.6 Switch I of Rab1A$_{1-175}$ contacts α2, α5, α6 and L$_F$ of SidM$_{317-545}$

In the crystal structure of SidM$_{317-545}$/Rab1A$_{1-175}$ complex, the larger part of the switch I region of Rab1A (residues 34 to 48) as well as L2 (α1$_R$-α2$_R$), α2$_R$ and L3 (α2$_R$-β2$_R$) contact the upper layer α5$_S$ and the bottom layer α2$_S$, α6$_S$ and L$_F$ (α6$_S$-α7$_S$) of SidM (Figure 3.18).

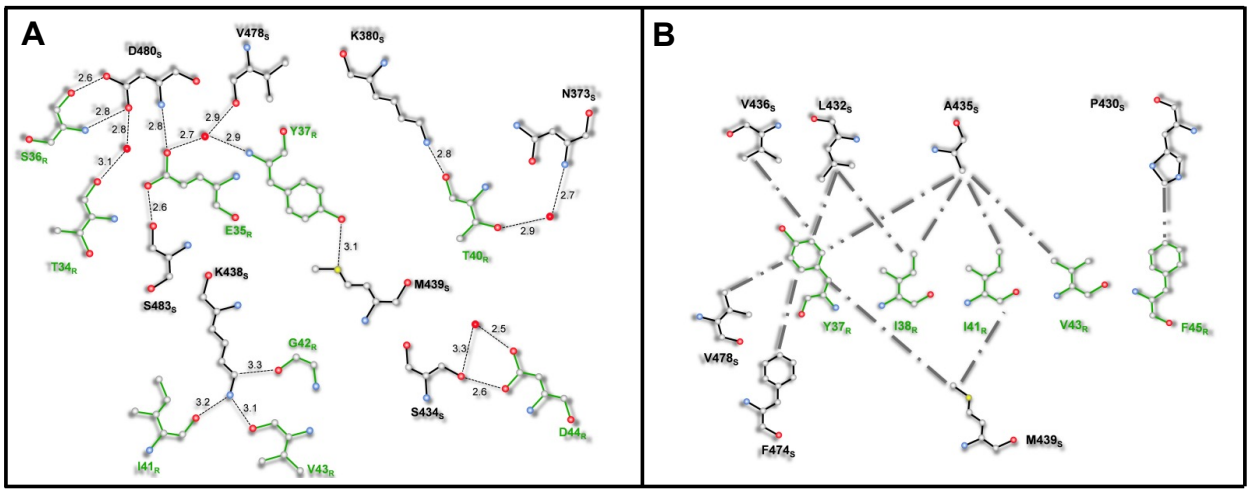

Figure 3.20: Interactions between Rab1A Switch I and SidM. (A) Hydrogen bond interactions between Switch I of Rab1A and SidM. Rab1A residues are represented in green, those of SidM in black. Hydrogen bonds are represented by black dotted lines. **(B)** Hydrophobic interactions between Switch I of Rab1A and SidM. Grey lines indicate hydrophobic interactions.

Contacts include several hydrogen bonds and hydrophobic interactions. Loop L2 ($\alpha1_R$-$\alpha2_R$) residues $T34_R$ (O), $E35_R$ (Oε1, Oε2) and $S36_R$ (N, Oγ) of Rab1A form strong direct and water-mediated hydrogen bond interactions with L_F ($\alpha6_S$-$\alpha7_S$) residues $D480_S$ (N) and $S483_S$ (Oγ) of SidM Fig (3.20A). The $\alpha2_R$ and L3 of Rab1A bears several hydrophobic residues $Y37_R$, $I38_R$, $I41_R$, $V43_R$ and $F45_R$, which makes extensive hydrophobic interactions with $\alpha5_S$ and $\alpha6_S$ residues $A345_S$, $V436_S$, $M439_S$, $F474_S$ and $V478_S$ of SidM (Fig 3.20B). The structural changes in the Switch I region of Rab1A, upon SidM binding is discussed in detail in section 4.2

3.5.7 Switch II contacts of $Rab1A_{1\text{-}175}$with $SidM_{317\text{-}545}$

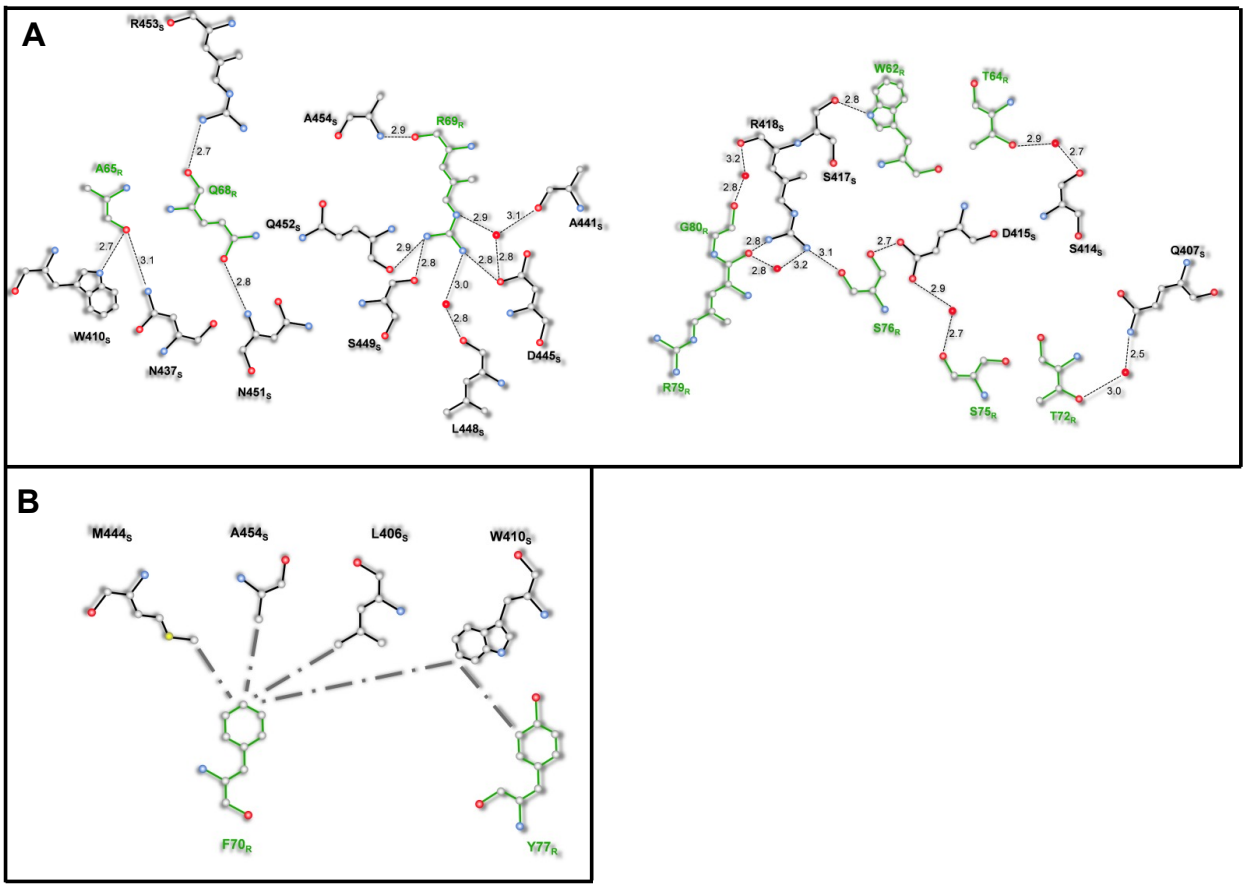

Figure 3.21: Interactions between Rab1A Switch II and SidM. (A) Hydrogen bonding interactions of Switch II of Rab1A and SidM. Rab1A residues are represented in Green and SidM residues in Black respectively. Hydrogen bonds are represented in black dotted lines. **(B)** Hydrophobic interactions between Switch II of Rab1A and SidM. Grey lines indicate hydrophobic interactions.

The structural elements L5, $\alpha3_R$ and L6 of Rab1A Switch II (residues 63-80) extensively interact with $\alpha4_S$, $\alpha5_S$, $\alpha8_S$ and L_E of SidM through hydrogen bonds and hydrophobic interactions (Fig

3.21A&B). Helix $\alpha3_R$ of Rab1A form strong interactions with L_E and $\alpha5_S$ of SidM through several hydrogen bonds between negatively charged $Q68_R$ of Rab1A with $N451_S$ (N) and $R453_S$ (NH1) of SidM. In addition, positively charged $R69_R$ of Rab1A interacts strongly with $A441_S$, $D445_S$, $L448_S$, $S449_S$, $A454_S$ and $Q452_S$ of SidM through several direct and water mediated hydrogen bonds (Fig 3.21A). Apart from these hydrogen-bonding interactions, L6 and $\alpha4_R$ of Rab1A also interact with $\alpha4_S$, $\alpha5_S$ and L_E of SidM through hydrophobic interactions. $F70_R$ of Rab1A forms multiple hydrophobic interactions with $L406_S$, $W410_S$, $M444_S$ and $A454_S$ of SidM, where $W410_S$ forms aromatic π-stacking interaction with $F70_R$ (Fig 3.21B).

3.5.8 P-Loop and other contacts of $Rab1A_{1-175}$ with $SidM_{317-545}$

Phosphate binding loop L1 of Rab1A (residues D16 and S17) contacts L_E of SidM through a salt bridge ($D16_R$ Oδ1/Oδ2 to $R453_S$ Nζ1/Nζ2) and two hydrogen bonds ($S17_R$ N/O to $N451_S$ Nδ2/Oδ1) (Fig 3.22).

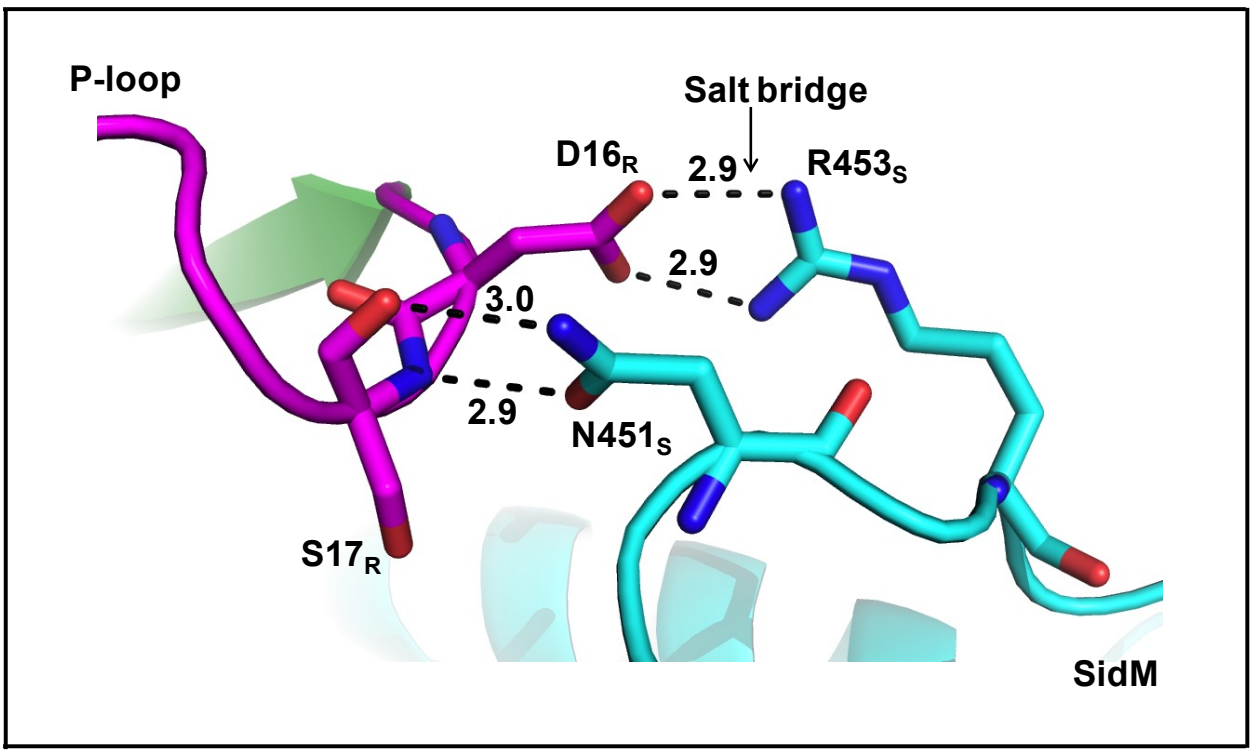

Figure 3.22: P-loop interactions of $Rab1A_{1-175}$ with $SidM_{317-545}$. P-loop residues of Rab1A are coloured magenta, SidM residues cyan. Hydrogen bonds are indicated by black dotted line.

Apart from the Switch I, II and P-loop of Rab1A, other regions are also involved in the interaction

with SidM (Fig 3.23). Thus the N-terminus of Rab1A contacts L_D of SidM through hydrogen bonds ($N2_R$ N ⋯ $L423_S$ O; $N2_R$ Nδ2 ⋯ $T424_S$ O; $Y5_R$ Oζ⋯ $T422_S$ O; $Y5_R$ Oζ ⋯ $S426_S$ Oγ; $K10_R$ Nζ⋯$A421_S$ O and $R418_S$ O; Fig 23A) and hydrophobic interactions ($L8_R$ = $A421_S$ and $Y5_R$ = $L423_S$; Fig 3.23B). Similarly, $L2_R$ hydrogen bonds L_D ($D31_R$ Oδ2 ⋯ $T427_S$ Oγ; $D31_R$ Oδ2 ⋯ $T427_S$ O; and $Y33_R$ O ⋯ $S426_S$ O [water mediated]) while $\beta3_R$ interact with $\alpha5_S$ ($K58_R$ NZ ⋯ $S426_S$ Oγ and $Q60_R$ Nε2 ⋯$S426_S$O [water mediated]).

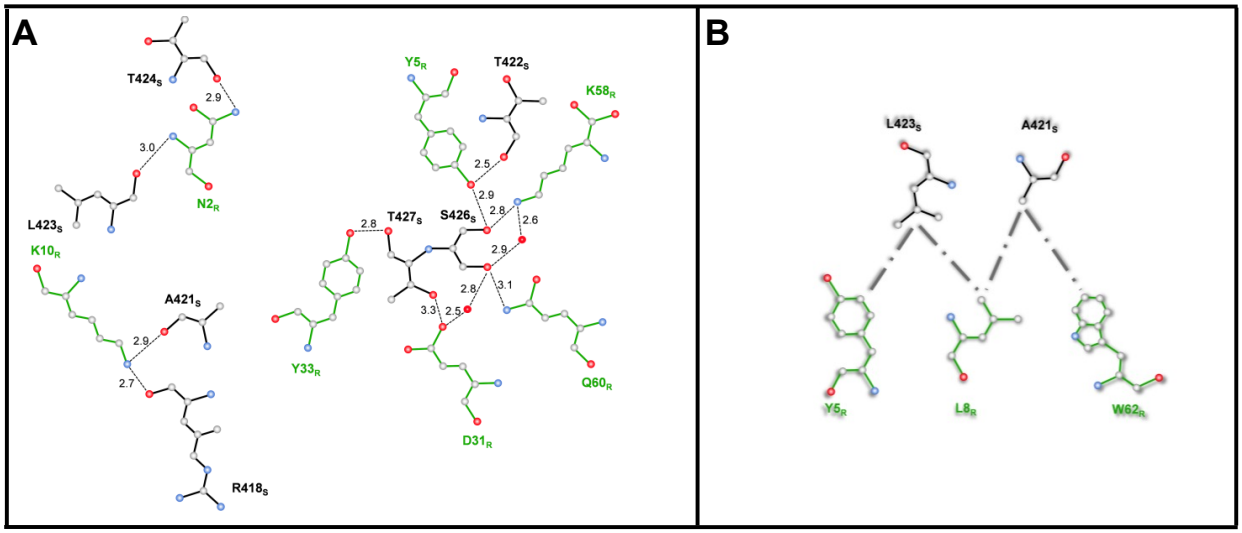

Figure 3.23: Other interactions between Rab1A and SidM. (A) Hydrogen bonding interactions of Rab1A and SidM. Rab1A residues are represented in green and SidM residues in black. Hydrogen bonds are represented by black dotted lines. **(B)** Hydrophobic interactions between Rab1A and SidM. Grey dashed-dotted lines indicate hydrophobic interactions.

3.6 Isothermal Titration Calorimetry (ITC) Measurements

The affinity of $SidM_{317-545}$ for $Rab1A_{1-175}$ was analyzed and quantified by Isothermal Titration Calorimetry (ITC) to complement earlier qualitative analyses by size exclusion chromatography (SEC). ITC is particularly sensitive and powerful in that it provides all the binding parameters such as binding affinity (K), binding stoichiometry (n), and binding enthalpy (ΔH) in a single experiment.

ITC experiments were performed on a Microcal ITC-200. Data is processed and evaluated using Microcal software integrated in Origin 7. $SidM_{317-545}$, and Rab1A (full length and variants) were purified and final buffer exchange was performed with 50 mM HEPES (pH 8.0) and 150 mM NaCl using a Superdex 75 1030 SEC column. The protein samples were concentrated to 100-1000

μM by vivaspin ultra centrifugal filter units of 10kDa molecular weight cut off and degassed for 10 minutes prior to any experiment.

In this experimental approach two states of Rab1A were used for the interaction analysis with $SidM_{317-545}$: In the first state, Rab1A: GDP was titrated to $SidM_{317-545}$. In the second state Rab1A: GDP was treated with 20 mM EDTA during all the purification steps to chelate Mg^{2+} and remove GDP.

3.6.1 State A- Rab1A: GDP/$SidM_{317-545}$

The binding affinity of Rab1A: GDP to $SidM_{317-545}$ was analyzed by titrating 18 x 2 μL injections of 1000 μM Rab1A: GDP from the syringe into the calorimetric cell containing 300 μL of 100 μM $SidM_{317-545}$ at 25 ºC. Fig 3.24A shows the ITC titration curves of Rab1A: GDP to $SidM_{317-545}$. Each peak from the upper panel, in pointing upwards, represents the amount of heat absorbed upon binding of Rab1A to $SidM_{317-545}$, indicating the reaction to be endothermic. The lower panel plots the integrated heat from each injection against the molar ratio of Rab1A to $SidM_{317-545}$. The binding affinity constant 'K', stoichiometry 'n' and binding enthalpy were derived by curve fitting using a "single set of independent sites" model. Analysis of the ITC data for Rab1A: GDP to $SidM_{317-545}$ generated the dissociation constant K_d of 790nM. Thermodynamic parameters obtained from the curve fitting are indicated in Table 3.1 .

3.6.2 State B: EDTA treatment of Rab1A/$SidM_{317-545}$

Recent studies have shown that, Rab1 binds $SidM_{317-545}$ with high affinity in its GDP-free state. In this study, Rab1A: GDP was treated with 20 mM EDTA during all the purification steps to chelate the Mg^{2+} and thereby reduces the binding affinity of GDP. In the final purification step, EDTA was removed by exchanging the buffer by 50 mM HEPES pH 8.0 and 150 mM NaCl. ITC experiments were performed similarly to those for Rab1: GDP (State A) to $SidM_{317-545}$. Interestingly, the binding affinity of $SidM_{317-545}$ for EDTA-treated Rab1A was two-fold higher than Rab1A: GDP:Mg^{2+} (Fig 3.24B). Again the binding of Rab1A to $SidM_{317-545}$ is an endothermic. In the lower panel the integrated heat from each injection is plotted against the molar ratio of Rab1A to $SidM_{317-545}$. Curve fitting indicates dissociation constant K_d of 420 nM for State B EDTA: Rab1A to $SidM_{317-545}$. Other derived thermodynamic parameters are listed in Table 3.1.

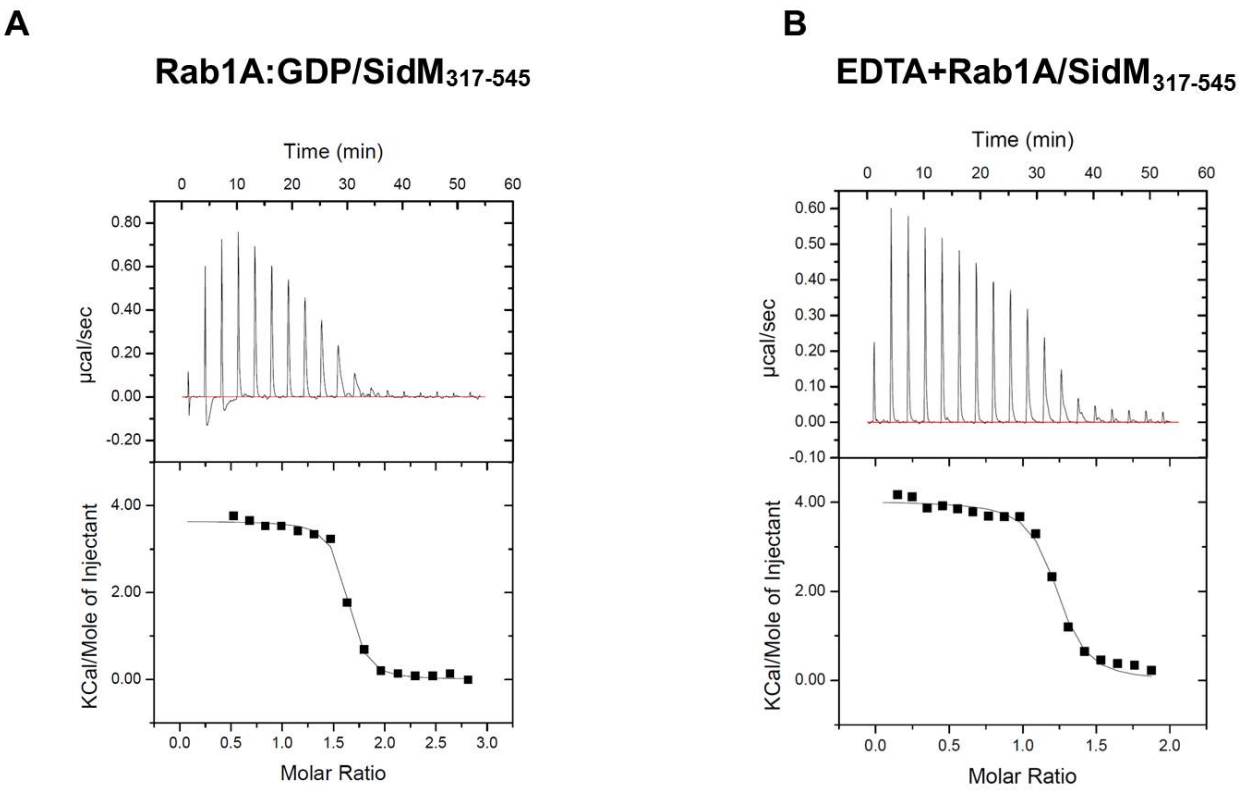

Figure 3.24: Isothermal titration curves of Rab1A: GDP/SidM and EDTA+Rab1A/SidM

(A) The titration curves of Rab1A: GDP against SidM represents the reaction to be endothermic. The top panel shows the raw data produced by titrating 1000 µM of Rab1A: GDP to 100 µM of SidM. The bottom panel represents the integration of peaks against the molar ratio of Rab1A: GDP to SidM. **(B)** The titration curves of EDTA+Rab1A: GDP against SidM represents the reaction to be endothermic.

3.6.3 Effect of Rab1A$^{K55A-K58S}$ variant on binding affinity with SidM

Prior to solving the structure of the Rab1A$_{1-175}$/SidM$_{317-545}$complex, Rab1A was surface engineered to facilitate its crystallization. As part of this strategy, surface residues K55 and K58 were exchanged by A55 and S58 by site-directed mutagenesis. Unexpectedly, SEC analysis indicated this variant to have a decreased affinity for SidM (Fig 3.13). The crystal structure of the Rab1A$_{1-175}$/SidM$_{317-545}$ complex, confirms K58 of Rab1A to contribute to the interaction with SidM$_{317-545}$ (Fig 3.25B). An ITC experiment undertaken to quantify the effect indicated a ten-fold decrease in affinity of Rab1A$^{K55A-K58S}$ for SidM compared to the wild-type protein (Fig 3.25 A) Thermodynamic binding parameters are listed in Table 3.1.

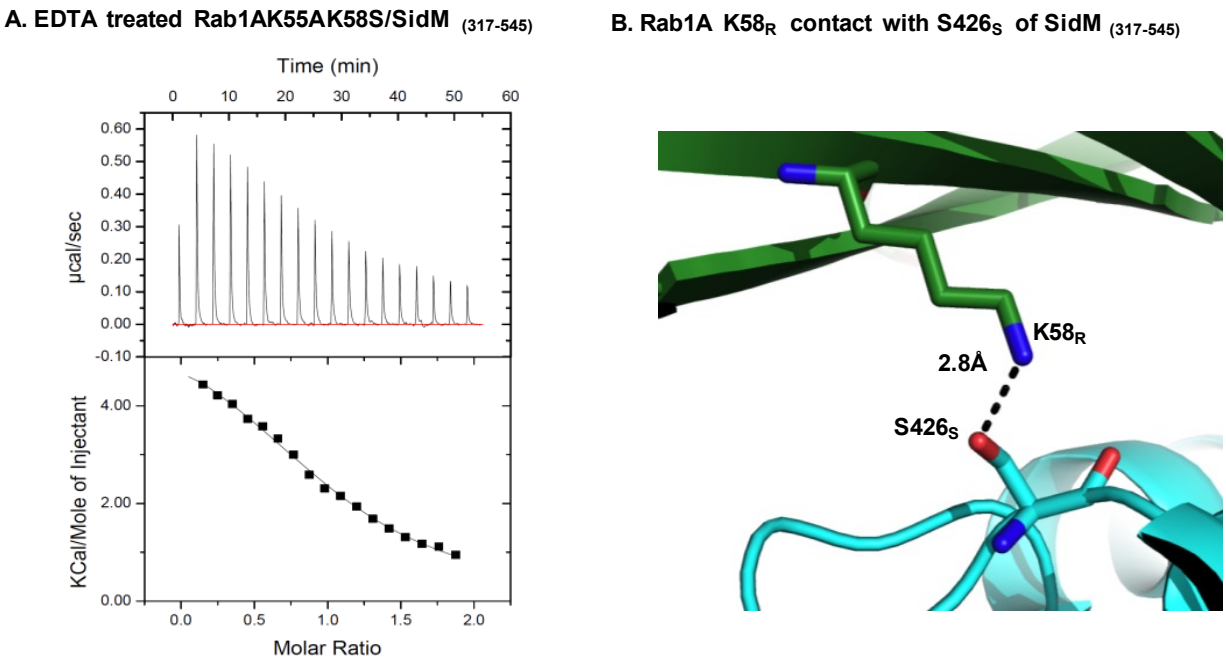

Figure 3.25: Decreased affinity of Rab1A$^{K55A-K58S}$ for SidM$_{317-545}$

(A) ITC titration curves of EDTA treated Rab1A$^{K55A-K58S}$ to SidM$_{317-545}$.The reaction is endothermic. The Top panel shows the raw data produced by titrating 1000 µM of Rab1A^{K55AK58S} variant to 100 µM of SidM$_{317-545}$. The Bottom panel represents the integration of above peaks against the molar ratio of Rab1A$^{K55A-K58S}$ to SidM$_{317-545}$. **(B)** The interaction of K58 of Rab1A (green) with S426 of SidM$_{317-545}$ (cyan) from the SidM$_{317-545}$ /Rab1A$_{1-175}$ crystal structure.

3.6.4 Effect of Rab1 variants E35A, Y37A and I41A on binding to SidM

Key residues of Rab1A$_{1-175}$ involved in the interaction with SidM$_{317-545}$ were identified from the crystal structure of Rab1A$_{1-175}$/SidM$_{317-545}$: E35$_R$, Y37$_R$ and I41$_R$ from the switch I region of Rab1A were classified as critical for the interaction with SidM$_{317-545}$ (Fig 3.20A&B). These residues were replaced by alanines by site-directed mutagenesis and corresponding pure samples prepared as described for wild-type Rab1A. The interaction of SidM$_{317-545}$ with Rab1 variants was analyzed by ITC as for wild-type Rab1A. ITC results reveal that all three Rab1A variants E35A, Y37A and I41A result in a significant decrease in the affinity towards SidM$_{317-545}$ (Fig 3.26A&B and Fig 3.27). The details of binding affinity are summarized in the Table 3.1.

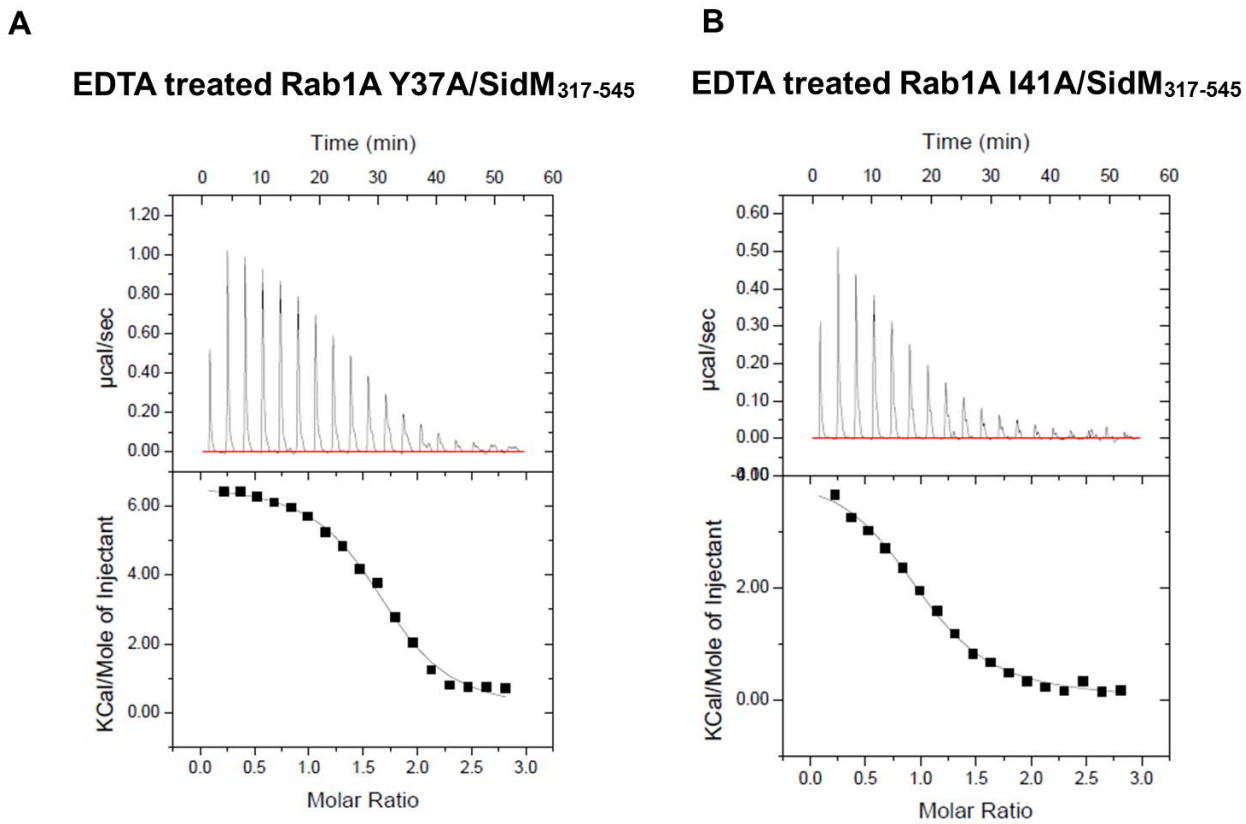

Figure 3.26: Isothermal titration curves of EDTA-treated Rab1A^{Y37A} and Rab1A^{I41A}/SidM (A) The titration curves of EDTA treated Rab1A^{Y37A} against SidM represents the reaction to be endothermic. Top panel: raw data from titrating 1000 µM Rab1A^{Y37A} to 100 µM of SidM. Bottom panel: integrated peaks from upper panel peaks plotted against the molar ratio of Rab1A^{Y37A} to SidM. (**B)**The titration curves of EDTA treated Rab1A I41A against SidM represents the reaction to be endothermic. Top panel shows the raw data produced by titrating 1000 µM of EDTA treated Rab1AI41A to 100 µM of SidM. Bottom panel represents the integration of above peaks against the molar ration of Rab1AI41Ato SidM.

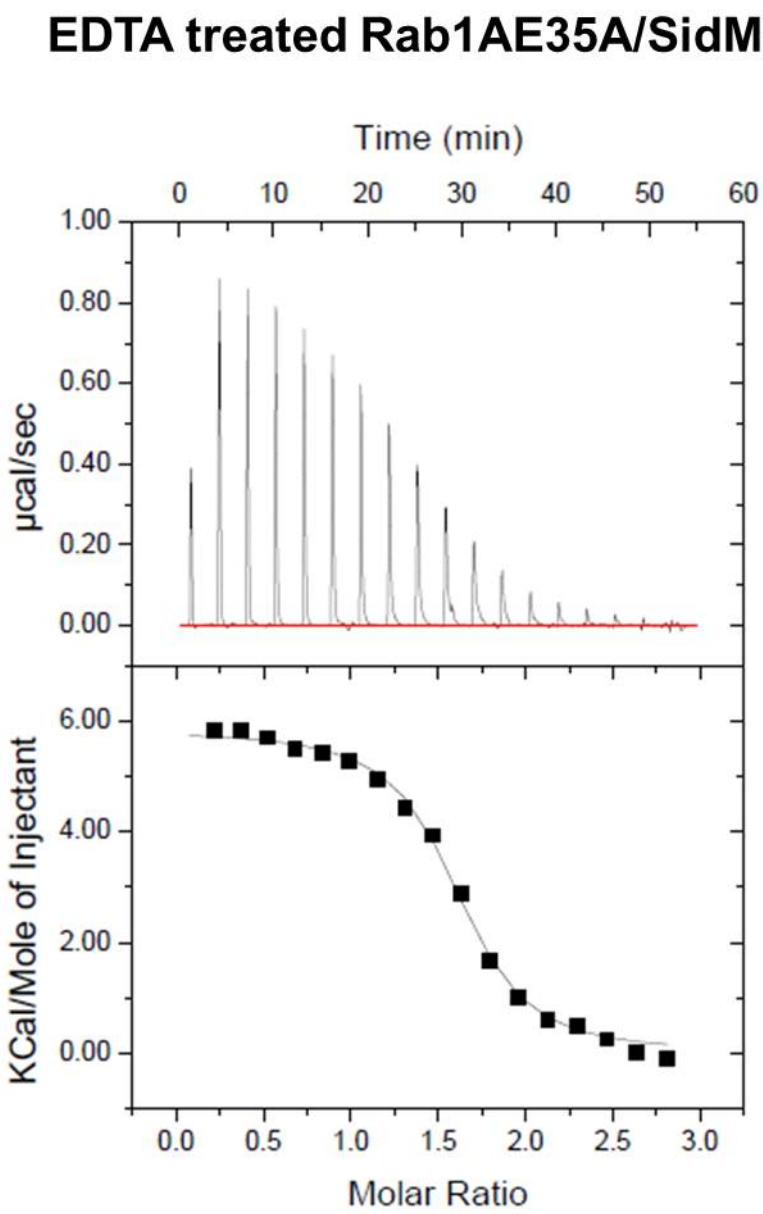

Figure 3.27: Isothermal titration curves of EDTA treated Rab1A^{E35A}/SidM. The titration curves of EDTA treated Rab1A^{E35A} against SidM identifies the reaction to be endothermic. The upper panel shows the raw data produced by titrating 1000 µM Rab1A^{E35A} to 100 µM SidM. The bottom panel represents the integration of above peaks against the molar ratio of Rab1^{AE35A} to SidM.

Table 4.1 Thermodynamic binding parameters for$SidM_{317-545}$ /$Rab1A_{1-175}$and Rab1A variants

Thermodynamic parameters	**Rab1A:GDP/$SidM_{317-545}$**	**EDTA:Rab1A/$SidM_{317-545}$**	**EDTA$Rab1A^{K55A-K58S}$/$SidM_{317-545}$**	**EDTA:$Rab1A^{E35A}$/$SidM_{317-545}$**	**EDTA:$Rab1A^{Y37A}$/$SidM_{317-545}$**	**EDTA:$Rab1A^{I41A}$/$SidM_{317-545}$**
k_a M^{-1}	$1.26x10^6$	$2.36x10^6$	$3.02x10^4$	$6.20x10^5$	$1.60x10^5$	$7.50x10^4$
k_d(μM)	0.793	0.423	33	1.6	6.25	13
N	1.19	1.56	1.07	1.5	1.6	1.0
ΔH kcal/mol	4.04	3.6	6.08	5.8	6.7	4.1

4 Discussion

4.1 SidM Manipulates Rab1A Function for Legionella pneumophila Survival

Rab1 is a small GTPase that regulates intracellular trafficking between the endocytoplasmic reticulum (ER) and the Golgi complex (Plutner, Cox et al. 1991; Tisdale, Bourne et al. 1992; Pind, Nuoffer et al. 1994; Wilson, Nuoffer et al. 1994; Somsel Rodman and Wandinger-Ness 2000; Moyer, Allan et al. 2001). In common with other GTPases, cytosolic Rab1 is normally kept in an inactive state by a dedicated GDP-dissociation inhibitor (GDI). To activate Rab1, a GDI-displacement factor (GDF) is required to remove the GDI before a GTP exchange factor (GEF) can induce the release of GDP to allow for subsequent uptake of GTP and activation of Rab1. SidM is a Type Four Secretion System effector protein from *L. Pneumophila* that has both GEF and GDF activity for Rab1GTPase (Machner and Isberg 2006). SidM recruits Rab1 to the *Legionella*-containing vacuole (LCV) as part of generating a specialized vacuole that resembles the host's rough endoplasmic reticulum. Within this vacuole *L. pneumophila* creates a replication niche allowing it to evade destruction by lysosomal fusion (Machner and Isberg 2006; Murata, Delprato et al. 2006).

Prior to the initiation of this study, no structural information for SidM was available. To understand the SidM/Rab1 complex at the atomic level, the central domain of $SidM_{317\text{-}545}$ and $Rab1A_{1\text{-}175}$ were each purified and co-crystallized. Complex formation of SidM/Rab1 was analysed by SEC and ITC experiments. The structure of the SidM/Rab1A complex was determined revealing that the GEF domain of SidM is structurally distinct from known eukaryotic GEFs. The structure of the complex further revealed that SidM induces several conformational changes in Rab1A to facilitate GDP release. ITC experiments show that SidM has a higher affinity for GDP-free Rab1A compared to Rab1:GDP.

4.2 SidM Induces Structural Changes on Rab1A

To identify SidM-induced rearrangements in Rab1A, Rab1A:GDP (PDB ID 2FOL) was superimposed on Rab1A from the Rab1A/SidM complex revealing a root mean square difference (RMSD) of 1.84 Å for C-α atoms. Major structural changes involve $\alpha1_{R,}$ P-loop, Switch I, Switch II and the $\beta5_R$-$\alpha5_R$ loop regions of Rab1A (Fig 4.1C).

4.2.1 Structural mechanism of nucleotide exchange by SidM

Rab GTPases bind GDP/GTP strongly, and GEFs decrease their binding affinity by inducing structural changes on Rab GTPases to catalyse nucleotide release (Schoebel, Blankenfeldt et al. 2010). Significant structural changes of Rab1A include the unravelling of $\alpha 1_R$ (residues 25-30) to form an extended loop and the translocation of Switch I away from the nucleotide-binding pocket–through several hydrophobic and hydrogen bond interactions with SidM. The central loop region of switch I (residues 36-41) adopts an α-helical conformation. Tyr33 and Glu34 in the switch I region bind the guanidine and sugar groups of the GDP in the Rab1:GDP structure and are significantly dislocated by about 21 and 28 Å respectively upon SidM binding. In the Rab:GDP structure, carbonyl oxygen (O) of I38 is involved in the interaction with Mg^{2+} and phosphate via a water molecule, whereas in the complex structure I38 is dislocated by about 17.2 Å (Fig 4.1B).

The P-loop of Rab1A consists of a conserved phosphate and Mg^{2+} binding motif (Vetter and Wittinghofer 2001). Mg^{2+} are essential for high affinity binding of GDP/GTP to the Rab GTPases (Hall and Self 1986). In the structure of Rab1:GDP, Lys21 of the P-loop binds the β-phosphate of GDP and Ser22 coordinates the Mg^{2+}. In the SidM/Rab1A complex, by contrast, SidM hydrogen bonds Asp16 and Ser17 moving Lys21 and Ser22 of the P-loop away from the phosphate and Mg^{2+}-binding sites, reducing the Rab1A affinity towards Mg^{2+} and thereby weakening the binding affinity for GDP.

In the Rab GTPase:GDP complexes, the switch II region is highly disordered (Eathiraj, Pan et al. 2005). In the structure of SidM/Rab1A, switch II is stabilized by multiple interactions with SidM. In Rab1:GDP, Asp63 of switch II coordinates Mg^{2+} via a water molecule. In the SidM/Rab1A complex, by contrast Asp63 forms a salt bridge to Lys21 of the P-loop thereby abolishing the interaction with Mg^{2+} and ultimately results in the decrease binding affinity of Rab1 for GDP (Fig 4.1B). Other SidM-induced changes include shifts of Rab1A loops $\beta 2_R$-$\beta 3_R$ by 4.9Å (by the engagement of Lys58) and β5R-$\alpha 5_R$ to a position that is occupied by guanosine base in Rab1A: GDP structure.

The described structural changes of Rab1A brought about by SidM binding combine to open the nucleotide binding pocket to release GDP explaining the GEF activity of SidM. The SidM mechanism of stabilizing nucleotide-free Rab1A is similar to that of other Rab:GEF complexes.

While our analyses were in progress, two competing groups reported crystal structures of Rab1 in complex with GEF domain of SidM (Schoebel, Blankenfeldt et al. 2010; Suh, Lee et al. 2010). To compare our SidM/Rab1A complex to the other two, the latter were

structurally aligned with our structure. This procedure yielded RMSD values of 0.51 and 0.59 Å for all C-α atoms of both proteins respectively. The low RMSDs imply essentially identical complexes, despite distinct crystal packing arrangements for each. Correspondingly, no major conformational changes are observed between these structures. Minor structural differences are likely to be caused by the crystal packing arrangement (Fig 4.2).

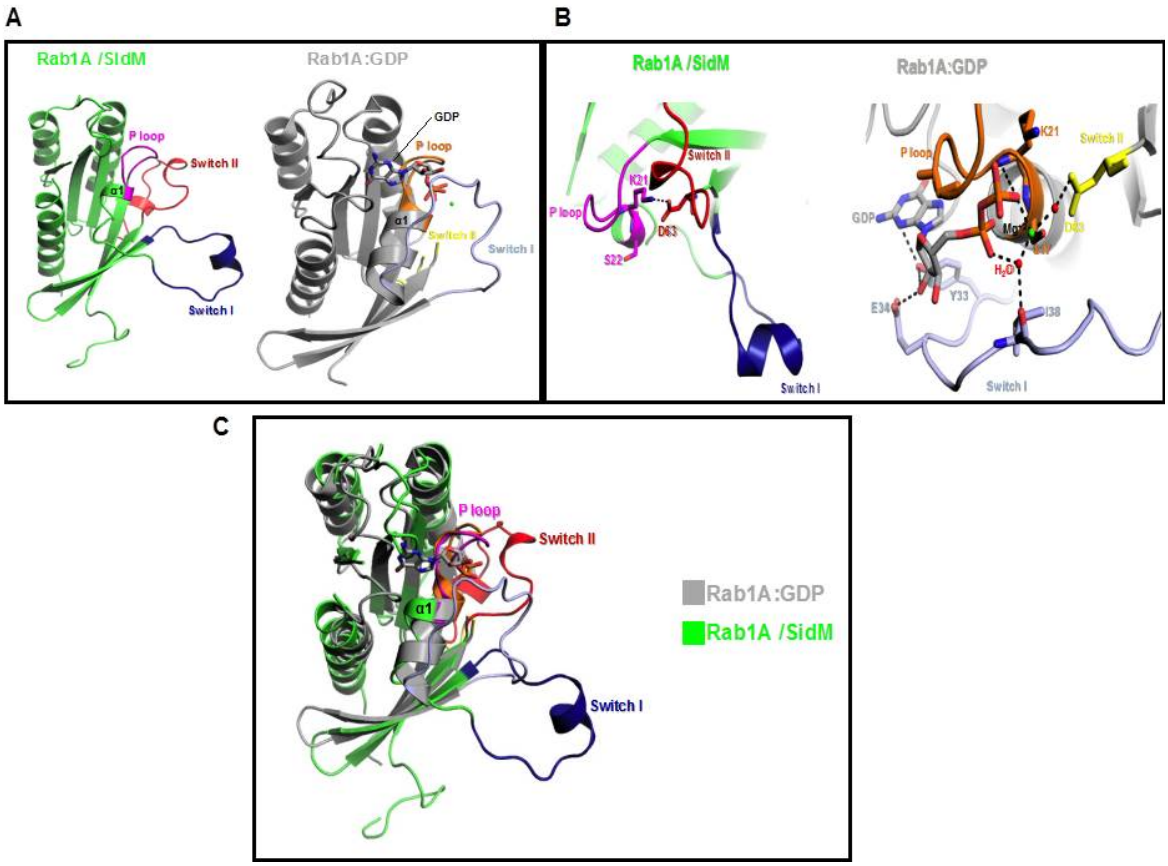

Figure 4.1: SidM-Induced Conformational changes in Rab1A (A). Conformational changes in Rab1A induced by SidM are identified by comparing Rab1A from its complex with SidM (green) to Rab1A:GDP (grey). Motifs Switch I, Switch II and P-loop are respectively shown in blue, red and magenta. $Mg^{2+}$and GDP are depicted in ball and stick representations. (B). left: Repositioning of Switch I and stabilization of P-loop in Rab1A/SidM; right: Mg^{+2} and GDP binding mode in Rab1A:GDP. (C) Superimposition of Rab1A:GDP (grey) and Rab1A from SidM/Rab1A.

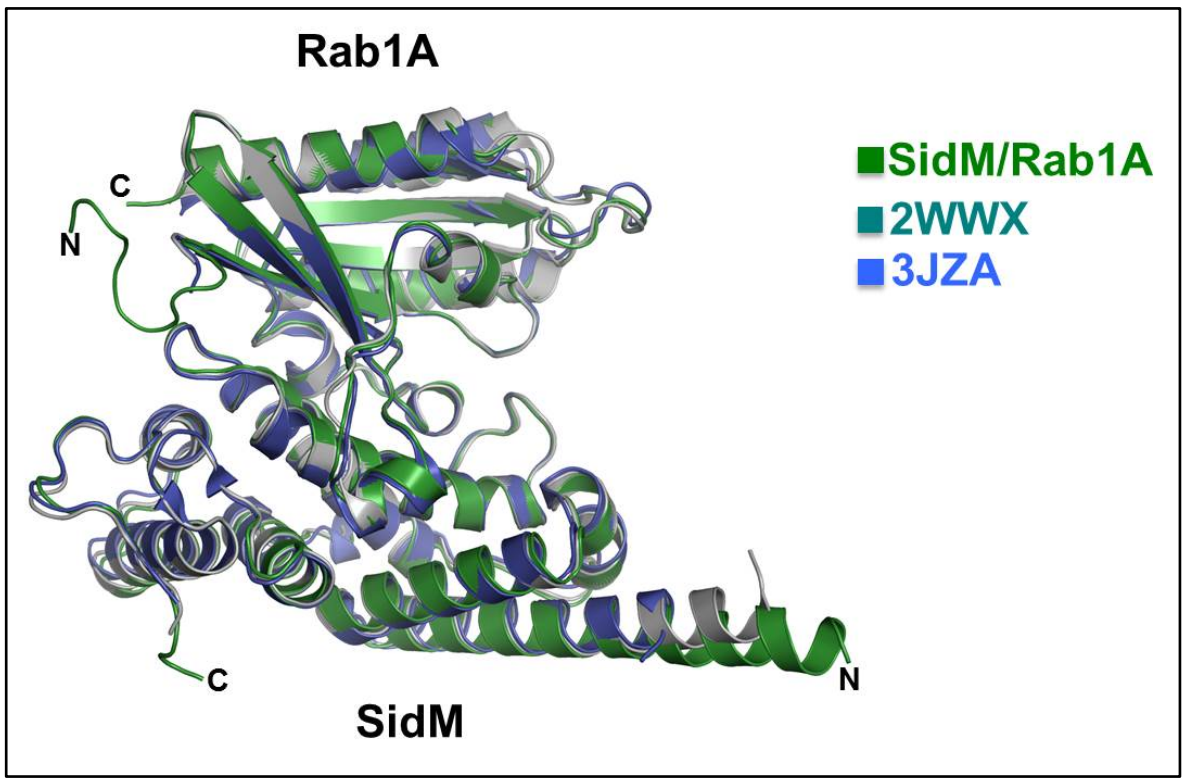

Figure 4.2: Alignment of SidM/Rab1A structure against other published structures of SidM/Rab1A (PDB ID: 2WWX & 3JZA). SidM/Rab1A is represented in green, 2WWX in grey and 3JZA in light blue

4.3 SidM affinity for nucleotide-free Rab1A is higher than for Rab1A:GDP

By interacting with the β-and γ-phosphate groups of GDP and GTP, Mg^{2+} ensures high affinity of Rab GTPases for these nucleotides (Hall and Self 1986; Goody, Pai et al. 1992). Exogenous EDTA removes Mg^{2+} from Rab GTPases inducing conformational changes that reduce affinity for GDP. GEFs bind nucleotide-free GTPases with higher affinity than nucleotide bound GTPases (Lai, Stubbs et al. 1994). In this study, Rab1A:GDP was treated with 20 mM EDTA during purification steps to remove Mg^{2+}. Prior to ITC experiments, the buffer was exchanged with Mg^{2+}- and EDTA-free buffer. The dissociation constant for SidM/Rab1A:GDP was found to be 700 nM (Fig 3.24A). By comparison the affinity of SidM for EDTA-treated Rab1A is increased roughly two-fold (K_D = 423 nM) (Fig 3.24B) confirming that the affinity of SidM for GDP-free Rab1A is higher than for GDP-bound Rab1A (Schoebel, Blankenfeldt et al. 2010). However, other studies have quantified the K_D for the SidM/GDP-free Rab1A to be in the pM range, implying that dissociation of GDP from Rab1A in our experiments was incomplete. Nevertheless, we do demonstrate that EDTA-induced loss of GDP does affect SidM affinity for Rab1A.

4.4 Role of Switch I in SidM binding

This and previous structural analyses of SidM/Rab1A have revealed that SidM predominantly interacts with switch I region of Rab1A dramatically changing its conformation. To assess the contribution of individual amino acids, Glu35, Tyr37 and Ile41 were substituted by alanine through site directed mutagenesis. Substituting Glu35 by alanine eliminates the hydrogen bonds linking Glu35 to Asp480 and Ser483 of SidM (Fig 3.20). ITC experiments correspondingly indicate that the affinity of SidM for $Rab1A^{E35A}$ is decreased ~four-fold relative to wild type Rab1A (Fig 3.27). The affinity of SidM for variant $Rab1A^{Y37A}$ is reduced ~15 fold (Fig 3.26A) possibly due to the loss of hydrophobic interactions with SidM residues Ala435, Phe474, Val478, Met439 and Asn373 (Fig 3.20B). Similarly, SidM affinity for $Rab1A^{I41A}$ is decreased ~30-fold (Fig 3.24B) probably due to the loss of hydrophobic and hydrogen bonding contact with Ala435, Met439, His376 and Lys438 of SidM (Fig 3.20A&B). Aligning different Rab sequences reveals that switch I residues Glu35, Tyr37 and Ile48 targeted by SidM are not conserved in other Rabs (Machner and Isberg 2006). This implies that Rab1A is highly specific for SidM.

Our site-directed mutagenesis and ITC experiments have shown that other amino acids at these positions resulted in decrease binding affinity of SidM for Rab1A. These findings imply that the switch I region is important for SidM binding.

4.4 Comparison of SidM/Rab1A with other GEF/Rab Complexes

Crystal structures of five eukaryotic GEFs in complex with nucleotide free Rab GTPases are currently available:Mss4/Rab8, Vps9/Rab21, Sec2/Sec4, TRAPP/Ypt1 and DENN/Rab27 [(Itzen, Pylypenko et al. 2006; Delprato and Lambright 2007; Dong, Medkova et al. 2007; Chin, Cai et al. 2009), 2FU5, 2OT3, 2OCY, 3CUE)]. SidM of the SidM:Rab1A complex presented in this study, does not share any obvious structural similarities with the remaining GEF domains. Nevertheless, the GEF mechanism of SidM is related to that of the other GEFs. Most importantly, SidM induces GDP-release exclusively through conformational changes in Rab1A, but without directly interacting with the nucleotide binding residues as observed in other GEFs.

Mss4 was shown to have low GEF activity for Rab8 relative to other GEFs. In the crystal structure of the nucleotide-free Mss4/Rab8 complex, Mss4 recognizes the switch I and β1-β2 inter-switch regions of Rab8 via an intermolecular β-sheet (Itzen, Pylypenko et al. 2006). Mss4 induces structural changes in switch I and α1 of Rab8, disrupting phosphate

and Mg^{2+} binding regions, opening of the nucleotide binding pocket. The Switch II region of Rab8 is not involved in the contact interface, in contrast to other GEF/Rab complexes (Fig 4.3).

In the structure of nucleotide free Rabex-5/Rab21, a helical-bundle Vps9 domain of the Rabex-5 catalytic core binds the switch/inter-switch regions and P-loop of Rab21 inducing an open conformation of the nucleotide binding pocket. Asp185 of Vps9 interacts with the conserved Lys21 from the Rab21 P-loop disrupting the phosphate and Mg^{2+} binding sites and stabilizing the disordered P-loop (Fig 4.3) and the switch II region (Delprato and Lambright 2007).

TRAPP1 is a multimeric membrane tethering complex and acts a GEF for Ypt1 of yeast. In contrast to other GEFs, the catalytic core of TRAPP1 is distributed among multiple subunits: Trs23p, Bet3p and Bet5p. In the crystal structure of TRAPP1/Ypt1, TRAPPI is seen to interact with the N-terminus, β1, Switch I, II and P-loop of Ypt1 (Fig 4.3). The C-terminus of Bet3p of TRAPP1 interacts with switch I region opening of the nucleotide binding pocket and disrupting the phosphate and Mg^{2+} binding sites to release GDP (Chin, Cai et al. 2009).

Sec2p functions as a GEF for the Rab GTPase Sec4p in yeast. The crystal structure of nucleotide free Sec2p/Sec4p revealed that Sec2p exhibits a parallel, homodimeric, coiled coil structure. Sec2p interacts with the Switch regions and the P-loop of Sec4p (Dong, Medkova et al. 2007; Sato, Fukai et al. 2007). Upon complex formation, Switch I residues involved in GDP base and sugar moiety binding undergo positional change, where Ile50 of Sec4p is forcibly placed close to the site occupied by Mg^{2+} in the nucleotide-bound forms. In this way, Ile50 disrupts the Mg^{2+} binding site of the P-loop, thus lowering the Sec4p affinity for GDP.

The GEF domain of SidM interacts with β1, switch I, II and P-loop of Rab1A displacing switch I away from the nucleotide binding site, stabilizing the P-loop and disrupting Mg^{2+} and phosphate binding site (Fig 4.2) releasing GDP from Rab1A.

Comparing the structures of GEF/Rab complexes indicates that Switch I displacement (including conserved residues involved in nucleotide binding) invariably induces nucleotide release. Similarly, all GEFs are seen to disrupt the Mg^{2+} and phosphate binding sites by inserting disruptive residues or by facilitating conformational changes. And finally, Switch II is forced to adopt an ordered conformation by GEFs.

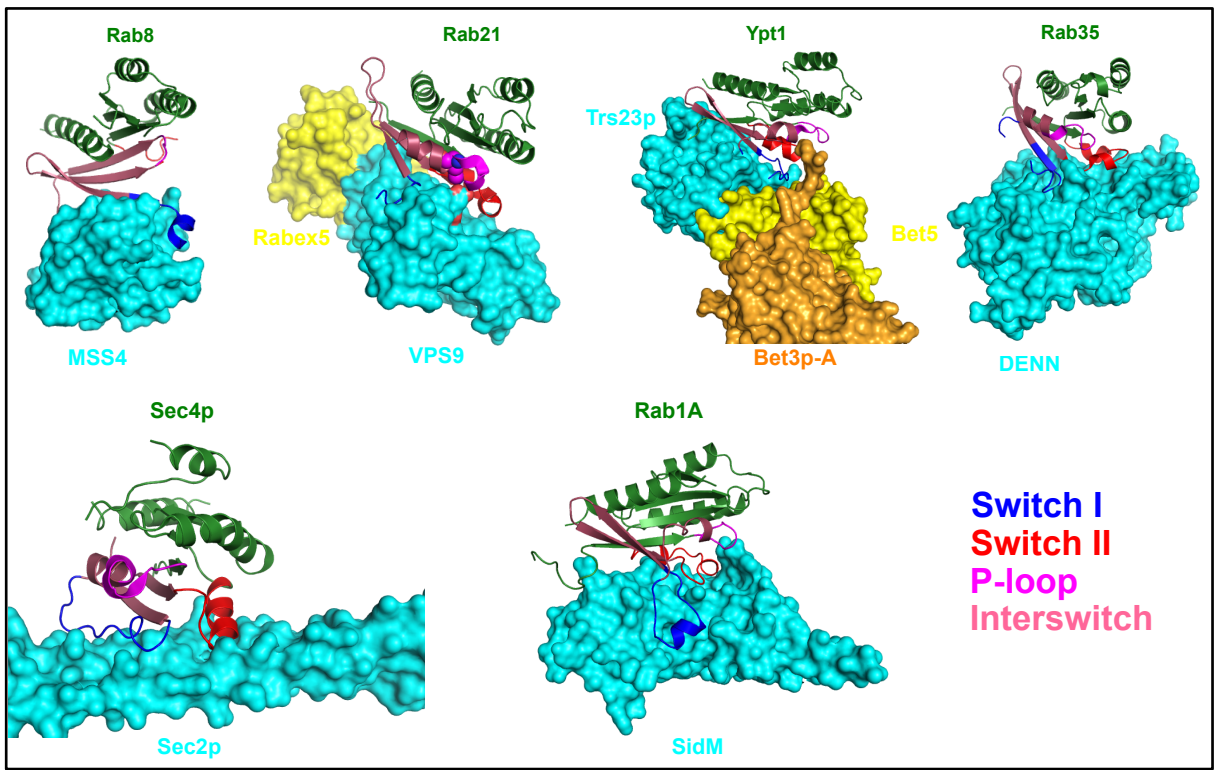

Figure 4.3: Comparison of the Crystal structures of different Rab:GEF Complexes. In the Rab: GEF complex structures, Rabs are color coded in green and GEF domains are represented in cyan. The structural elements of Rab GTPases involved in the interaction are color coded as switch I- blue, switch II- red, inter-switch region- salmon and P-loop in magenta. Images were drawn by pymol using coordinates of crystal structures with the following PDB codes: 2FU5 (Mss4: Rab8), 2OT3 (Rabex-5: Rab21), 2COY (Sec4: Sec2) and 3CUE (TRAPP: Ypt1).

5 Conclusions and Outlook

In this thesis, full length and six C-terminal truncation variants of human Rab1A were produced to study the interaction with C-terminal domain of SidM (317-545). Each of them was screened over a wide variety of conditions to produce crystals in complex with $SidM_{317-545}$ with the aim of solving the crystal structure of the complex. All truncation variants showed tight interaction with $SidM_{317-545}$. However only the complex consisting of $SidM_{317-545}$ and $Rab1A_{1-175}$ and where both genes were co-expressed in *E. coli* was successfully crystallized. This implies that the C-terminus of Rab1A is flexible and hinders the crystallization of the complex.

The interaction between two proteins were analysed by SEC, ITC and X-ray crystallography methods. The crystal structure of the SidM/Rab1A complex was solved, revealing that the GEF domain of SidM is structurally distinct from other known eukaryotic GEFs. The structure of the complex further revealed that SidM interacts mainly

with switch I, switch II and P-loop of Rab1A and induces conformational changes by dislocating switch I away from the nucleotide binding site and thereby disrupting Mg^{2+} and phosphate binding site releasing GDP from Rab1A. This is how SidM acts as an efficient GEF for Rab1A.

Based on the structural information of the complex, SidM interacting residues Glu35, Tyr37 and Ile41 of switch I of Rab1A were substituted by alanine to assess the role of switch I in the binding affinity with SidM. ITC experiments have shown that these variants bind SidM with weaker affinity than wild type Rab1A. These results indicate that Switch I is critical for SidM binding. On the other side, critical Rab1A interacting residues of SidM can also be targeted for mutational and structural analysis. Co-crystallizing these variants in complex and solving their crystal structures would give us detail insight on the mode of interaction between two proteins.

6 References

Alory, C. and W. E. Balch (2001). "Organization of the Rab-GDI/CHM superfamily: the functional basis for choroideremia disease." Traffic **2**(8): 532-543.

Altman, E. and G. Segal (2008). "The response regulator CpxR directly regulates expression of several Legionella pneumophila icm/dot components as well as new translocated substrates." J Bacteriol **190**(6): 1985-1996.

Andres, D. A., M. C. Seabra, et al. (1993). "cDNA cloning of component A of Rab geranylgeranyl transferase and demonstration of its role as a Rab escort protein." Cell **73**(6): 1091-1099.

Berger, K. H. and R. R. Isberg (1994). "Intracellular survival by Legionella." Methods Cell Biol **45**: 247-259.
Bock, J. B., H. T. Matern, et al. (2001). "A genomic perspective on membrane compartment organization." Nature **409**(6822): 839-841.

Brand, B. C., A. B. Sadosky, et al. (1994). "The Legionella pneumophila icm locus: a set of genes required for intracellular multiplication in human macrophages." Mol Microbiol **14**(4): 797-808.

Brombacher, E., S. Urwyler, et al. (2009). "Rab1 guanine nucleotide exchange factor SidM is a major phosphatidylinositol 4-phosphate-binding effector protein of Legionella pneumophila." J Biol Chem **284**(8): 4846-4856.

Bucci, C. and M. Chiariello (2006). "Signal transduction gRABs attention." Cell Signal **18**(1): 1-8.

Cai, H., K. Reinisch, et al. (2007). "Coats, tethers, Rabs, and SNAREs work together to mediate the intracellular destination of a transport vesicle." Dev Cell **12**(5): 671-682.

Campodonico, E. M., L. Chesnel, et al. (2005). "A yeast genetic system for the identification and characterization of substrate proteins transferred into host cells by the Legionella pneumophila Dot/Icm system." Mol Microbiol **56**(4): 918-933.

Conover, G. M., I. Derre, et al. (2003). "The Legionella pneumophila LidA protein: a translocated substrate of the Dot/Icm system associated with maintenance of bacterial integrity." Mol Microbiol **48**(2): 305-321.

Cunha, B. A. and U. Syed (2010). "Legionella pneumophila community acquired pneumonia (CAP) presenting with myoclonus." J Infect **61**(6): 505-507.

C.W. Carter, Jr. & R. M. Sweet, Eds (1997). " Processing of X-ray Diffraction Data Collected in Oscillation Mode." Methods in Enzymology, Volume **276:** 307-326

De Buck, E., J. Anne, et al. (2007). "The role of protein secretion systems in the virulence of the intracellular pathogen Legionella pneumophila." Microbiology **153**(Pt 12): 3948-3953.

de Felipe, K. S., S. Pampou, et al. (2005). "Evidence for acquisition of Legionella type IV secretion substrates via interdomain horizontal gene transfer." J Bacteriol **187**(22): 7716-7726.

de Renzis, S., B. Sonnichsen, et al. (2002). "Divalent Rab effectors regulate the sub-compartmental organization and sorting of early endosomes." Nat Cell Biol **4**(2): 124-133.

Delprato, A. and D. G. Lambright (2007). "Structural basis for Rab GTPase activation by VPS9 domain exchange factors." Nat Struct Mol Biol **14**(5): 406-412.

Derre, I. and R. R. Isberg (2004). "Legionella pneumophila replication vacuole formation involves rapid recruitment of proteins of the early secretory system." Infect Immun **72**(5): 3048-3053.

Dong, G., M. Medkova, et al. (2007). "A catalytic coiled coil: structural insights into the activation of the Rab GTPase Sec4p by Sec2p." Mol Cell **25**(3): 455-462.

Eathiraj, S., X. Pan, et al. (2005). "Structural basis of family-wide Rab GTPase recognition by rabenosyn-5." Nature **436**(7049): 415-419.

Edelstein, P. H. (2007). "Urine antigen tests positive for Pontiac fever: implications for diagnosis and pathogenesis." Clin Infect Dis **44**(2): 229-231.

Emsley, P. and K. Cowtan (2004). "Coot: model-building tools for molecular graphics." Acta Crystallogr D Biol Crystallogr **60**(Pt 12 Pt 1): 2126-2132.

Esters, H., K. Alexandrov, et al. (2001). "Vps9, Rabex-5 and DSS4: proteins with weak but distinct nucleotide-exchange activities for Rab proteins." J Mol Biol **310**(1): 141-156.

Gerlach, R. G. and M. Hensel (2007). "Protein secretion systems and adhesins: the molecular armory of Gram-negative pathogens." Int J Med Microbiol **297**(6): 401-415.

Goody, R. S., E. F. Pai, et al. (1992). "Studies on the structure and mechanism of H-ras p21." Philos Trans R Soc Lond B Biol Sci **336**(1276): 3-10; discussion 10-11.

Gurkan, C., H. Lapp, et al. (2005). "Large-scale profiling of Rab GTPase trafficking networks: the membrome." Mol Biol Cell **16**(8): 3847-3864.

Hall, A. and A. J. Self (1986). "The effect of Mg2+ on the guanine nucleotide exchange rate of p21N-ras." J Biol Chem **261**(24): 10963-10965.

Hammer, J. A., 3rd and X. S. Wu (2002). "Rabs grab motors: defining the connections between Rab GTPases and motor proteins." Curr Opin Cell Biol **14**(1): 69-75.

Horwitz, M. A. (1983). "The Legionnaires' disease bacterium (Legionella pneumophila) inhibits phagosome-lysosome fusion in human monocytes." J Exp Med **158**(6): 2108-2126.

Horwitz, M. A. and S. C. Silverstein (1980). "Legionnaires' disease bacterium (Legionella pneumophila) multiples intracellularly in human monocytes." J Clin Invest **66**(3): 441-450.

Hubber, A. and C. R. Roy (2010). "Modulation of host cell function by Legionella pneumophila type IV effectors." Annu Rev Cell Dev Biol **26**: 261-283.

Chin, H. F., Y. Cai, et al. (2009). "Kinetic analysis of the guanine nucleotide exchange activity of TRAPP, a multimeric Ypt1p exchange factor." J Mol Biol **389**(2): 275-288.

Ingmundson, A., A. Delprato, et al. (2007). "Legionella pneumophila proteins that regulate Rab1 membrane cycling." Nature **450**(7168): 365-369.

Itzen, A., O. Pylypenko, et al. (2006). "Nucleotide exchange via local protein unfolding--structure of Rab8 in complex with MSS4." EMBO J **25**(7): 1445-1455.

Jordens, I., M. Marsman, et al. (2005). "Rab proteins, connecting transport and vesicle fusion." Traffic **6**(12): 1070-1077.

Khosravi-Far, R., R. J. Lutz, et al. (1991). "Isoprenoid modification of rab proteins terminating in CC or CXC motifs." Proc Natl Acad Sci U S A **88**(14): 6264-6268.

Kubori, T., A. Hyakutake, et al. (2008). "Legionella translocates an E3 ubiquitin ligase that has multiple U-boxes with distinct functions." Mol Microbiol **67**(6): 1307-1319.

Laguna, R. K., E. A. Creasey, et al. (2006). "A Legionella pneumophila-translocated substrate that is required for growth within macrophages and protection from host cell death." Proc Natl Acad Sci U S A **103**(49): 18745-18750.

Lai, F., L. Stubbs, et al. (1994). "Molecular analysis of mouse Rab11b: a new type of mammalian YPT/Rab protein." Genomics **22**(3): 610-616.

Lee, M. T., A. Mishra, et al. (2009). "Structural mechanisms for regulation of membrane traffic by rab GTPases." Traffic **10**(10): 1377-1389.

Luo, Z. Q. and R. R. Isberg (2004). "Multiple substrates of the Legionella pneumophila Dot/Icm system identified by interbacterial protein transfer." Proc Natl Acad Sci U S A **101**(3): 841-846.

Machner, M. P. and R. R. Isberg (2006). "Targeting of host Rab GTPase function by the intravacuolar pathogen Legionella pneumophila." Dev Cell **11**(1): 47-56.

Matthews, B. W. (1968). "Solvent content of protein crystals." J Mol Biol **33**(2): 491-497.

Moyer, B. D., B. B. Allan, et al. (2001). "Rab1 interaction with a GM130 effector complex regulates COPII vesicle cis--Golgi tethering." Traffic **2**(4): 268-276.

Muller, M. P., H. Peters, et al. (2010). "The Legionella effector protein DrrA AMPylates the membrane traffic regulator Rab1b." Science **329**(5994): 946-949.

Murata, T., A. Delprato, et al. (2006). "The Legionella pneumophila effector protein DrrA is a Rab1 guanine nucleotide-exchange factor." Nat Cell Biol **8**(9): 971-977.

Murshudov, G. N., A. A. Vagin, et al. (1997). "Refinement of macromolecular structures by the maximum-likelihood method." Acta Crystallogr D Biol Crystallogr **53**(Pt 3): 240-255.

Nagai, H., J. C. Kagan, et al. (2002). "A bacterial guanine nucleotide exchange factor activates

ARF on Legionella phagosomes." Science **295**(5555): 679-682.

Neunuebel, M. R., Y. Chen, et al. (2011). "De-AMPylation of the small GTPase Rab1 by the pathogen Legionella pneumophila." Science **333**(6041): 453-456.

Neunuebel, M. R. and M. P. Machner (2012). "The taming of a Rab GTPase by Legionella pneumophila." Small GTPases **3**(1): 28-33.

Ninio, S., D. M. Zuckman-Cholon, et al. (2005). "The Legionella IcmS-IcmW protein complex is important for Dot/Icm-mediated protein translocation." Mol Microbiol **55**(3): 912-926.

Novick, P., M. Medkova, et al. (2006). "Interactions between Rabs, tethers, SNAREs and their regulators in exocytosis." Biochem Soc Trans **34**(Pt 5): 683-686.

Otwinowski Z, Minor W (1997) Processing of X-ray diffraction data collected in oscillation mode. In: Methods in Enzymology - Macromolecular Crystallography Part A (Charles WC, ed), pp 307-326. Academic Press

Pancer, K. and H. Stypulkowska-Misiurewicz (2003). "[Pontiac fever--non-pneumonic legionellosis]." Przegl Epidemiol **57**(4): 607-612.

Pereira-Leal, J. B., A. N. Hume, et al. (2001). "Prenylation of Rab GTPases: molecular mechanisms and involvement in genetic disease." FEBS Lett **498**(2-3): 197-200.

Pereira-Leal, J. B. and M. C. Seabra (2000). "The mammalian Rab family of small GTPases: definition of family and subfamily sequence motifs suggests a mechanism for functional specificity in the Ras superfamily." J Mol Biol **301**(4): 1077-1087.

Pfeffer, S. and D. Aivazian (2004). "Targeting Rab GTPases to distinct membrane compartments." Nat Rev Mol Cell Biol **5**(11): 886-896.

Pind, S. N., C. Nuoffer, et al. (1994). "Rab1 and Ca2+ are required for the fusion of carrier vesicles mediating endoplasmic reticulum to Golgi transport." J Cell Biol **125**(2): 239-252.

Plutner, H., A. D. Cox, et al. (1991). "Rab1b regulates vesicular transport between the endoplasmic reticulum and successive Golgi compartments." J Cell Biol **115**(1): 31-43.

Samrakandi, M. M., D. A. Ridenour, et al. (2002). "Entry into host cells by Legionella." Front Biosci **7**: d1-11.

Sato, Y., S. Fukai, et al. (2007). "Crystal structure of the Sec4p.Sec2p complex in the nucleotide exchanging intermediate state." Proc Natl Acad Sci U S A **104**(20): 8305-8310.

Segal, G., J. J. Russo, et al. (1999). "Relationships between a new type IV secretion system and the icm/dot virulence system of Legionella pneumophila." Mol Microbiol **34**(4): 799-809.

Segal, G. and H. A. Shuman (1997). "Characterization of a new region required for macrophage killing by Legionella pneumophila." Infect Immun **65**(12): 5057-5066.

Segev, N. (2001). "Ypt/rab gtpases: regulators of protein trafficking." Sci STKE **2001**(100): re11.

Shohdy, N., J. A. Efe, et al. (2005). "Pathogen effector protein screening in yeast identifies Legionella factors that interfere with membrane trafficking." Proc Natl Acad Sci U S A **102**(13): 4866-4871.

Schoebel, S., W. Blankenfeldt, et al. (2010). "High-affinity binding of phosphatidylinositol 4-phosphate by Legionella pneumophila DrrA." EMBO Rep **11**(8): 598-604.

Schwartz, S. L., C. Cao, et al. (2007). "Rab GTPases at a glance." J Cell Sci **120**(Pt 22): 3905-3910.

Sivars, U., D. Aivazian, et al. (2003). "Yip3 catalyses the dissociation of endosomal Rab-GDI complexes." Nature **425**(6960): 856-859.

Somsel Rodman, J. and A. Wandinger-Ness (2000). "Rab GTPases coordinate endocytosis." J Cell Sci **113 Pt 2**: 183-192.

Stenmark, H. (2009). "Rab GTPases as coordinators of vesicle traffic." Nat Rev Mol Cell Biol **10**(8): 513-525.

Stenmark, H. and V. M. Olkkonen (2001). "The Rab GTPase family." Genome Biol **2**(5): REVIEWS3007.

Stenmark, H., A. Valencia, et al. (1994). "Distinct structural elements of rab5 define its functional specificity." EMBO J **13**(3): 575-583.

Storoni, L. C., A. J. McCoy, et al. (2004). "Likelihood-enhanced fast rotation functions." Acta Crystallogr D Biol Crystallogr **60**(Pt 3): 432-438.

Suh, H. Y., D. W. Lee, et al. (2010). "Structural insights into the dual nucleotide exchange and GDI displacement activity of SidM/DrrA." EMBO J **29**(2): 496-504.

Tan, Y. and Z. Q. Luo (2011). "Take it and release it: The use of the Rab1 small GTPase at a bacterium's will." Cell Logist **1**(4): 125-127.

Tisdale, E. J., J. R. Bourne, et al. (1992). "GTP-binding mutants of rab1 and rab2 are potent inhibitors of vesicular transport from the endoplasmic reticulum to the Golgi complex." J Cell Biol **119**(4): 749-761.

Tronel, H. and P. Hartemann (2009). "Overview of diagnostic and detection methods for legionellosis and Legionella spp." Lett Appl Microbiol **48**(6): 653-656.

Ullrich, O., H. Stenmark, et al. (1993). "Rab GDP dissociation inhibitor as a general regulator for the membrane association of rab proteins." J Biol Chem **268**(24): 18143-18150.

van den Ent, F. and J. Lowe (2006). "RF cloning: a restriction-free method for inserting target genes into plasmids." J Biochem Biophys Methods **67**(1): 67-74.

van Schaik, E. J., C. Chen, et al. (2013). "Molecular pathogenesis of the obligate intracellular

bacterium Coxiella burnetii." Nat Rev Microbiol **11**(8): 561-573.

VanRheenen, S. M., Z. Q. Luo, et al. (2006). "Members of a Legionella pneumophila family of proteins with ExoU (phospholipase A) active sites are translocated to target cells." Infect Immun **74**(6): 3597-3606.

Vetter, I. R. and A. Wittinghofer (2001). "The guanine nucleotide-binding switch in three dimensions." Science **294**(5545): 1299-1304.

Vincent, C. D., J. R. Friedman, et al. (2006). "Identification of the core transmembrane complex of the Legionella Dot/Icm type IV secretion system." Mol Microbiol **62**(5): 1278-1291.

Vogel, J. P., H. L. Andrews, et al. (1998). "Conjugative transfer by the virulence system of Legionella pneumophila." Science **279**(5352): 873-876.

Wennerberg, K., K. L. Rossman, et al. (2005). "The Ras superfamily at a glance." J Cell Sci **118**(Pt 5): 843-846.

Wilson, B. S., C. Nuoffer, et al. (1994). "A Rab1 mutant affecting guanine nucleotide exchange promotes disassembly of the Golgi apparatus." J Cell Biol **125**(3): 557-571.

Wu, Y. W., K. T. Tan, et al. (2007). "Interaction analysis of prenylated Rab GTPase with Rab escort protein and GDP dissociation inhibitor explains the need for both regulators." Proc Natl Acad Sci U S A **104**(30): 12294-12299.

Zerial, M. and H. McBride (2001). "Rab proteins as membrane organizers." Nat Rev Mol Cell Biol **2**(2): 107-117.

Zhu, Y., L. Hu, et al. (2010). "Structural mechanism of host Rab1 activation by the bifunctional Legionella type IV effector SidM/DrrA." Proc Natl Acad Sci U S A **107**(10): 4699-4704.

Zusman, T., G. Aloni, et al. (2007). "The response regulator PmrA is a major regulator of the icm/dot type IV secretion system in Legionella pneumophila and Coxiella burnetii." Mol Microbiol **63**(5): 1508-1523.

Acknowledgements

I would like to thank my supervisor Prof.Dr. Wolf-Dieter Schubert for his kind support, guidance and giving me the opportunity to work independently in his group. His expertise and commitment were essential to the success of this work, not least by his ever-open ear for questions and discussion. With untiring efforts he has done everything to complete the elaborate move to South Africa and quickly organized and to ensure good conditions in South Africa for successful research at a high level. He also helped us to all problems away from the lab, so bring a move to a new country with him, always a helping hand to the side, and thus has made us feel at home. He helped me and my wife a lot to have a comfortable stay in South Africa. His accommodative nature and encouragement have made my time here a truly comfortable yet enriching learning experience.

I would like to thank Prof. Dirk Heinz for giving me the opportunity to work in his department and the making available of a modern laboratory equipment and infrastructure during the time at HZI. Even after moving to South Africa, we were still actively supported by his department. I thank you also for joining my initial "Thesis Committee," and very helpful suggestions and discussions.

I am very grateful to Prof. Dr. Michael Steinert for joining my thesis committee and being my examiner. I also thank him for accepting my courses to complete my PhD successfully. I also would like to thank Prof. Ralf-Rainer Mendel for the takeover of the Presidency examination.

I would like to thank Dr. Joop van den Heuvel and his team for the regular production of Rab1 protein during my stay at HZI. I am very thankful to Prof. David Pugh and Prof. Trevor Sewell for being my thesis committee members at UWC, South Africa.

I also would like to thank Dr. Mathias Machner for providing us the constructs of Rab and SidM proteins. I would like to thank Christine Holland for her help and training me in the lab during my initial days at HZI. I thank Dr. Manfred Nimtz and team, Rita and Salome Smit Getzlaff for mass spectrometric and N-terminal sequencing.

My special thanks to Nils and Lilia for their kind support and suggestions in the lab. It was very nice working with you. Your friendly nature had made me and my wife feel at home. I always cherish the moments that we spend together in South Africa being like family members.

A big "thank you" goes to Ute Widow, the best TA ever. If we missed a person in Cape Town on the work, then you.

I also thank, Maike Bublitz for her suggestions during my stay at HZI. I also thank Uwe and all the other members of HZI for their nice working environment. I thank Muzi, Donne, Rowan, Clive and all the other members of the lab at UWC, South Africa.

I am very thankful to Dr. Konrad Bussow for spending his valuable time in correcting my thesis. I thank all current and former colleagues in the Structural Biology at the HZI and Biotechnology at UWC in South Africa, I would like to unreservedly thank you for the great working atmosphere, fun lunch breaks and various "After Work" events.

I thank Madhu Nagaraj for his friendly nature and for his cooking skills during my stay in Braunschweig.

This work would not have been possible without the great support of my wife Devi. Devi, I cannot write here, for your kind support and love that you gave me all the time. Thank you, thank you very much. I thank my family members for their kind support. Last but not the least, I thank my almighty GOD for his blessings.

Curriculum Vitae

ADDRESS

Edukondalu Mullapudi
Research Associate
Department of Structural Virology
Central European Institute of Technology (CEITEC)
Kamenice 753/5, Building A35
62500 Brno, Czech Republic
Email: mullapudiedukondalu@gmail.com

Phone: +420702930988

PERSONAL DETAILS

Name	: Edukondalu Mullapudi
Date of Birth	: 03-04-1984
Gender	: Male
Marital	: Married
Nationality	: Indian

EDUCATION

PhD (2009-2014) in Structural Biology, **Helmholtz Centre for Infection Research**, Braunschweig, Germany and **University of the Western Cape**, South Africa

MSc (2007) in Molecular biology, **University of Skövde**, Skövde, Sweden

B.Sc (2005) in Biotechnology, Biochemistry, Chemistry, SPACES Degree College, **Andhra University**, Vishakhapatnam, India

PROFESSIONAL CAREER

Research Associate (August 2013- till date) at Central European Institute of Technology (CEITEC), Brno, Czech Republic

Research Associate (March 2012-Dec 2012) at Institute for Microbial Biotechnology and Metagenomics (IMBM), University of the Western Cape, Cape Town.

Research Expertise

Biochemistry, Molecular Biology, Protein Chemistry, Structural Biology and Microbiology

CONFERENCES

2010 Talk: Structural and functional characterization of the protein SidM of Legionella Pneumophilia and its complex with human guanosine triphosphatase Rab1A, awarded prize at **Biotechnology Research Open Day**, University of the Western Cape, Cape Town, South Africa

2008: Attended **3rd Colloquium DFG Priority Program SPP 1150, Signal Pathways to the cytoskeleton and Bacterial Pathogenesis**, Freiburg, Germany, September 7-9, 2008

2008: Attended **11th Heart of Europe Bio-Crystallography Meeting (HEC 11)**, Greifswald, Germany, September 25 - 27, 2008

CERTIFICATE COURSE

First Aid-Level 2 Training from Department of Labour Approved First Aid Training Organization, SAFENET, South Africa (21-24 June 2010)

Chemical Safety Training from THE SAFETY NETWORK, SAFENET, South Africa (18 June 2010)

Laboratory Safety Training from, THE SAFETY NETWORK, SAFENET, South Africa (15 June 2010)

Standardization of Protocol for PCR based amplification of SY-83 (Sep-Nov 2005), Genetech Professional Education and Training, Hyderabad, India